T.C.
ALTINBAS UNIVERSITY
Graduate School of Science and Engineering
Electrical and Computer Engineering

ANALYSIS AND EVALUATION OF OFDM IN LTE NETWORK

Abdunaser Sasi A Algnash

Master Thesis

Supervisor

Prof. Dr. Oguz Bayat

Istanbul, 2020

ANALYSIS AND EVALUATION OF OFDM IN LTE NETWORK

by

Abdunaser Sasi A Algnash

Electrical and Computer Engineering

Submitted to the Graduate School of Science and Engineering

in partial fulfillment of the requirements for the degree of

Master of Science

ALTINBAŞ UNIVERSITY

2020

This is to certify that we have read this thesis and that in our opinion it is fully adequate, in scope and quality, as a thesis for the degree of Master of Science.

Prof. Dr. Oguz BAYAT

Supervisor

Examining Committee Members (first name belongs to the chairperson of the jury and the second name belongs to supervisor)

Prof. Dr. Oguz BAYAT	School of Engineering and Natural Sciences, Altinbas University	_____
Asst. Prof. Dr. Abdullahi Abdu IBRAHIM	School of Engineering and Natural Sciences, Altinbas University	_____
Asst. Prof. Dr. Adil Deniz DURU	Faculty of Sport Sciences, Marmara University	_____

I certify that this thesis satisfies all the requirements as a thesis for the degree of Master of Science.

Asst. Prof. Dr. Cagatay AYDIN
Head of Department

Approval Date of Graduate School of Science and Engineering: ____/____/____

Prof. Dr. Oguz BAYAT
Director

I hereby declare that all information in this document has been obtained and presented in accordance with academic rules and ethical conduct. I also declare that, as required by these rules and conduct, I have fully cited and referenced all material and results that are not original to this work.

Abdunaser Sasi A Algnash

DEDICATION

I dedicate this work to my parents. Also special dedication to my wife and my daughters Ghazl and Dania. They were my help, patience and my passion in exile.

ACKNOWLEDGEMENTS

Firstly, I thank my God who grant me the ability and rightness to fulfill this writing to the fullest, and I hope it is purely done for his great face. Secondly, I appreciate Dr. Oguz Bayat for his advice and proper guidance through the period of doing this research. His recommendations were very helpful and beneficial. I firstly owe the fulfilling of this thesis writing to my God and after that to the efforts that are given by him.

I also appreciate the advice that was given to me by Dr. Cagatay Aydin. He is always existing in the right time. And special grateful to the postgraduate department of Altinbas University. As well as the library team, international office and registration office. They all were flexible and their assistance must not be forgotten.

I would also appreciate all of my colleagues during my studies as their participation was really helpful in filling the gaps.

Finally, I appreciate my parents, brothers and sisters for their continuous support. Without their advice and encouragement this work might be done improperly.

ABSTRACT

ANALYSIS AND EVALUATION OF OFDM IN LTE NETWORK

Algnash, Abdunaser

M.Sc. Electrical and Computer Engineering, Altınbaş University,

Supervisor: Prof. Dr. Oguz Bayat

Date: February, 2020

Pages: 158

Orthogonality of OFDM is a dominant solution to achieve a reliable fast speed data rates. OFDM is implemented according to the concept of dividing the available bandwidth into sub-streams, and that is accomplished by splitting the data stream into parallel data sub-streams. In OFDM a various set of orthogonal narrow sub-carriers are transmitted in parallel and they overlap orthogonally. OFDM provides a high data rates across frequency selective channels including multipath fading, phase noise and frequency offset. OFDM changes the selectivity of multipath channel frequency into a more stable channel with flat fading characteristics, and therefore, minimize inter-symbol-interference ISI. Although it is highly sensitive to synchronization errors, it is simplifying the process of equalization at receiver. Multiple input multiple output MIMO-OFDM is implemented within OFDM systems which uses multiple antennas to rise the throughput without maximizing the power of transmitter or receiver. OFDM is configured within LTE Long Term Evolution as down-link air-interface. Despite the fact that OFDM system achieves many advantages, it is facing serious issues. Particularly, PAPR peak to average power ratio, which is considered as a problematic drawback [1]. PAPR occurs due to highly variated fluctuations in transmitted signal

that leads to the requirement of having linearity of high power amplifiers HPA. Frequency offset is another problem encountering OFDM systems which is caused by Doppler shift frequency. The main purpose of this thesis is studying an OFDM system mathematically and proposing a Matlab simulation demonstrates each of the components of the OFDM system, analyze and evaluate its performance with respect to the bit error ratio BER using quadrature amplitude modulation QAM. The simulation is modeled under different environmental conditions such as Rayleigh fading and AWGN additive white Gaussian noise. After that, many proposed techniques are analyzed and simulated to reduce PAPR, frequency offset, channel estimation, synchronization and phase noise effects from the received signal. Finally, OFDM system optimization can be achieved by applying techniques that give better results within the system. Simulations and analysis are studied with consideration of using LTE as the technology that is using the OFDM modulation.

Keywords: Orthogonal Frequency Division Multiplexing OFDM, Analogue-To-Digital ADC, Additive White Gaussian Noise AWGN, Demodulation, Peak-To-Average-Power-Ratio PAPR, Serial-To-Parallel S/B, Multiple-Input-Multiple-Output MIMO, Modulation, Channel Estimation, Synchronization, Cyclic Prefix CP.

TABLE OF CONTENTS

Pages

LIST OF TABLES

Pages

LIST OF FIGURES

Pages

LIST OF ABBREVIATIONS

OFDM	:	Orthogonal Frequency Division Multiplexing
MIMO	:	Multi Input Multi Output
BER	:	Bit Error Ratio
PAPR	:	Peak To Average Power Ratio
LTE	:	Long Term Evolution
HPA	:	High Power Amplifier
QAM	:	Quadrature Amplitude Modulation
AWGN	:	Additive White Gaussian Noise
CP	:	Cyclic Prefix
ISI	:	Inter Symbol Interference
ADC	:	Analogue To Digital Converter
DAC	:	Digital To Analogue Converter
P/S	:	Parallel To Serial Conversion
S/P	:	Serial To Parallel Conversion
DFT	:	Discrete Fourier Transform
TDMA	:	Time Division Multiple Access
CDMA	:	Code Division Multiple Access
ACI	:	Adjacent Channel Interference

1. INTRODUCTION

OFDM is a mapping and modulation technique which is particularly appropriate for high density data-rate transmission in delayed-dispersive-channel conditions. It changes over a speedy rate of information stream into various decreased rate of information sub streams that are sent over parallel way, and narrow-band channels that become simple to be equalized effectively[2].

Initially, considering to investigate why conventional modulation techniques made problematic issues at higher transmission data-rates, a symbol-duration Ts needs to be very tiny to obtain the necessary data-rate and the transmission bandwidth appears to be significantly large, delay-dispersion channel conditions is essentially given by nature, not by a transmission system itself. Subsequently, if the symbol-duration becomes exceptionally small, then the impulse-response becomes very long regarding to the symbol duration. Therefore, the receiver's equalizer become more complicated and the signal detection computation need expensive equipment to achieve that goal. For instance, the global-system-for-mobile-communication GSM requires 200kz bandwidth and transmits information at 200 Kbit/s, while the wireless local area network IEEE-802-11 transmits data at 54 Mbit/s and requires 20Mhz bandwidth. In delay-dispersion channel of 1 μS in GSM uses 2-tab equalizer, on the other hand the 20Mhz bandwidth requires 20-tabs, OFDM expands the symbol-duration for every sub-carrier with comparison to the single-carrier system [3]. Thus, OFDM system reduces inter-symbol-interference ISI to an acceptable level.

1.1 HISTORY OF OFDM

OFDM has to be one of the most energizing advancements in broadband wireless communication. Despite the fact that multi-carrier multiplexing (such as frequency-division-multiplexing FDM) can be gone back to 1950s, high efficiency spectrum and minimal cost practical implementation become conceivable during the 1970s and 1980s with the obvious advances of Digital-Fourier-Transform DFT, up to the 1990s until the first appearance of OFDM as a commercial implementation in digital-audio-broadcasting DAB. In 1970 initial patent issued for OFDM, after that initial OFDM-Based digital audio broadcasting system was implemented in 1995, then in 1997 the first terrestrial digital-video-broadcasting DVB was invented, next in 1999 wireless LAN standards was distributed for HIPER LAN /2 and IEEE-802.11a, then the first fixed-wireless-MAN was developed in 2004 as the IEEE-802.16a/d standards, in 2005 IEEE-802.16e WIMAX

standard was developed for cellular OFDM-based networks [4]. Finally, in 2009 the first commercial cellular mobile network was emerged in Sweden and Norway as the long-term-evolution LTE that uses the spectral efficiency OFDM scheme [5] . Since then, OFDM was implemented in mobile communication systems and up to the present day where the LTE OFDM based system is being widely used.

1.2 WIRELESS COMMUNICATION MULTIPLE ACCESS TECHNIQUES

Practically, it is difficult to transmit a high singular data-rate stream through the air channel from a transmitter towards a receiver. Thus, a communication system must be able to deal with multiple-users simultaneously. The technique that allow various users to use the system simultaneously is aimed to the process of multiple-access MA. In wireless cellular communication systems, the coverage land is split into smaller places named cells and each of them is served via a central base station. Information transfer from user device to the central base station is referred to the term reverse link or uplink, and information transfer from the central base station to the used device is named downlink or forward link. Both up-link and down-link use different operational frequencies. And the method permitting multiple-users to interchange information simultaneously is called multiple-access technique [6]. Two multiple access techniques are adopted by LTE, the OFDM for downlink direction between the base station and user equipment and SC-FDMA for the reverse direction.

1.2.1 OFDM

Higher rate of data-stream normally is subject to have a symbol-period Ts less than channel time-delay Td, that is occurred when sending the data-stream in a serial form. As a result, this causes the problem of ISI inter symbol interference that is only recovered by configuring a complicated equalizer. In OFDM method the data-stream is converted from serial to parallel sub-carriers. Subsequently, the symbol-duration is expanded and become longer than the channel time-delay.

This process reduces the complexity of equalization and changes the frequency selectivity of channel characteristics into a reliable channel with flat fading properties. It also increases the efficiency of spectrum, and higher data-rate streams can be transmitted among an OFDM system Thus, LTE practically takes advantage of OFDM theory and it is implemented in the down-link

physical air-interface. Figure 1.1 illustrates the effects of dispersive channel on the transmitted signal.

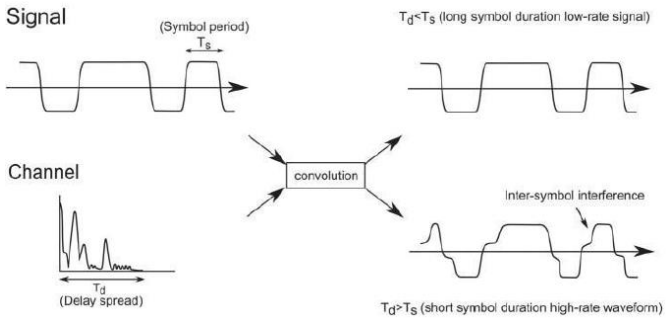

Figure 1.1: Effects of dispersive channel on transmitted signals [7]

1.2.2 SC-FDMA

SC FDMA means a multiplexing method employed in LTE uplink stream, that is because it was the best technique was practiced to reduce PAPR levels of the transmitted signal. High PAPR requires high consumption power amplifiers at the user equipment UE, which in practice, impossible to implement due to the limitation of mobile batteries [7]. The SC-FDMA principle can be achieved by two operations, one at the transmitter, and the other at the receiver. DFT discrete Fourier transform M Points process is applied prior to N-Point IFFT stage at the transmitter. At the receiver an IDFT M Point inverse discrete Fourier transform is applied afterwards the OFDM-FFT process. As a consequence, SC-FDMA multiplexing data as in normal OFDM, but with a lower PAPR levels and achieving an optimized power efficiency of spectrum. SC-FDMA employed by either of two types, localized subcarrier assignment and distributed subcarrier assignment [8].

1.3 THESIS OBJECTIVES AND EXCUTION SUMMARY

1.3.1 Thesis Aims and Target

The general aim of this writing is to enrich readers to the LTE-OFDM technique principles and keep them in knowledge of various LTE-OFDM system components. Furthermore, it provides the readers how an LTE-OFDM system works and shows them every stage of the modulation process from the transmitter who transmits the signal in binary format until the receiver get the data and

retrieve it to its original state. This thesis describes LTE architecture and studies the LTE OFDM system mathematically, and demonstrates the main key factors that affect the performance of the system. Channel estimation and synchronization process are studied and modeled with respect to the frequency-selective channel and multipath-fading effects. Finally, the main aim of this writing is to study PAPR and analyze different proposed methods that decrease PAPR levels, and therefore, increase system efficiency. Furthermore, this thesis, simulates the LTE-OFDM system modulation process using Matlab software. Firstly, it analyses the performance of the system regarding to BER bit error ratio using various digital mapping schemes in different channels. For instance, QAM16 and QAM64 quadrature amplitude modulation, QPSK quadrature phase shift keying and BPSK binary phase shift keying. Then, the simulation goes further and simulates various PAPR reduction methods. Finally, different frequency offset, timing offset estimators, encoding processors and channel estimators are simulated and their impacts on the OFDM system are evaluated.

1.3.2 Thesis Organization Preview

1. Chapter one gives an introduction to OFDM modulation technique and shows its history, then it briefly explains various multiple access methods. Finally, it lists the thesis objectives and targets.

2. Chapter two shows a brief description of LTE architecture and illustrates different components of the LTE network. Also ways how LTE allocating bandwidth spectrum are explained. LTE Time framing and transmission procedure are discussed in details. Finally, MIMO principles and adaptive modulation are briefly demonstrated.

3. Chapter three explains how the digital modulation pulse is shaped in different ways. And both the baseband and passband signals are illustrated mathematically. After that various LTE modulation techniques are theoretically demonstrated including BPSK, QPSK, 16-QAM and 64-QAM.

4. Chapter four demonstrates the principle of orthogonal OFDM multicarrier transmission. After that a mathematical representation of OFDM is illustrated in details. Also, the OFDM system components and processing steps are explained in details. Finally, synchronization errors effects, different frequency and timing offset methods are studied in details.

5. Chapter five illustrates the PAPR in OFDM systems and a further mathematical explanation is demonstrated. Finally, various PAPR decreasing techniques are mathematically explained in details.

6. Chapter six presents the Matlab simulation models and shows the simulation results of the OFDM system performance and the performance of its different components. All the factors that affect the OFDM system are tested and evaluated such as coding and interleaving, different constellation mapping, synchronization, PAPR reduction methods, windowing and multipath fading channel are simulated in terms of BER and reception quality.

7. Chapter seven shows the conclusion and the summary of the OFDM system simulation results. Moreover, this chapter gives the things that are to be researched further in the future.

1.3.3 Literature Review

The design of OFDM system is illustrated in [9] and [10]. And the performance of OFDM system using BPSK and QPSK is tested and evaluated in [11], adaptive modulation is evaluated in [12] and OFDM using different modulation techniques is tested in [13]. OFDM performance using M-QAM is evaluated in [14] and [15].

The hybrid PAPR decreasing method with clipping and companding is evaluated in [16] and [17]. The tangent rooting PAPR decreasing method is evaluated in [18]. Also various companding techniques are evaluated in [19] and [20]. Different PAPR methods are evaluated in [21].

The LS and MMSE channel estimators are evaluated in [22], [23] and [24]. The CFO estimation is evaluated in [25], [26] and [27]. The STO estimation is evaluated in [28], [29] and [30].

2. LTE NETWORK

For a long period of time cellular mobile communication systems play a key role in every aspect of life. Both voice calls and internet multimedia services changed our lifestyle. Voice calls dominate against data traffic because of the little growth of cellular networks traffic. In 2007 multimedia services traffic increased significantly because of the spreading of 3.5G universal mobile telecommunication service UMTS technology. As a result, the number of mobile users raised dramatically and therefore, the UMTS incapable of adopting this trend. Consequently, the demand for increasing capacity become high priority to the third-generation-partnership-project 3GPP. 3GPP made a decision to re-design and re-build both the UMTS air-interface and core-network. The new emerged design standardized as the fourth generation long term evolution 4G-LTE [31] [5]. The release 8 issued in 2008 for LTE standards [31].

2.1 LTE AECHITECTURE

LTE is simply comprised of four sections, UE user equipment refers to the mobile device, EPC evolved packet core refers to the network heart, E-UTRAN refers to the radio air interface and external services section [32]. LTE is structured from scratch to be internet protocol IP-Oriented network that provides continuous connectivity. IP-based LTE dominates in transporting data as it is only built to operate above the transport layer. IP-Multimedia-Subsystem IMS is an example of external-services that is intended to provide internet connectivity to the LTE users.

2.1.1 E-UTRAN Evolved-NodeB (eNB)

The eNB is the most complicated part of the LTE, it is implementing all radio access functions. Typically, it performs the functions of a bridging device in layer two in between the core network EPC and the UE [33]. eNB manages the radio resources and performs encoding, modulation and resource mapping. eNB communicates with another eNBs via X2 air interface, manages a connection with the UE via Uu air interface, provides communication links with the MME mobility management entity via S1-MME, and communicates with the S-GW serving gateway through S1-U. The eNB comprises of three main parts , the first part is the actual antennas that reside close to the eNB, the second part is the radio elements, that provide modulation and demodulation

processes of all transmitted and received radio signals and finally the digital signal elements that carry out all digital signal processing of all transmitted and received signals [34].

2.1.2 User Equipment UE

UE is the mobile handheld equipment which provides voice and data communications to LTE users. The UE provides connections to E-UTRAN via air interface Uu. The UE contains a separable module called USIM universal subscriber identity module. The USIM is designed to be integrated into a smart chip named UICC universal integrated circuit card [35]. USIM is responsible for establishing and authenticating the mobile user to the radio access network.

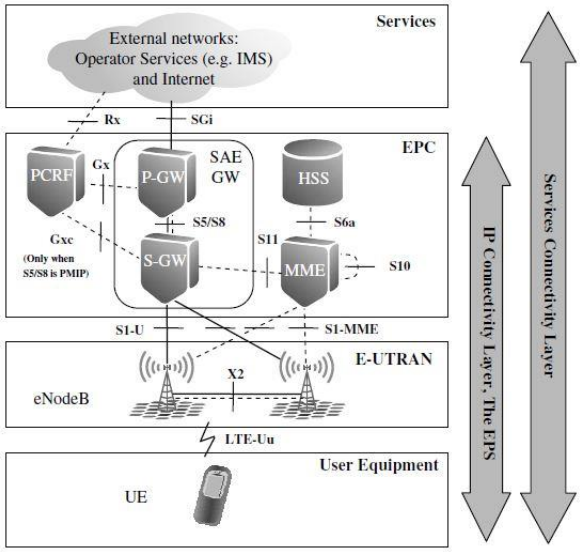

Figure 2.1: Simple LTE architecture configuration [33]

2.1.3 Mobility Management Entity MME

The MME implements all signal functions between eNBs and EPC and between core EPC network and UEs. As the MME is not part of the air interface components, therefore, MME is intended to be the main part of the EPC and carries out all control-plane signaling with eNBs and UEs. The MME is responsible for authentication and security functions [36]. MME manages mobility by keeping track of positions of all UEs exist in the coverage area. MME also administer user subscription profile. Each mobile user is assigned to one MME, and in large LTE networks multiple MMEs can be exist. MME support handovers and exchange handover-messages between two particular eNBs [37]. Figure 2.1 shows a simple LTE architecture block diagram.

2.1.4 Serving Gateway S-GW

Serving GW establishes connections and administer user data channels among eNBs and PDN-GW packet data network gateway through the S1-U, S5/S8 interfaces. PDN-GW plays a role as a gateway-router to external networks. User data channels are administered by MME and orders are sent to the S-GW through S11 interface which performs the CP signaling. In large networks there might be more than one S-GW.

2.1.5 Packet Data Network Gateway PDN-GW

PDN GW is an external gateway interface that interacts with outside networks such as the internet, IMS IP multimedia sub system evaluated as the main integration with PDN GW, the PSTN public switched telephone network another example of the outside world can PDN GW interacts with. The PDN-GW is also intended to assign UEs a specific IP-address [7]. After the UE have been authenticated by the MME the PDN-GW assigns an IP-Address to that particular user.

2.1.6 Home Subscriber Server HSS

HSS aims to the main place for storing all permanent subscriber information and user profiles that contain the specified permitted services and allowed PDN connections for each user. The HSS stores the secret key that is used for authentication process to get the authentication vectors which is preserved in AUC authentication center. HSS communicates with each MME in the whole network [33]. HSS stores the locations for each UE for each visited network.

2.1.7 Policy and Charging Resource Function PCRF

PCRF is the LTE part that is designed to control policy and charging services. PCRF manages and controls the quality of service QOS for LTE subscribers.

2.2 BANDWIDTH SPECTRUM ALLOCATION

LTE allocating bandwidth spectrum from 1.4MHz range to 20MHz range. LTE divides the available spectrum into different resource blocks RBs, each individual resource block comprises of twelve sub carriers separated by 15KHz. Therefore, the overall resource block bandwidth is 180KHz. By allocating the spectrum from 1.4MHz to 20MHz. As a result, the transmission

bandwidth is varied from 6 to 100 resource blocks among a particular carrier [8]. This mechanism of allocating the available spectrum leads to a flexible way for achieving the required spectrum.

2.3 TIME FRAMING AND TIME FREQUENCY REPRESENTATION

LTE manages data transmission in Time-Domain as a sequence of 10ms time frames. Every time frame is split into a set of ten sub frames has a length of 1ms period of time. Then every particular sub frame is split into two time slots with a length of half millisecond each. Lastly, 7 or 6 transmission symbols is stored in each time slot regarding to the length of the inserted cyclic prefix. Whether a normal CP or an extended one. The structure of LTE time framing is demonstrated in figure 2.2 and table 2.1.

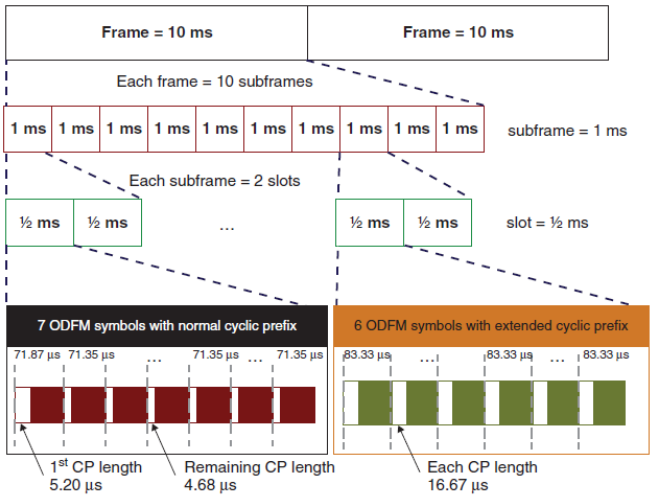

Figure 2.2: LTE time framing structure [8]

Table 2.1: LTE bandwidth allocation parameters

OFDM Down-Link Transmission Parameters with 1ms Sub-Frame and 15-KHz Spacing						
Channel Spectrum (MHZ)	1.4	3	5	10	15	20
Frequency of Samples (Fs)	1.92	3.84	7.68	15.36	23.04	30.72
FFT-Size	128	256	512	1024	1536	2048
Symbols Per Each Sub Frame	14 Normal CP			12 Extended CP		
Cyclic Prefix Length	4.7 Normal CP			5.6 Extended CP		

One of the most beneficial features of LTE is using a resource grid that maps the transmitted signal into a time-frequency-representation after coding and modulation stages. The x-axis refers to the

time that OFDM symbol belongs to. The y-axis refers to the frequency that belongs to an OFDM subcarrier. Each RB is verified as a set of resource elements REs. In normal cyclic prefix the RB contains eighty-four REs. On the contrary, in an expanded cyclic prefix each RB contains seventy-two resource elements [8].

2.3.1 Time Framing and Transmission Procedure

In LTE the smallest part can be transmitted is binary data bits zero or one. A collection of bits forms one OFDM symbol, and the total count of binary bits per OFDM symbol relies on the type of used mapping technique. The OFDM symbol refers to the term RE. Thus, seven or six OFDM symbols are combined together to form one subcarrier. 12 subcarriers form one-time slot of 0.5ms. Two-slots form one sub frame of 1ms. The created sub-frame refers to the LTE network scheduling time. In this time the eNB determines which subscribers to be queued and ordered also decides which RBs are to be assigned to which subscriber. System bandwidth determines the overall number of parallel RBs in every sub-frame. For example, in 10MHz bandwidth system, 600-subcarriers can be achieved. Therefore, a total of 50-RBs are obtained, since each RB comprises of 12-subcarriers.

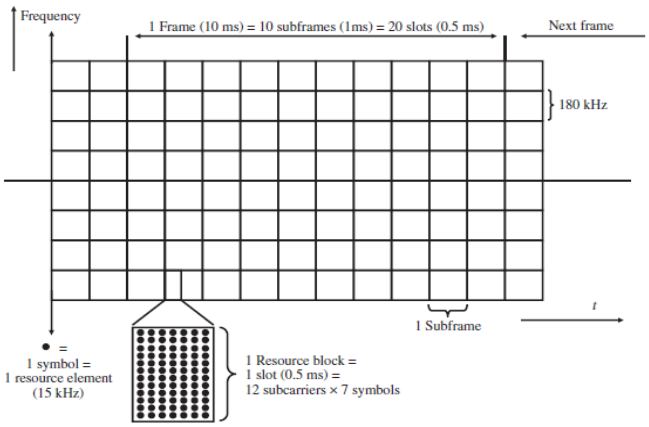

Figure 2.3: LTE resource blocks and resource grid [34]

LTE use either two ways to transmit a sub-frame, the first way DVRBs distributed virtual resource blocks or the second way LVRBs localized virtual resource blocks [34]. In LVRBs method the RBs are transmitted in a coherent way. And the eNB requests a feedback channel of narrow band from the UE to perform the scheduling of the RBs over sub carriers incapable of facing narrow band fading. On the other hand, the DVRBs method scatters the RB symbols among the available

bandwidth. The UE returns either a channel of wide band through the available bandwidth or no feedback at all. In conclusion, 10-subframes are grouped together to form an LTE-Frame. The illustration of resource blocks and the illustration of resource grid are shown in figure 2.3.

2.4 LTE MIMO BASICS AND ADAPTIVE MODULATION

In high data-rate mapping techniques such as 64-QAM where 6-bits transmitted per symbol, multi-antenna technology is used in the down-link. In the release-8 of 3GPP it is called the Multiple-Input-Multiple-Output MIMO technology. The principle of MIMO is transmitting various independent streams of data through the same radio channel simultaneously. In practice, LTE uses only two streams of data in the case of excellent channel conditions. Otherwise only one stream of data is used. At the transmitter two independent transmit hardware and two antennas are necessary, one transmits a vertical polarized signal, whether the other transmits a horizontal polarized signal [34]. The MIMO requires that both transmitted signals must be remaining independent all the way between the MIMO-Transmitter and the MIMO-Receiver. This can be obtained when the transmitted signals have reached the UE within multipath. Theoretically, the received signals gain will be doubled when using two antennas. Unfortunately, in practice the throughput gain is decreased because the occurred interference between the signals [34]. If the interference is little a high order modulation technique is used such as 64- QAM with MIMO. Otherwise, only a low order mapping scheme is applied such as 16-QAM with MIMO. According to the channel characteristic conditions. This process is called adaptive modulation in which the eNB decides how to transmit signals properly. When the distance between the transmitter and the received is short, this gives good signal to noise ratio SNR levels in which 64-QAM and MIMO would be suitable for transmission. To sum up, a modulation scheme and the usage of MIMO is changing in every millisecond depends on channel conditions. Transmission and reception diversities can be achieved by using MIMO, in which the data stream is transferred through multiple antennas using various modulation techniques. Although the UE can transmit only one data stream, the eNB can request multiple UEs to transfer signals among the same specified RB, and after that it implements MIMO to receive individually transmitted data streams. This operation is referring to the term multiuser MIMO [34].

3. LTE DIGITAL MODULATION SCHEMES

Modulation is the process of source data mapping to a signal waveform that can be transferred through an analogue channel. Which is in turn, becomes compatible with that specified channel. Since, the digital communication system represents the data source in digital format. As the source coder encodes the data into binary bits. On the other hand, the medium channel transfers only analogue signals. Therefore, the transmitter modulator makes a process of conversion from digital to analogue waveform. The analogue signal has the ability to represent one or multiple bits depending on the modulation type. And the receiver demodulator converts the received signal back into a digital waveform, the receiver recovers the original signal data bits [3]. Modulation process is typically formed by two operations baseband and passband [6]; baseband mapping modulates the source data into a low frequency baseband signal. The passband mapping transforms the high carrier frequency according to properties of the achieved baseband signal. Modulation process is required due to the limitation of making a practical transmission antennas capable of transmitting baseband signals.

3.1 BASEBAND AND PASSBAND MODULATION THEORY

The high frequency carrier can be reformed by:

$$S(t) = A(t).\cos\big(\omega ct + \emptyset(t)\big) \tag{3.1}$$

Where $A(t)$ denotes the amplitude and $\emptyset(t)$ denotes the phase and $\omega c = 2\pi fc$. The passband modulation is formed according to the variation of these three key factors amplitude, frequency and phase. As a result, several analogue modulation schemes are achieved AM, FM and PM respectively. In digital modulation the binary bits are transmitted in an analogue passband channel. The variation of carrier frequency key factors is limited to a period of time T. In T time duration a limited number of symbols can be transmitted according to the modifying of amplitude, frequency and phase of the carrier.

The process of representing binary bits into an analogue form is called shift keying. Subsequently, ASK, FSK and PSK digital modulation techniques are achieved. Passband waveform is always illustrated by using the product of both exponential functions of the baseband signal and the carrier signal [6].

$$\text{Exp}(j\,x) = \cos(x) + j \cdot \sin(x) \tag{3.2}$$

Thus, the carrier signal can be verified by:

$$s(t) = \text{Re}\left\{A(t) \cdot \text{Exp}\left(j\left(\omega ct + \varphi(t)\right)\right)\right\} \tag{3.3}$$

$$s(t) = \text{Re}\,\{A(t) \cdot \exp(j\varphi(t)) \cdot \exp(j\omega ct)\}$$

$$s(t) = \text{Re}\,\{b(t) \cdot \exp(j\omega ct)\}$$

Where: $b(t) = A(t) \cdot \exp\left(j\varphi(t)\right) = \text{baseband signal}$

$$\exp(j\omega ct) = \text{unmodulated carrier}$$

A signal is represented as a vector magnitude by using both pairs inphase (I) and quadrature (Q) parts as it is illustrated in figure 3.1 where:

$$A = \sqrt{(I^2.Q^2)} \tag{3.4}$$

$$And\ the\ phase, \theta = \arctan(\frac{Q}{I})$$

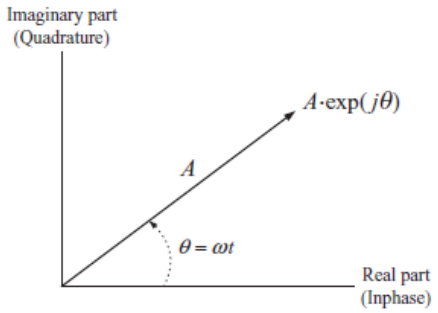

Figure 3.1: I Q signal representation

$$s(t) = sI\,(t)\cos(2\pi fct) - sQ(t)\sin(2\pi fct) \tag{3.5}$$

Where:

$$sI\,(t) = A(t)\cos\varphi(t), \quad \text{In} - \text{phase part}$$

$$sQ\,(t) = A(t)\sin\varphi(t), \quad \text{Quadrature part}$$

3.2 DIGITAL PULSE SHAPING

Digital binary data is represented by baseband waveform and every transmitted symbol has a time duration of T. Hence, the easy and more convenient way to reform sequences of binary data in baseband signal within a time domain is to perform rectangular signal shape. The rectangular shaped pulse is limited in time interval, and out of this period the signal power is zero. On the contrary, in the representation of frequency domain [38]. The signal has infinite spectrum, and the signal power is not limited. The time domain signal can be transferred to a frequency domain signal by fulfilling Fourier Transform.

$$B(f) = \int_{-\infty}^{\infty} b(t) \cdot exp(-j2\pi f\ t)dt \tag{3.6}$$

Where $b(t)$ denotes the signal in time domain. The rectangular function represents the signal in time domain. And sinc function is conversely used in frequency domain.

$$sinc(x) = \frac{\sin(\pi x)}{\pi x} \tag{3.7}$$

And vice versa. If the sinc function is used in time domain such as the Nyquist signal shape, the rectangular function is used in frequency domain. In practice, the infinite spectrum found by the rectangular shaped signal is not allowed due to the limitation of the propagation channel spectrum. Therefore, the rectangular pulse is filtered by a low pass filter. This operation converts the pulse to a shape similar to the Nyquist pulse [3]. This filtration refers to the term pulse shaping. As a consequence, any signal has limitless time duration and a limited spectrum causes ISI and a severe signal distortion can be occurred. Since, the Nyquist pulse shaping goes to zero in all periods $t = \mp KT,\ k = 0,1,2,.,.,.,$ etc. And also the ISI is measured zero in those points. If shaped pulses is moved by a constant period of integer multiplies of time duration T. Subsequently, the receiver gets the signal in the central symbol duration. If the sampling frequency is synchronized, which is in turn prevents ISI in the transmission operation [6]. Any *b(t)* time domain signal must fulfill Nyquist theory as it is shown in figure 3.2 by:

$$b(kT) = \begin{cases} A, & k = 0 \\ 0, & k \neq 0 \end{cases} \tag{3.8}$$

The b(t) is required to apply (3.7) by fulfilling the B(f) this condition:

$$\sum_{k=-\infty}^{\infty} B\left(f + \frac{k}{T}\right) = AT, |f| \leq \frac{1}{2T} \tag{3.9}$$

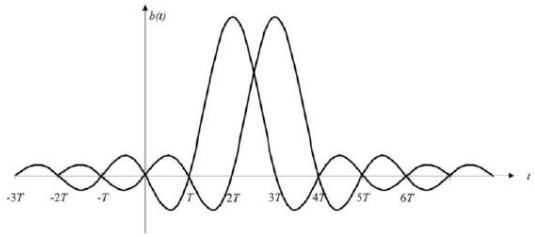

Figure 3.2: Nyquist theory [6]

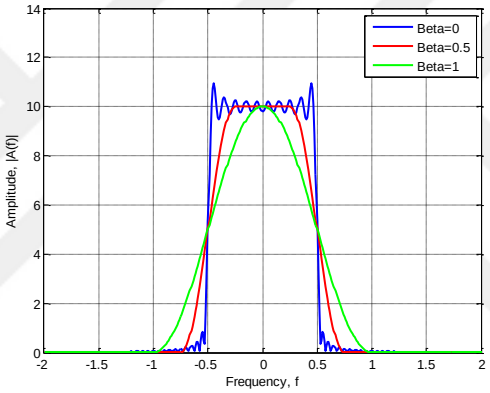

Figure 3.3: Raised cosine filter representation in frequency domain

The Nyquist theory requires perfect synchronization. In practice, the communication system uses Nyquist pulse which utilizes spectrum optimally, but unfortunately, it faces large synchronization errors. Figures 3.3, 3.4 and 3.5 illustrate the effects of raised cosine filter with the variation of β.

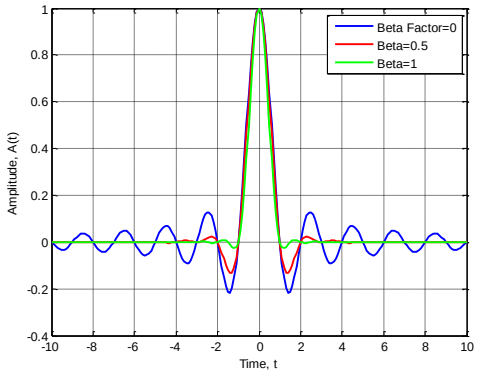

Figure 3.4: Raised cosine filter representation in time domain

To cope this issue, the receiver applies the raised cosine filter with a roll-off factor $0 \leq \beta \leq 1$.

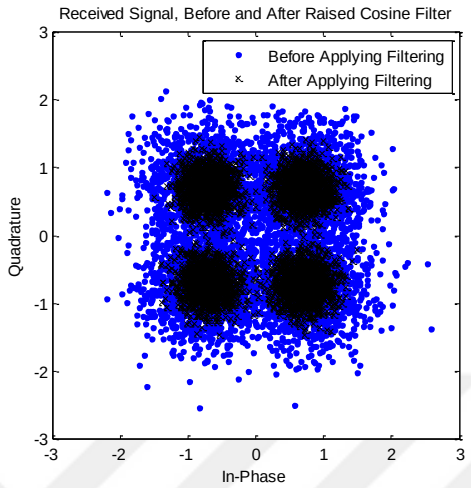

Figure 3.5: Filtering a signal using raised cosine filter

3.3 PHASE AND AMPLITUDE ENCODING

The source binary data bits are encoded either in phase or amplitude through a period of time T. The transmitted signal s(t) is modulated according to the variation of phase or frequency.

$$\mathrm{s(t)} = sI\ (t)\cos(2\pi fct) - sQ(t)\ \sin(2\pi fct) \tag{3.10}$$

Where K denotes the number of bits and equals $K = log2M$ and T denotes the symbol period and it is limited to this range $\{0 \leq t < T\}$. The components in-phase sI(t) and quadrature sQ(t) are baseband parts that are characterized by the pulse shape properties. Thus, their spectrum equals to the spectrum of pulse shape. The bandwidth B depends on the Beta factor.

$$B = Beta/T \tag{3.11}$$

Beta depends on the pulse shape type. The transmitted signal s(t) has a central frequency fc and a bandwidth of $2B$. Thus, the $s(t)$ has a spectrum of $1/T$. Consequently, the amplitude and phase are determined by the constellation point $\mathrm{Si} = (\mathrm{Si1}, \mathrm{Si2}), \mathrm{i} = 1,2,.,.,\mathrm{M}.Si$ refers to the symbol has a number of bits K equal to the log2M [39]. The received signal x(t) is defined by:

$$x(t) = sI\ (t) + jsQ(t) = (Si1 + jSi2)e(t) \tag{3.12}$$

Where $e(t)$ denotes the pulse shape type.

3.3.1 ASK Modulation

ASK processes the principle of switching the carrier signal high and low levels using unipolar binary bits. ASK is determined as the first modulation scheme that is used afterwards analogue modulation techniques. ASK also refers to the term on-off keying OOK. ASK codes binary stream on the carrier signal according to the amplitude variation of the carrier wave. The ASK modulated signal is defined by:

$$\mathrm{s(t)} = \mathrm{Ac.\,m(t).\cos(\omega ct + \emptyset)} \tag{3.13}$$

Where $\mathrm{Ac.\,m(t)}$ denote the complex envelope $g(t)$. Or in the complex definition by:

$$\mathrm{s(t)} = \mathrm{Ac.\,m(t).\,[Cos(2\pi fct + \emptyset) + iSin(2\pi fct + \emptyset)]} \tag{3.14}$$

Where $\mathrm{m(t)}$ denotes the baseband signal and equals to $m(t) = \{0,1\}$. Figure 3.6 illustrates the form of the ASK modulated signal.

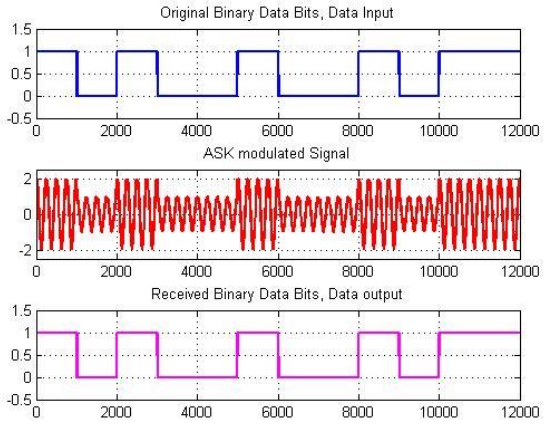

Figure 3.6: Modulation of ASK scheme

In ASK only cosine wave is modulated which refers to the In-Phase component. ASK modulated signal can be detected coherently by product detector or non-coherently by envelope detector [38]. Product detector achieves best results of receiving an ASK modulated signal mixed with noise regarding to the BER. ASK transmission spectrum equals to the double of baseband spectrum. If the received signal is filtered by a raised cosine filter, then the baseband spectrum B is defined by:

$$B = \frac{1}{2}(1 + beta)R \tag{3.15}$$

Where $beta$ denotes the roll-off factor and R denotes the bit rate. Thus, the total transmission spectrum BT is defined by:

$$BT = (1 + Beta)R \tag{3.16}$$

3.3.2 PSK Modulation

PSK modulation variates the phase of the carrier signal according to the source data binary bits. Thus, the binary data bits are encoded by comprising the phase of the carrier signal. PSK is widely used that is because of its immunity to noise. The transmitted PSK signal is identified by:

$$si\,(t) = gTx(t)\cos(\omega ct\ +\ \emptyset i\,) \tag{3.17}$$

Where $gTx(t)$ denotes the pulse shape filter impulse response and $\{i = 1,.,.,M = 2^k\}$ where M denotes the number of phase changes. And $\emptyset i$ is defined by:

$$\emptyset i = \frac{2\pi(i-1)}{M} \tag{3.18}$$

Also, PSK signal can be defined by:

$$si(t) = Re\left\{gTx(t)e^{\frac{j2\pi(i-1)}{M}}e^{j2\pi fct}\right\}, \qquad 0 \le t \le T \tag{3.19}$$

$$si(t) = gTx.cos\left[2\pi fct + \frac{2\pi(i-1)}{M}\right]$$

$$si(t) = gTx.cos\left[\frac{2\pi(i-1)}{M}\right]cos2\pi fct - gTx.sin\left[\frac{2\pi(i-1)}{M}\right]sin2\pi fct$$

As a result, the symbols or constellation dots $(\mathrm{Si1}, \mathrm{Si2})$ can be calculated by:

$$Si1 = A.\mathrm{Cos}(\frac{2\pi(i-1)}{M}) \tag{3.20}$$

$$Si2 = A.\mathrm{Sin}(\frac{2\pi(i-1)}{M})$$

BPSK and QPSK are examples of LTE-OFDM modulation schemes [40]. Figure 3.7 illustrates the form of the PSK modulated signal.

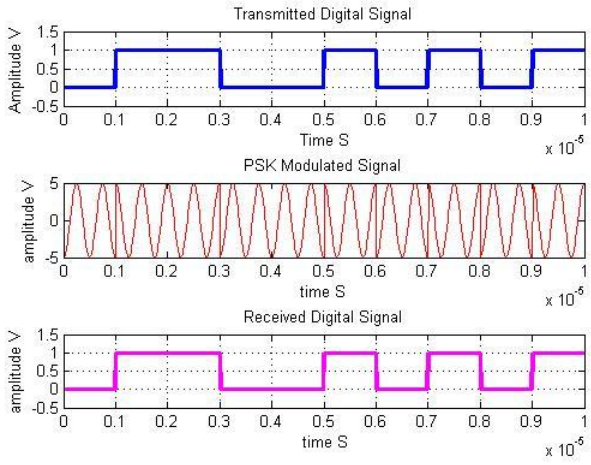

Figure 3.7: Modulation of PSK scheme

3.3.3 BPSK Modulation

BPSK is evaluated as the simplest mapping scheme. BPSK changes the phase of the consistent amplitude of the carrier signal regarding to the pair of possible data source binary bits zero 0 and one 1. Typically, the phase is switched by 180° between them. Considering a carrier signal with an amplitude of A, a symbol time T and energy for each bit Eb. Where the average power is:

$$p = \frac{A^2}{2}, \qquad A = \sqrt{2p} \tag{3.21}$$

$$Eb = p.T \ = \frac{1}{2}A^2T$$

Thus, the representation of BPSK transmitted signal as it is shown in figure 3.8 is defined by:

$$s(t) = \sqrt{\frac{2Eb}{T}}\cos(2\pi fct + \emptyset), \qquad 0 \le t \le T\ (binary\ bit\ 1) \tag{3.22}$$

$$s(t) = \sqrt{\frac{2Eb}{T}}\cos(2\pi fct + \pi + \emptyset), \qquad 0 \le t \le T\ (binary\ bit\ 0)$$

$$= -\sqrt{\frac{2Eb}{T}}\cos(2\pi fct + \emptyset), \qquad 0 \le t \le T\ (binary\ bit\ 0)$$

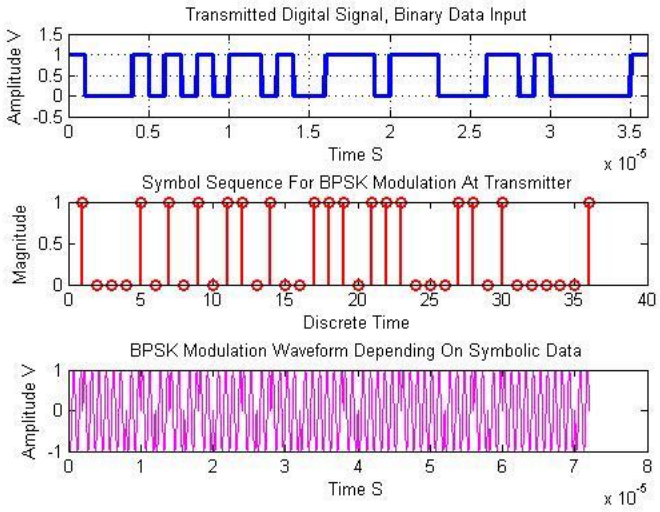

Figure 3.8: Modulation of BPSK scheme

If the source binary data $(0, 1)$ are represented by $m1$ and $m2$ respectively. Therefore, the binary data signal $m(t)$ can be entered to the transmitted BPSK signal as:

$$s(t) = m(t)\sqrt{\frac{2Eb}{T}}\cos(2\pi fct + \emptyset) \tag{3.23}$$

$$s(t) = \sqrt{\frac{2Eb}{T}}\cos\big(2\pi f_C t + \pi(1 - m(t))\big); \qquad m(t) \in \{0,1\}$$

The BPSK transmitted signal can be defined in complex way by:

$$s(t) = \sqrt{\frac{2Eb}{T}}\ e^{(2\pi fct++m(t)+\emptyset)} \tag{3.24}$$

The constellation diagram of BPSK is shown in figure 3.9. The BPSK baseband is defined by:

$$s_m(t) = \cos(\pi m);\ m \in \{0,1\} \tag{3.25}$$

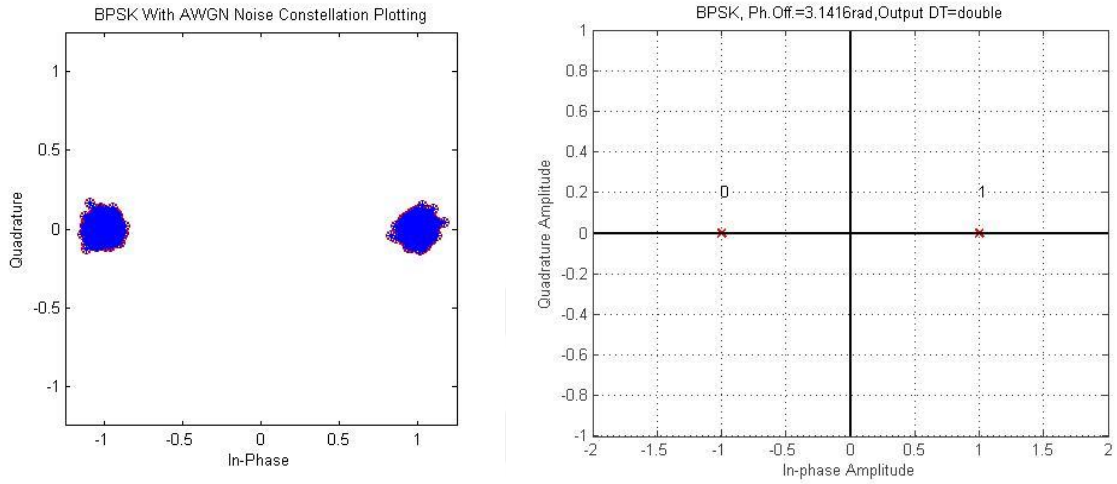

Figure 3.9: BPSK constellation diagram

BPSK can be implemented in two ways, the first way is performed similar to the phase modulation. The phase is shifted according to the source binary data to $\frac{\pi}{2}$ or $-\frac{\pi}{2}$. The second way as PAM modulation in which the rectangular pulse shaping and Nyquist pulse shaping with amplitude of binary 1 are used [3]. As the rectangular pulse shape has limitless spectrum it is difficult to be applied in practical situations. Thus, raised cosine filter is used instead. The bit rate *R* in BPSK is one bit per symbol duration of T. The constellation points of BPSK employ only the x-axis with two dots have the values $\sqrt{\frac{2Eb}{T}}$ or $-\sqrt{\frac{2Eb}{T}}$ depending on the input bit 0 or 1.

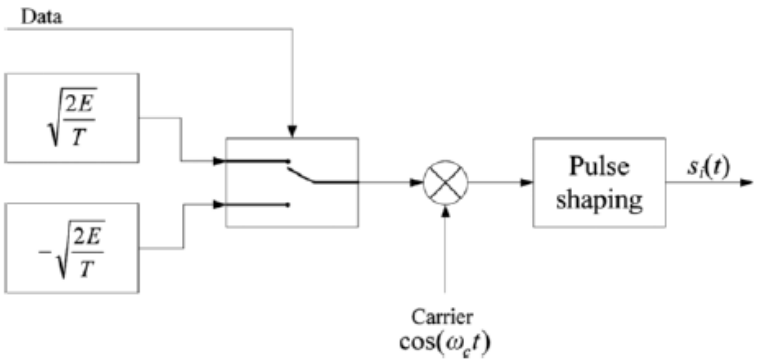

Figure 3.10: Modulator of BPSK scheme [6]

At the BPSK demodulator a synchronous detector must be used to coherently detect the original signal from the BPSK modulated signal. Therefore, the used phase and frequency of the carrier signal in the BPSK demodulator must synchronize with the carrier that is used at the transmitter [11]. Figures 3.10 and 3.11 demonstrate the block diagrams of BPSK modulator and de-modulator.

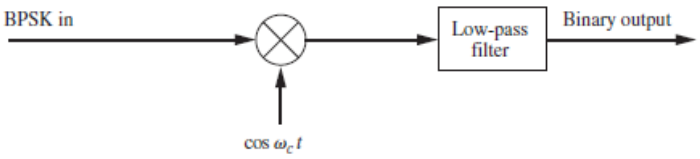

Figure 3.11: Demodulator of BPSK scheme [6]

3.3.4 QPSK Modulation

QPSK mapping scheme obtains the double of bandwidth efficiency achieved by BPSK. Two binary bits are transmitted in every symbol with a time duration of T on both in-phase and quadrature signal components. The phase of the carrier signal is shifted between four equally spaced measurements such as $\{\frac{\pi}{4}, \frac{3\pi}{4}, \frac{5\pi}{4}, \frac{7\pi}{4}\}$ or $\{0, \frac{\pi}{2}, \pi, \frac{3\pi}{2}\}$ where each phase measurement refers to a particular pair of binary bits. The QPSK transmitted signal is defined by:

$$s(t) = \sqrt{\frac{2Eb}{T}} \cos\left(2\pi f_c t + (\mathrm{i}-1)\frac{\pi}{2} + \emptyset\right), \qquad 0 \le t \le T, \qquad i = \{1,2,3,4\} \tag{3.26}$$

Where T denotes the symbol period that equals to double bits time duration. By applying the trigonometric property to (3.26) the QPSK signal is identified by:

$$s(t) = \sqrt{\frac{2Eb}{T}} \cos\left(2\pi f_c t + (\mathrm{i}-1)\frac{\pi}{2}\right) - \sqrt{\frac{2Eb}{T}} sin\left(2\pi f_c t + (\mathrm{i}-1)\frac{\pi}{2}\right) \tag{3.27}$$

The two components I(t),Q(t) over the period $0 \le t \le T$ are referring to the basis functions:

$$I(t) = \sqrt{\frac{2}{T}} \cos(2\pi f_c t) \quad \text{and} \quad Q(t) = \sqrt{\frac{2}{T}} sin(2\pi f_c t) \tag{3.28}$$

Therefore, the QPSK transmitted signal as it is shown in figure 3.14 is defined by:

$$s(t) = \sqrt{Eb}.\mathrm{Cos}\left((\mathrm{i}-1)\frac{\pi}{2}\right)I(t) - \sqrt{Eb}.Sin\left((\mathrm{i}-1)\frac{\pi}{2}\right)Q(t) \tag{3.29}$$

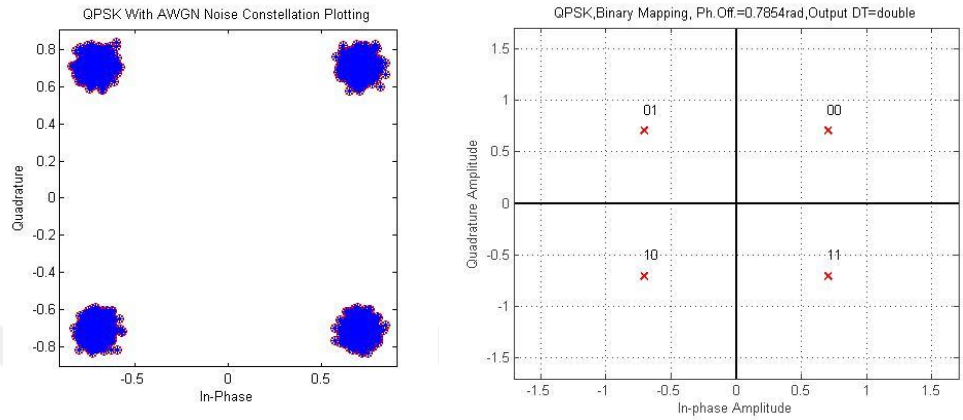

Figure 3.12: QPSK constellation diagram

Thus, By considering the use of rectangular pulse shaping theory the constellation diagram of QPSK is formed by $2X2$ dimensional array. Therefore, four values are contained within the constellation block which refer to the phase shifts of the carrier signal. They are possible to be $0°, 90°, 180°, \text{and } 270°$ or $45°, 135°, 225°, \text{and } 315°$. The constellation diagram of QPSK is shown in figure 3.12.

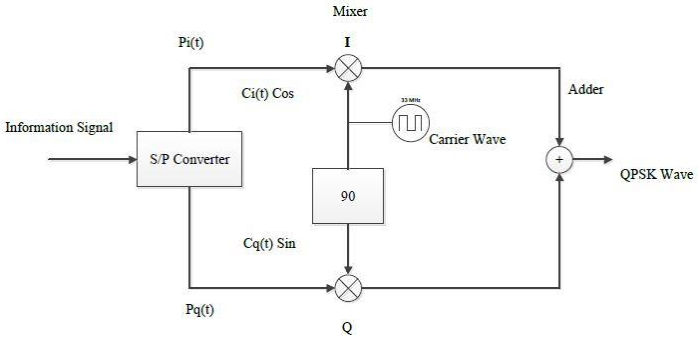

Figure 3.13: Modulator of QPSK scheme [11]

From the constellation block of QPSK mapping, the distance between two adjacent dots equals to $\sqrt{2Es}$, where $Es = 2Eb$ since each QPSK symbol consists of two bits. Therefore, the distance becomes equal to $2\sqrt{Eb}$. The QPSK receiver filters the undesirable noise and then divides the filtered output into two parts. Each part is passed through coherent demodulator. Finally, the original binary data bits are recovered [41].

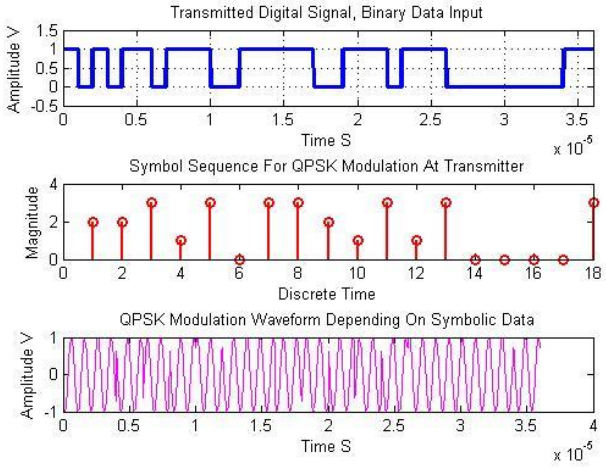

Figure 3.14: Modulation of QPSK scheme

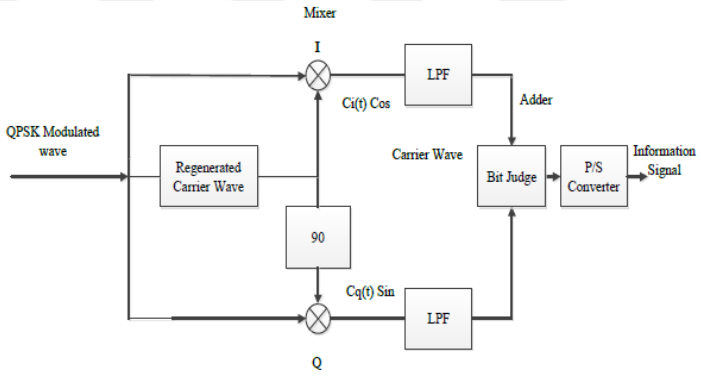

Figure 3.15: Demodulator of QPSK scheme [11]

Figures 3.13 and 3.15 show block diagrams of QPSK modulator and de-modulator respectively.

3.3.5 QAM Modulation

QAM signal mapping modulates the source binary data bits regarding to the variation of both phase and amplitude. To be specific QAM can be determined as an extension to QPSK, as the QAM modulated signal is formed in both in-phase and quadrature parts but the distribution of constellation points in this case is covering all the constellation block as square form which is different from QPSK circular form [6]. This squared constellation diagram is obtained by multiple amplitude variations for each In-phase and Quadrature parts. Therefore, QAM mapping can be called multi-level modulation technique [6]. M-QAM is an efficient signal mapping comparing to other mapping schemes due to the resulted spectral efficiency.

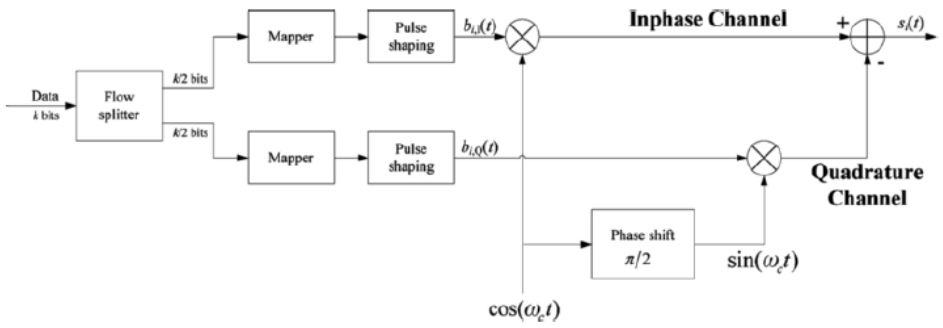

Figure 3.16: Modulator of QAM scheme [6]

The M-QAM transmitted signal as it shown in figure 3.17 is defined by:

$$Si(t) = \sqrt{\frac{2Emin}{T}}\, ai.\cos(2\pi fct) + \sqrt{\frac{2Emin}{T}}\, bi.\sin(2\pi fct) \tag{3.30}$$

$$0 \le t \le T, \qquad i = \{1,2,\ldots\ldots,M\}$$

Where $Emin$ denotes the signal energy that has the minimum amplitude. And (ai, bi) denote the matrix dimension integers that refer to particular locations. The ith point coordinates are $ai\sqrt{Emin}\ and\ bi\sqrt{Emin}$ and (ai, bi) which is an item of DxD matrix that is given by:

$$\{ai, bi\} = \begin{bmatrix} (-D+1, D-1) & (-D+3, D-1) & .. & (D-1, D-1) \\ (-D-1, D-3) & (-D+3, D-3) & .. & (D-1, D-3) \\ \vdots & \vdots & :: & :: \\ (-D+1, -D+1) & (-D+3, -D+1) & .. & (D-1, -D+1) \end{bmatrix} \tag{3.31}$$

Where $D = \sqrt{M}$ and $M = 2^k$ and K denotes the number of bits per symbol $K = log2(M)$. The low pass filter at the demodulator is used to dismiss undesirable high frequency terms. QAM is a signaling in which the source binary data is divided into two binary streams $K/2$ which consists of even and odd data symbols refer to the In-phase and Quadrature parts respectively. Each binary data stream is independently mapped. And after that, they are summed together and transmitted over the channel.

The M-QAM receiver splits the received signal into two In-phase and Quadrature streams, then each stream is passed through a LPF and finally the original binary bits are retrieved. M-QAM is implemented in various levels such as 16-QAM, 64-QAM and 256-QAM. But only 16-QAM and

64-QAM mapping schemes are used with LTE network. Two kinds of mapping are used in M-QAM gray mapping and binary mapping. Figures 3.16 and 3.17 show block diagrams of QAM modulator and QAM de-modulator respectively.

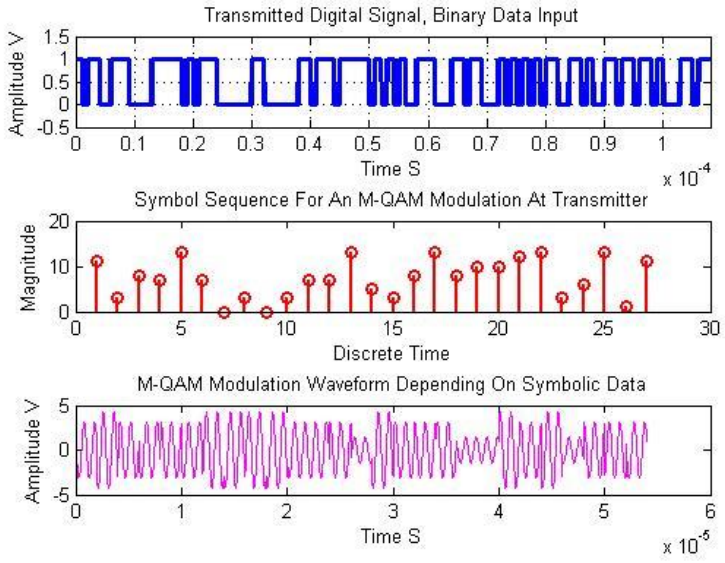

Figure 3.17: Modulation of 16-QAM scheme

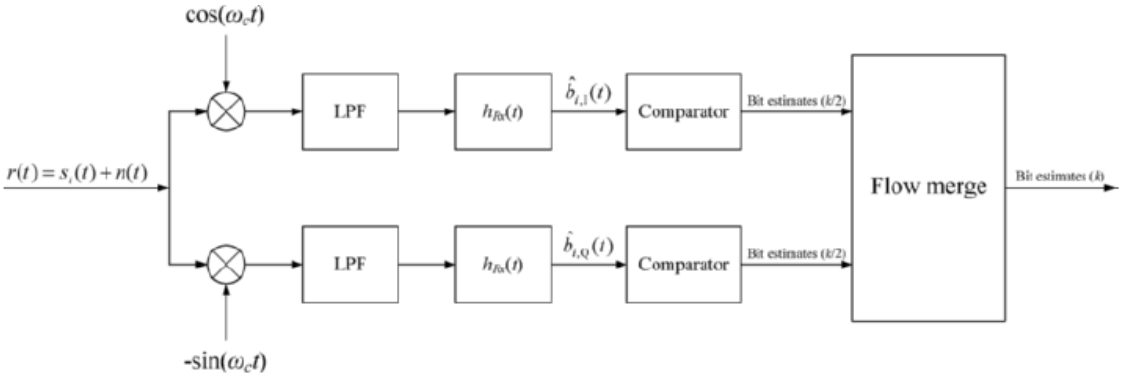

Figure 3.18: Demodulator of QAM scheme [6]

3.3.5.1 16-QAM

In 16-QAM source binary bit stream is grouped into 4-bits to create one symbol and total symbols are represented as 16-symbol. The constellation diagram of 16-QAM is shown in figure 3.19.

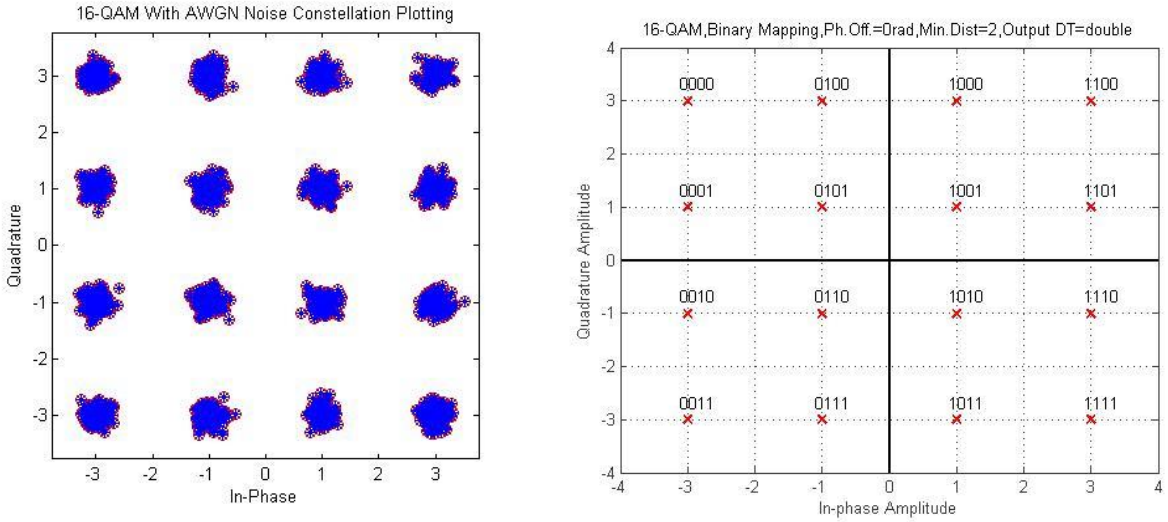

Figure 3.19: 16-QAM constellation diagram

3.3.5.2 64-QAM

In 64-QAM source binary bit stream is grouped into 6-bits to represent one symbol and finally the total symbols are represented as 64-symbol block. The constellation diagram of 16-QAM is shown in figure 3.20.

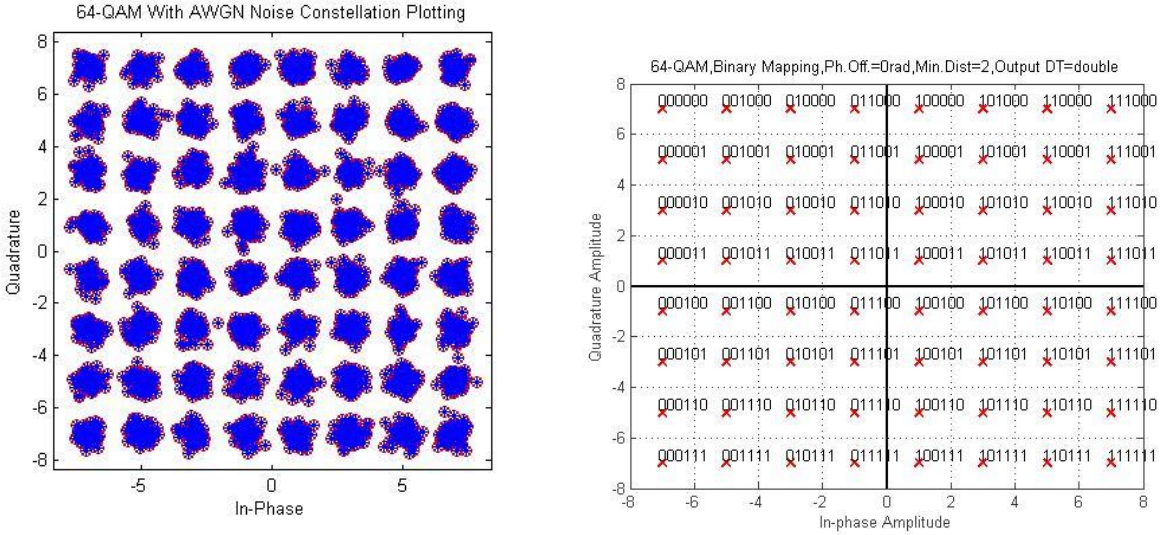

Figure 3.20: 64-QAM constellation diagram

4. LTE-OFDM

LTE implements OFDM technology from scratch where OFDM is used in downlink stream and SC-FDMA in uplink stream. LTE air interface is complemented by OFDMA which provides user diversity within the system. OFDM deploys the principle of orthogonality of transmitting multi-carrier signals. The raised bandwidth is achieved for LTE, the high number of low rate sub carriers are used [42].

4.1 TRANSMISSION OF MULTI-CARRIER THEOTY

The principle of multicarrier transmission such as FDMA as shown in figure 4.1 is splitting the single wideband carrier spectrum into multiple sub narrow channels. Every sub channel is assigned to a particular user [43]. This method overcomes the selectivity of frequency of the propagation channel occurs when using the single carrier. As the narrow channels become flat fading instead of selective fading ones. And therefore, the ISI will cause change to only one or two of the sub channels. The disadvantage of FDMA multicarrier transmission is that it requires guard intervals positioned between the sub channels which reduce the spectral efficiency [44].

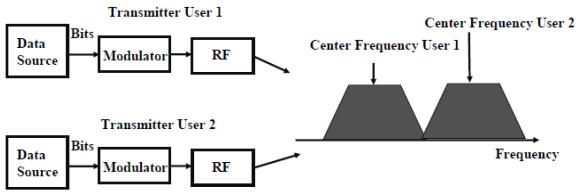

Figure 4.1: Transmission of multicarrier principle (FDMA) [33]

By considering i^{th} subcarrier and the data transmitted on the i^{th} subcarrier is xi, the modulated signal for each subcarrier is identified by:

$$si(t) = xi.g(t).e^{j2\pi fit} = xi.g(t).e^{j2\pi\frac{B}{N}it} \tag{4.1}$$

$$si(t) = xi.g(t).\cos(2\pi fit + \emptyset i)$$

Where f denotes the center frequency of the i^{th} subcarrier and N denotes the number of subcarriers and $g(t)$ denotes the pulse shape. Hence, there are N data streams as xi is the i^{th} data stream. The transmitted composite modulated signal of all subcarriers are calculated by:

$$s(t) = \sum_{i}^{N-1} si(t) = \sum_{i}^{N-1} xig(t).e^{j2\pi\frac{B}{N}it} = \sum_{i}^{N-1} xig(t).e^{j2\pi fit} \tag{4.2}$$

$$s(t) = \sum_{i}^{N-1} xig(t).\cos(2\pi fit + \emptyset i)$$

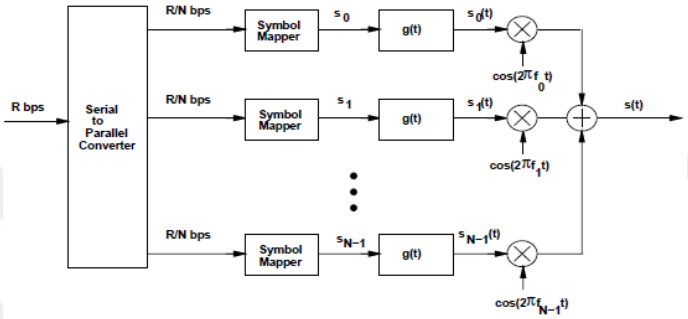

Figure 4.2: Principle of multicarrier system [39]

Therefore, a bank of modulators is used as shown in figure 4.2, one modulator for each subcarrier. Then the transmitted signal is the sum of these modulators. By demodulating each data stream coherently with $e^{j2\pi flt}$ at N/B corresponding subcarrier. The demodulated signal is calculated by:

$$yi(t) = \int_{0}^{N/B} si(t).e^{-j2\pi flt}\,dt \tag{4.3}$$

$$y(t) = \int_{0}^{N/B} s(t).e^{-j2\pi flt}\,dt$$

$$y(t) = \sum_{l}^{N-1} \int_{0}^{N/B} \left(xig(t).e^{j2\pi fit}\right).e^{-j2\pi flt}\,dt$$

Where l denotes the l^{th} subcarrier. The rectangular window of time associated with the detection of multicarrier signal is N/B which is the integration period. Hence, multicarrier system transmits N symbols using N subcarriers in time period of N/B. The symbol rate equals to B. As can be seen that the single carrier symbol rate is equal to multicarrier symbol rate, which equals to B.

4.2 OFDM MULTICARRIER THEOTY

The OFDM multicarrier system as shown in figure 4.3 is similar to the conventional multicarrier transmission except that the sub channels are overlapping among each other with no interference due to the orthogonality. The orthogonality is achieved by replacing The bank of modulators at the transmitter by a bank of IFFT operations and by changing the demodulators at the receiver by a set of FFT operations. As a result, the spectral efficiency is increased and the system becomes capable of transmitting higher data rates.

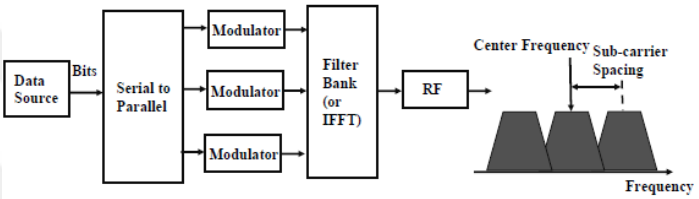

Figure 4.3: Principle of OFDM multicarrier [33]

4.2.1 Principle of Orthogonality

In conventional multicarrier transmission systems such as FDMA the sub carriers are separated by a long frequency spacing. As a consequence, that method wastes spectral efficiency. Fortunately, the spacing efficiency can be increased by overlapping the sub carriers in an orthogonal way in which the interference between them is avoided at all [45].

The principle of orthogonality of a set of complex signals $\{e^{j2\pi fit}\}\ \begin{matrix} i = N-1 \\ i = 0 \end{matrix}$ with a symbol of period T that forming OFDM multi subcarriers at different center frequency $fi = i/T$ values. With the condition of $0 \leq t \leq T$ is satisfied. These sub carriers are to be called orthogonal if the result of the integration at their fundamental time period is equal to zero [46]. That can be defined by:

$$Si(t) = \frac{1}{T}\int_0^T e^{j2\pi fit}.e^{-j2\pi flt}dt = \frac{1}{T}\int_0^T e^{j2\pi\frac{i}{T}t}.e^{-j2\pi\frac{l}{T}t}dt \tag{4.4}$$

$$Si(t) = \frac{1}{T}\int_0^T e^{j2\pi\frac{i-l}{T}t}\,dt = \begin{Bmatrix} 1, & i = l \\ 0, & else\ where \end{Bmatrix}$$

By taking various samples at a time period of $t = \frac{nT}{N} = nTsa$, where Tsa is the sampling time. Thus, equation (4.4) can be identified in discrete time by:

$$S(t) = \frac{1}{N}\sum_{n=0}^{N-1}\int_0^T e^{j2\pi\frac{i}{T}t}.e^{-j2\pi\frac{l}{T}t}\,dt = \frac{1}{N}\sum_{n=0}^{N-1}\int_0^T e^{j2\pi\frac{i\,nT}{T\,N}}.e^{-j2\pi\frac{l\,nT}{T\,N}}\,dt \tag{4.5}$$

$$S(t) = \frac{1}{N}\sum_{n=0}^{N-1}\int_0^T e^{j2\pi\frac{(i-l)}{N}n}\,dt = \begin{Bmatrix}1, & i = l\\ 0, & else\ where\end{Bmatrix}$$

This orthogonality condition must be satisfied in an OFDM system in order to avoid ISI interference between sub channel streams.

4.3 MATHEMATICAL REPRESENTATION OF OFDM

The main idea of OFDM system is dividing a high rate bit stream into various parallel sub bit streams overlapping with each other and never interfere due to the orthogonality. This methodology enables the transmitted symbol duration to be increased and therefore, exceeds the frequency dispersive channel time period. As a result, ISI is minimized to the lowest limits and in some channel conditions is eliminated at all. In a mathematical way, the bit stream is mapped by a complex signal mapping schemes such as BPSK, QPSK and QAM. Therefore, the mapped signal is represented by:

$$Xi(t) = Ai(t).e^{j(2\pi fit+\emptyset i(t))} \tag{4.6}$$

$$Xi(t) = Ai(t).\cos\big(2\pi fit + \emptyset i(t)\big) + jAi(t).\sin\big(2\pi fit + \emptyset i(t)\big)$$

$$Xi(t) = I(t) + jQ(t)$$

Where Ai denotes the amplitude, $\emptyset i$ denotes the phase of the carrier, $I(t)$ denotes the inphase real part and $Q(t)$ denotes the quadrature imaginary part.

4.3.1 Mathematical Principle of OFDM Modulator

OFDM modulator maps the binary bit stream into series of complex QAM or PSK integer symbols that are divided into parallel N symbol streams using a serial to parallel inverter. Each N block of

symbols are implemented by a particular subcarrier and each symbol has a time period of T [46]. By supposing B is the total OFDM signal bandwidth of N sub channels. Each sub channel is allocated bandwidth equals to $\Delta f = B/N$ which is the subcarrier spacing frequency for $(i = 0,1,2, \dots, N-1)$. And therefore each symbol period $T = 1/\Delta f = N/B$. Each subcarrier has a frequency that is calculated by $fi = i.\Delta f = i(B/N) = i/T$.

Supposing the symbols are mapped by a mapping scheme such as QAM. This defines the pulse shaping basis signal by:

$$\varphi(t) = \begin{Bmatrix} \frac{1}{\sqrt{T}}.e^{j2\pi fit} & where\ 0 \le t \le T,\ \ for\ i = 0,1,2,3, \dots\dots, (N-1) \\ 0 & else\ where \end{Bmatrix} \tag{4.7}$$

Since it is a normalized signal at the frequency fi. According to the orthogonality characteristics. Therefore, it can be illustrated by:

$$\{\varphi(t) = \varphi i(t), \varphi l(t)\} = \int_{-\infty}^{\infty} \frac{1}{\sqrt{T}}.e^{j2\pi fit}.\frac{1}{\sqrt{T}}.e^{j2\pi flt}\, dt \tag{4.8}$$

$$\{\varphi(t) = \varphi i(t), \varphi l(t)\} = \frac{1}{T}\int_{-\infty}^{\infty} e^{j2\pi(fi-fl)t}\, dt$$

$$\{\varphi(t) = \varphi i(t), \varphi l(t)\} = \begin{Bmatrix} \frac{1}{T}\int_0^T e^{j2\pi t(0)}\, dt. & where\ i = l \\ \frac{1}{T}\int_0^T e^{j2\pi t(fi-fl)}\, dt. & where\ i \ne l \end{Bmatrix}$$

$$\{\varphi(t) = \varphi i(t), \varphi l(t)\} = \begin{Bmatrix} \frac{1}{T}\int_0^T e^{j2\pi t(0)} = 1. & where\ i = l \\ \frac{1}{T}\int_0^T e^{j2\pi t(fi-fl)} = 0. & where\ i \ne l \end{Bmatrix}$$

Thus, the orthogonality is achieved between N sub channels. As a consequence, the OFDM signal is comprised of orthogonal vectors represent the symbols of subcarriers [47]. By supposing that $\{Xs(i,k), Xs(i,l)\}$ representing complex symbol for k^{th} MQAM symbol at i^{th} subcarrier. The transmitted OFDM baseband symbol is defined by:

$$Sk(t) = \sum_{i=0}^{N-1} Xs(i,k).\varphi i(t - KT)\,, \qquad KT \le t \le KT + nTsa \tag{4.9}$$

$$Sk(t) = \frac{1}{\sqrt{N}} \sum_{i=0}^{N-1} Xs(i,k).e^{j2\pi fit}\,, \qquad 0 \le t \le T$$

Where $1/\sqrt{N}$ is the normalizing factor and $Xs(i,k)$ is the k^{th} MQAM symbol. Hence, the transmitted passband signal is defined by:

$$S(t) = \sum_{k=-\infty}^{\infty} Sk(t)_{,,} \qquad 0 \le t \le T \tag{4.10}$$

$$S(t) = \sum_{k=-\infty}^{\infty} \frac{1}{\sqrt{N}} \sum_{i=0}^{N-1} Xs(i,k).\varphi i(t - KT)$$

Due to the propagation channel has response of infinite impulse all other symbols have to contribute to the present symbol. Therefore, the OFDM baseband and passband transmitted signals can also be illustrated in continuous time respectively by:

$$Sk(t) = \textstyle\sum_{i=0}^{N-1} Xs(i,k).e^{j2\pi fi(t-kT)}\,,\ 0 \le t \le T \quad \text{and} \tag{4.11}$$

$$S(t) = RE\left\{\frac{1}{T}\right\} \sum_{k=-\infty}^{\infty} \left\{\sum_{i=0}^{N-1} Xs(i,k)\,.\,e^{j2\pi fi(t-kT)}\right\}, \qquad 0 \le t \le T$$

The continuous OFDM complex signal can be represented in discrete time form by sampling at $t = kT + nTSa$ where Tsa denotes the sampling frequency $Tsa = T/N$. The generated final discrete OFDM signal by IFFT algorithm is identified by:

$$S(n) = \sum_{i=0}^{N-1} Xs(i,k)\,.\,e^{j2\pi in/N}\,, \qquad n = 0,1,2,3,\ldots,(N-1) \tag{4.12}$$

$$S(n) = \frac{1}{\sqrt{N}} \sum_{i=0}^{N-1} Xs(i,k)\,.\,e^{j2\pi in/N}\,, \qquad \text{after power normalization by } 1/\sqrt{N}$$

4.3.2 Mathematical Principle of OFDM Demodulator

The received OFDM symbol for the k^{th} data symbol at i^{th} subcarrier is defined by:

$$Yk(t) = \sum_{i=0}^{N-1} Xs(i,k).e^{j2\pi fi(t-kT)}, \qquad kT < t \leq kT + nTsa \tag{4.13}$$

The transmitted symbol $X(i,k)$ can be recovered at $l^{th}, l = 0\ to\ (N-1)$ due to the orthogonality characteristics by:

$$Yk(i) = \frac{1}{T}\int_{-\infty}^{\infty} Yk(t).e^{-j2\pi ifi(t-kT)}\ dt \tag{4.14}$$

$$Yk(i) = \frac{1}{T}\int_{-\infty}^{\infty}\left\{\sum_{l=0}^{N-1} Xs(l,k).e^{j2\pi fl(t-kT)}\right\}.e^{-j2\pi fi(t-kT)}\ dt$$

$$Yk(i) = \sum_{l=0}^{N-1} Xs(l,k)\left\{\frac{1}{T}\int_{-\infty}^{\infty} e^{j2\pi(fl-fi)(t-kT)}\ dt\right\} = Xs(i,k)$$

By supposing the $\{Yk(n), \text{where}\ n = 0\ to\ (N-1)\}$ is the instance samples of the OFDM received symbol $yk(t)$ at the period $t = kT + nTsa$ at the integration window can be represented in discrete form by:

$$Yk(i) = \sum_{n=0}^{N-1} yk(n).e^{j2\pi in/N} \tag{4.15}$$

$$Yk(i) = \sum_{n=0}^{N-1}\left\{\frac{1}{N}\sum_{l=0}^{N-1} Xs(l,k).e^{j2\pi ln/N}\right\}.e^{-j2\pi in/N}$$

$$Yl(i) = \frac{1}{N}\sum_{n=0}^{N-1}\sum_{l=0}^{N-1} Xs(l,k).e^{j2\pi(l-i)n/N} = Xs(i,k)$$

Where $Xs(i,k)$ is the original OFDM symbol and this process can be implemented efficiently by applying IFFT algorithm at the OFDM demodulator.

4.3.3 Mathematical Principle of AWGN OFDM Demodulator

By supposing that the channel is AWGN the received signal with i^{th} subcarrier is defined by:

$$Yk(t) = Sk(t) + n(t) \tag{4.16}$$

Where $n(t)$ is the associated noise within the received signal. This received signal can be demodulated after correlation with a matched filter $\varphi i^*(t)$ according to the orthogonal characteristics. The result will be {1 when $i = l$ and 0 when $i \neq l$}. Finally, the l^{th} symbol can be recovered at the i^{th} subcarrier by:

$$\overline{Xs}(i,k) = \int_0^T Yk(t).\varphi i^*(t)\, dt \tag{4.17}$$

$$\overline{Xs}(i,k) = \int_0^T [Sk(t) + n(t)].\varphi i^*(t)\, dt$$

$$\overline{Xs}(i,k) = \int_0^T [\sum_{l=0}^{N-1} Xs(l,k).\varphi l(t).\varphi i^*(t)\, dt + \int_0^T \varphi i(t).n(t)\, dt$$

$$\overline{Xs}(i,k) = \sum_{l=0}^{N-1} Xs(l,k) \int_0^T Xl(t)\, Xi^*(t)\, dt + n(t)$$

$$\overline{Xs}(i,k) = \sum_{l=0}^{N-1} Xs(l,k) \int_0^T \varphi l(t)\, \varphi i^*(t)\, dt + n(t)$$

$$\overline{Xs}(i,k) = Xs(i,k) + n(t)$$

Where $Xs(i,k)$ denotes the original OFDM symbol.

4.3.4 Mathematical Principle of Multipath OFDM Demodulator

By supposing that the OFDM signal is passed through a multipath fading channel. Thus, the transmitted k^{th} symbol with i^{th} subcarrier OFDM signal is defined by:

$$Sk(t) = \sum_{i=0}^{N-1} Xk(i) \cdot e^{j2\pi fi(t-kT)}, \qquad kT \le t \le kT + nTsa \tag{4.18}$$

Where $Xk(i)$ is a QAM symbol and Tsa is the sampling frequency. and $Hk(t)$ is the channel impulse response. The received signal that is passed via multipath channel is identified by:

$$Yk(t) = Sk(t) * Hk(t) + N(t), \qquad kT \le t \le kT + nTsa \tag{4.19}$$

$$Yk(t) = \int_0^{\infty} Hk(\tau).Sk(t-\tau)\, dt + N(t)\ , \qquad kT \le t \le kT + nTsa$$

Where $N(t)$ denotes the added AWGN noise, by applying a sampling rate of $nTsa = nT/N$. Therefore, the received signal can be formed in discrete time by:

$$Yk(n) = Sk(n) * Hk(n) + N(n) \tag{4.20}$$

$$Yk(n) = \sum_{m=0}^{\infty} Hk(m).Sk(n-m) + N(n)$$

The demodulated multipath faded OFDM signal is effected by ISI that is produced by the delay dispersive channel. As a result, a part of the received OFDM symbol is combined with another symbol causing a severe ISI that leads to loss of orthogonality between subcarriers. This is avoided by adding a sufficient cyclic prefix CP.

4.4 IMPLEMENTATION OF LTE OFDM TRANSCEIVER

The LTE-OFDM transceiver consists of two important parts, the OFDM modulation transmitter and the OFDM modulation receiver. At the transmitter the binary data stream that forms the digital signal is coded and interleaved for error correction. After that the binary bit stream is mapped using either M-QAM or PSK modulation schemes to complex-value symbols, the constellation mapping assigns sinusoid with a particular phase and/or amplitude instances to the binary data stream. Then the complex serial mapped symbols are divided into parallel low data symbol streams after pilot symbols are inserted for channel estimation. Regarding to the LTE downlink physical layer the constellation mapped symbols and the inserted pilot symbols are mapped on a resource grid. The block diagram of OFDM transceiver is demonstrated in figure 4.4.

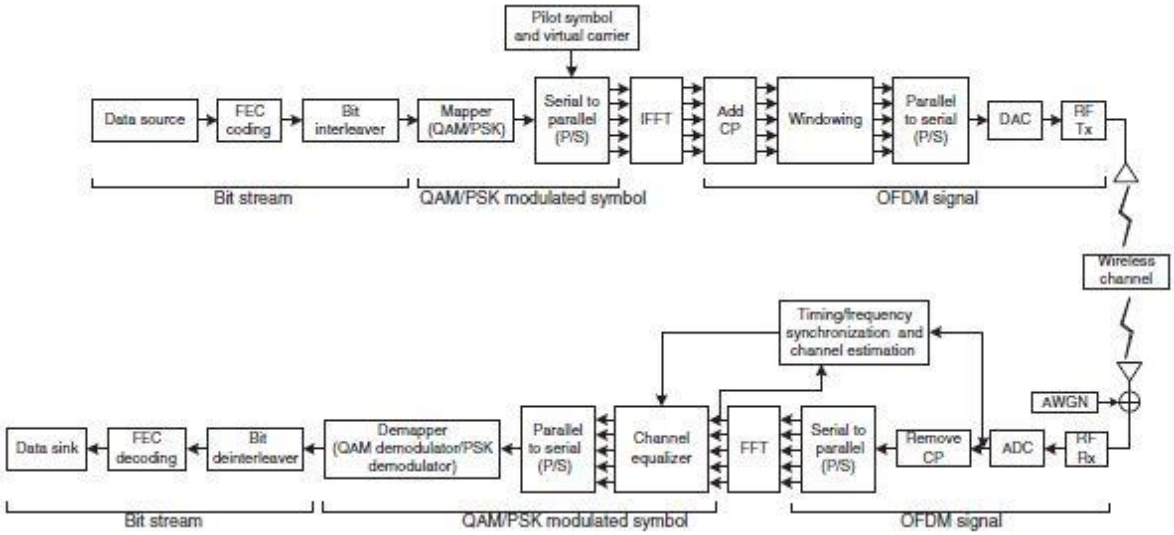

Figure 4.4: Schematic diagram of OFDM transceiver [48]

The next stage is that the frequency domain parallel subcarrier symbol chunks are entered to the IFFT process where the complex orthogonal OFDM baseband subcarriers are generated in time domain. If the symbols of the constellation mapper are less than the size of the IFFT, then the rest of values are zero padded. Afterwards that, the addition of the cyclic prefix takes place which works as guard interval that prevents ISI among transmitted symbols. Then, some pulse shaping windowing is applied to the IFFT output symbols to avoid or minimize the side lopes of the spectral waveform. The parallel streams are then converted back to serial form. Finally, the serial stream of complex OFDM baseband signal are converted from digital to analogue signals for transmission by radio frequency circuit as passband signal over the propagation channel.

At the receiver, the OFDM signal is received by the radio frequency circuit and then it is converted to digital waveform stream using ADC. After that, the guard intervals are removed from the received binary stream. Next stage, the serial stream of time domain signal is converted from serial to parallel data streams that are fed into the FFT process where it is converted back to frequency domain data stream. The output of the FFT process is synchronized by the timing frequency and channel estimation process. Then the parallel FFT outputs are equalized and converted back from parallel to serial form. After that, the complex serial stream is de-mapped back to a binary data stream using either MQAM or PSK according to the scheme that is used at the transmitter. Finally, the binary stream data is de-interleaved and decoded where errors are fixed and the output gives the original transmitted binary stream.

4.4.1 FEC Coding and Decoding

Error correction algorithms are applied in the OFDM input data mainly to minimize bit errors to the optimum level. Therefore, reduce the probability of decoding a bit in error position. OFDM binary data stream is initially encoded and interleaved before processing OFDM modulation. Many encoding techniques are existed nowadays for encoding data in wireless communication systems. But LTE downlink physical layer applying either turbo coding algorithm or Viterbi algorithm (soft or hard) [39]. For instance, in turbo coding a cyclic redundancy check CRC code is attached to the input user binary bit stream and then is segmented into a tiny blocks called sub-blocks. after that channel coding implementing a rate matching process that determine the count of output binary bits that referring to the requested coding rate [39]. And lastly, the sub-blocks are regenerated into code words [8]. The decoding process at the receiver is the way how the received signal is decoded and detected free of errors according to the encoding algorithm.

In the forward error correction mechanism, the transmitted data bits are formed in code words of two or three times of the original number of bits. The added bits play as redundant data bits that are used by the receiver to reconstruct the original data source. The source binary bits are divided by the transmitted coded bits count is called the rate of the encoding process. In LTE the OFDM transmitter determine the rate of coding process in two steps. In the first step, the source binary bits go through a turbo coding algorithm with a coding rate of $\{1/3\}$ [5]. In the second step the process of rate matching is carried out where some of the bits are transmitted and the rest are directed to an algorithm process called puncturing where the bits are discarded. The OFDM receiver is provided by the same puncturing algorithm that is capable of replacing dummy bits into the discarded bits at the transmitter and finally the bit sequence is forwarded to turbo decoder for correcting bits with errors. In LTE as shown in figure 4.5. a technique called hybrid automatic repeat request HARQ is performed where the transmitter transmits CRC bits in combination with the source bits. The receiver demodulated the received signal. After that, zero soft decisions are added in place of any bits that are discarded at the transmitter and keeps the produced code word inside a buffer [34]. Later to be passed into a process of detecting and correcting bit errors. Finally, the receiver sends an acknowledgement to the transmitter. If the redundancy check is unsuccessful, then the transmitter sends the data another once. The HARQ implements stop-and-wait mechanism where the transmitter waits from the receiver an ACK prior to transmitting the data again [7].

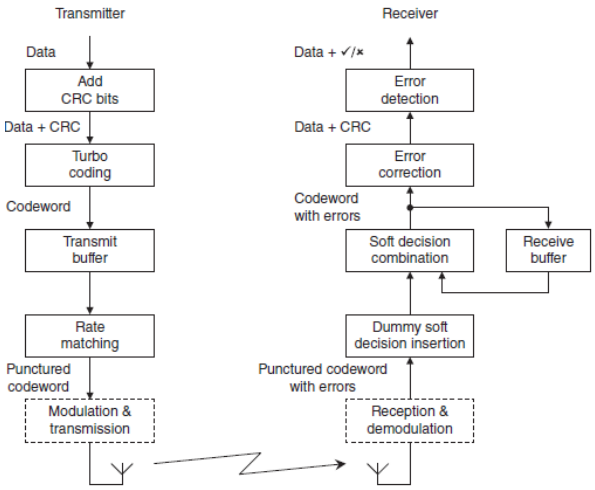

Figure 4.5: LTE turbo coding and HARQ process [5]

4.4.2 Symbol Interleaving and De-interleaving

To verify that the transmitted signal is only affected by a lower level of multipath fading. The binary data stream is symbolic interleaved in which the sequence of bit stream is rearranged in a way different from the original bit stream. The benefits of using interleaving process is avoiding the damage of the complete sequence of symbols. Fortunately, one symbol is lost because of multipath fading effects. The interleaving process provides lower fading levels rather than severe fading effects. The receiver de-interleaved the original sequence of the binary bits by using the same interleaving method that is used at the transmitter.

4.4.3 Constellation Mapping and De-mapping (M-QAM or PSK)

In LTE-OFDM system the encoded and interleaved binary bit stream is mapped and modulated using various constellation mapping techniques into a resource mapping grid with complex symbols where an adaptive way is performed depending on the channel quality. If the channel condition is worse. Therefore, low-order constellation mapping is selected such as BPSK or QPSK. Otherwise, high-order modulation scheme is performed such as 16-QAM or 64-QAM. The binary bit stream is represented in a sinusoid signal that varies in phase or/and amplitude according to the value of bit zero or one.

In BPSK LTE symbol contains one bit. Thus, meaning that the possibility of having only two values is achieved (zero or one) which is represented in an I-Q way as the following in table 4.1:

Table 4.1: BPSK I and Q bit constellation values

Binary Value	I-Component	Q-Component
0	1	0
1	-1	0

Where in QPSK constellation mapping the LTE symbol contains two bits. Such that only four values are possible of a combination of two bits that are represented in an I-Q form as the following in table 4.2:

Table 4.2: QPSK I and Q bit constellation values

Binary Value	I-Component	Q-Component
00	$1/\sqrt{2}$	$1/\sqrt{2}$
01	$1/\sqrt{2}$	$-1/\sqrt{2}$
10	$-1/\sqrt{2}$	$1/\sqrt{2}$
11	$-1/\sqrt{2}$	$-1/\sqrt{2}$

In 16-QAM the LTE symbol contains four bits and the possibility of 16 values are obtained. While in 64-QAM mapping provides 64 possible values where the LTE symbol is comprising of six bits. The constellation de-mapping at the receiver applies the reverse process of the constellation mapping at the transmitter. De-mapping of the received symbols converts the state from an inphase and quadrature forms to the original binary bits using the same mapping technique that is used at the transmitter.

4.4.4 Serial to Parallel

The principle of S-P conversion is that the serial constellation mapped symbols are split into various parallel sub streams according to the subcarriers count. In terms of mathematical representation, the serial scalar vector is inverted into an array of several columns. Therefore, the number of subcarriers determine how many columns to be exist within the represented matrix. The number of parallel sub streams must be less or equal to the size of the IFFT process.

The OFDM receiver receives the OFDM signal and converts it to a digital waveform and then removes the inserted cyclic prefix guard bands. The produced serial signal is divided into sub values that are generating the feed of the FFT process.

4.4.5 Zero Padding

If the parallel symbol sub streams are less than the size of the IFFT the zero padding process adds zeros sub streams until the size of subcarriers is equal to the IFFT size [48]. Thus, zero padding is taking place if the sampling rate of IFFT is higher than the spectrum of the transmitted subcarriers.

4.4.6 Pilot Reference Symbols Insertion for Channel Estimation

One of the main difficulties that encounter OFDM transmission and reception is the multipath fading channel. Since, it impacts and distorts the transmitted signal. As a result, the propagation channel must be estimated to verify that the receiver can detect and compensate the effects of the selectivity of channel that is caused by the delayed multipath signals. The user equipment receives the downlink reference symbols which are used in two functions. The first function instantly provides the user equipment with the phase and amplitude reference signals that to be used for implementing channel estimation [5]. The second function enables the user equipment measuring the power of the received signal in terms of frequency function for manipulating the channel quality levels. In order to detect and compensate the channel effects at the OFDM receiver, each transmitted subcarrier to be considered as a separate channel that works independently if there is no existence of ICI among subcarriers. Therefore, the received subcarrier can be determined as the product of the response of the channel frequency and the transmitted OFDM signal [48]. As a result, the transmitted OFDM signal can be reconstructed by implementing pilot signals that are previously known to both the transmitter and the receiver. Three different forms of pilots are used block, comb and lattice types. Which are called reference signals as are illustrated in figure 4.6.

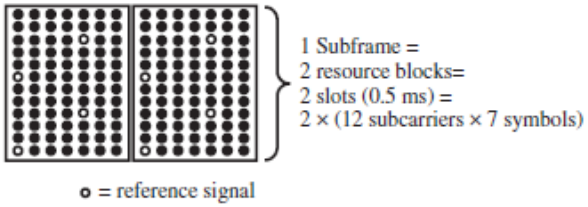

Figure 4.6: OFDM reference signals insertion [34]

The channel estimation process is required when demodulating the received OFDM signal coherently where an instant different locations of both time and frequency of the modulated symbols are interchanged with predefined pilot symbols in which the propagation channel can be

estimated properly [40]. One disadvantage of pilot addition is that it reduces the efficiency of both spectrum and power. Many techniques are used for inserting pilot signals such as least square channel estimation and linear mean minimum square error estimation scheme.

4.4.7 Frequency and Timing Synchronization

In an OFDM transceiver the frequency and clock offset are critical issues as if the receiver lose synchronization with the transmitter, this leads to the loss of orthogonality between subcarriers and therefore, severe ICI and ISI will occur. As a result, an OFDM system requires a precise estimation of the frequency offset compensator and an accurate clock processor. In OFDM two methods are used for frequency offset compensation, pilot type and non-pilot type [49]. The LTE system implements the pilot type because it is more accurate and reliable. In LTE the base station eNB broadcasts synchronization signals periodically to the mobile users to preserve the synchronization alignment in both frequency and clock [48].In LTE the time is synchronized to the eNB's downwards reference time clock and synchronization signals that are periodically transmitted to all mobile terminals. The eNB reference clock must be extremely accurate. Fortunately, mobile terminals do not require complex frequency and time estimators which simplifies the design of the OFDM receivers [50].

4.4.8 IFFT and FFT Processes

At the transmitter side, the complex mapped symbols using QAM or PSK are split into parallel blocks of i^{th} subcarriers of M size which are identified in frequency representation. These complex vectors are used as an input to the inverse fast fourier transform IFFT algorithm with the N size. If $\{M < N\}$ then zero padding is added to the M values. The produced IFFT output N values are expressed in time domain representation [12]. The inphase and quadrature components of the mapped symbols using either QAM or PSK are divided into parallel subcarriers. These subcarriers are summed together and divided by IFFT N size scaling factor. The resulted signal is represented in time format rather than frequency format. The receiver gets the transmitted analogue signal and mixes it with the complex Inphase and quadrature components of the original carrier frequency used at the transmitter. After filtration, the signal is converted to digital time representation format using an ADC and then the serial channel is divided into parallel sub channels equals to the N size of FFT algorithm. The FFT transforms the inphase and quadrature components of the signal from

time function to frequency function. Hence, the implementation of IFFT and FFT is substantially quick and highly accurate without any complexity and calculation load that affects the performance of the system [5].

4.4.9 Cyclic Prefix Addition and Removal

The LTE system performance is measured according to various terms, but the main term that affected the performance degradation is the ISI that is caused by multipath channel [51]. In OFDM systems, even if the orthogonality theory was implemented within the system, the system is still exposed to ISI because of the delayed multipath transmission. If the assumption of the transmitter and the receiver are properly synchronized, in the selectivity of multipath fading environment the synchronization errors are considered to be high because the orthogonality between the original source signal and the delayed received signal are mismatched [52]. Therefore, severe ISI levels are occurred. A developed technique that is performed in a way in which these levels of ISI can be avoided. This technique justifies the transmitted OFDM signal by adding guard intervals that preserve the orthogonality between multi-delayed signals in the existence of multipath fading environment. These guard intervals are named cyclic prefix as illustrated in figure 4.7, the prefix means that an end part of the OFDM symbol is copied to the first part of the transmitted OFDM symbol. Thus, the OFDM symbol duration Tex is extended by Tcp ($Tex = T + Tcp$ [3].

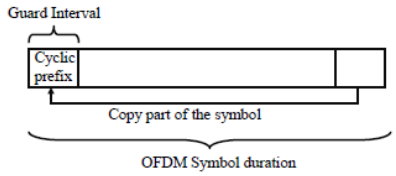

Figure 4.7: OFDM cyclic prefix addition [33]

This extension of OFDM symbol prevents interference with symbols are transmitted previously. The cyclic prefix is added for many purposes, mainly it maintains the receiver's subcarriers orthogonality. It also transforms the operation of the linear convolution that is caused by the channel on the transmitted signal into a circular convolution operation [8]. This convolutional format helps the implementation of FFT process where the frequency domain representation is performed only if the response of the channel operates in a convolutional way. The CP extension length is an important parameter in which it must be longer than the channel response delay that

is caused by multipath fading $Tcp > Tch$. LTE-OFDM uses a sufficient length of CP to avoid reducing the efficiency of spectrum. The 3GPP standardized three CP lengths as the following:

Table 4.3: LTE-OFDM cyclic prefix length

Type	CP Length	No Symbols Per Subcarrier	No Subcarriers Per Resource Block	Spacing Of Subcarriers
Normal CP	4.7 μs	7	12	15 Khz
Extended CP	16.6 μs	6	12	15 Khz
Special Ext CP	33 μs	3	24	7.5 Khz

At the receiver side the cyclic prefix extension is discarded as it contains the interference with the previously transmitted symbols and therefore, the ISI is avoided or minimized to a very tiny level.

4.4.10 DAC and ADC

In LTE-OFDM the transmitted signals are digital waveforms that simplify the signal processing by implementing the developed DSP circuits such as the IFFT and FFT. The IFFT computed time domain values that are converted to analogue format using DAC in order to be suitable for RF transmission. At the receiver side the received analogue signal is converted back to a digital format to be suitable for processing using a digital FFT algorithm. The bits count required for ADC and DAC depends on various factors. In high order constellation 64-QAM requires at least 8-bits for the transmitter DAC and 10-bits or more for the receiver ADC. As a result, an average tradeoff is achieved between performance and complexity factors [50]. In order to prevent any issues with aliasing the frequency of sampling fsa must be equals to or greater than the double of the total frequency of the signal.

$$Fsa = \frac{1}{Tsa} = \frac{N}{T} = B \tag{4.21}$$

4.4.11 Windowing of Square Root Raised Cosine Filter

In pulse shaping of rectangular waveform and with the existence of overlapped sub channels the ISI will affect not only one sub channel but various sub channels. This can be avoided in OFDM system if each sub channel is bandlimited so it only overlaps with only neighboring sub channels.

If each individual sub channel bandwidth is $1/T$ the interference only affects one subcarrier. Therefore, the pulse shaping of Nyquist is required for each sub channel to achieve the transmitted signal free of ISI interference. This implementation requires a higher rate sampling rather than N/T. The pulse shaping of Nyquist is identified by:

$$S_{Nyquist}(t) = \begin{cases} \dfrac{sin\left[\frac{\pi t}{T'}(1-\beta)\right] + \frac{4\beta t}{T'}\cos\left[\frac{\pi t}{T'}(1-\beta)\right]}{\frac{\pi t}{T'}\left[1-(\frac{4\beta t}{T'})^2\right]} & for\ t \in \{-4T', 4T'\} \\ 0 & Else\ where \end{cases} \quad (4.22)$$

Where $T' = (1+\beta)T$ and β is the roll-off factor.

4.4.12 OFDM Transmitter and OFDM Receiver RF Circuits

The OFDM Transmitter RF circuit consists of a frequency carrier $\{fc\}$ local oscillator generates $\cos(2\pi fct)$ *and* $\sin(2\pi fct)$ components that each is summed with the digital to analogue I and Q converted signals and after that they pass through LPFs and then the two streams are mixed together where a passband filter is applied to the produced signal and finally the signal is passed through a high power amplifier for obtaining a robust coverage area via the RF antenna [50].

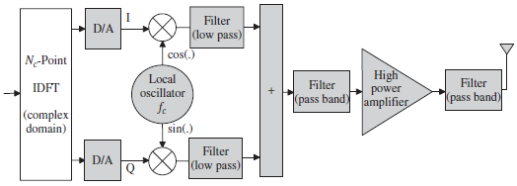

Figure 4.8: OFDM transmitter RF circuit [50]

The OFDM receiver antenna receives the signal and passes it to the RF circuit which is comprising of the same components of the transmitter RF circuit that is applying the inverse process. Figures 4.8 and 4.9 demonstrate the RF circuits block diagrams of the transmitter and the receiver.

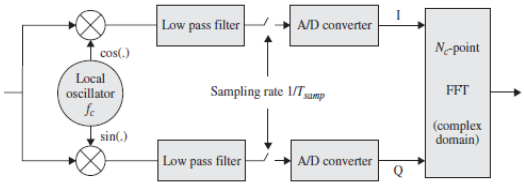

Figure 4.9: OFDM receiver RF circuit [50]

4.5 FREQUENCY AND TIME OFFSET TECHNIQUES

The OFDM system performs well in the case that the orthogonality is perfectly maintained. Otherwise the performance is degraded because of the occurred ICI and ISI. The loss of orthogonality is caused by the symbol timing offset STO and carrier frequency offset CFO. Therefore, the received OFDM signal with the existence of STO θ and the CFO φ is identified by:

$$rl(t) = IFFT[yl(k)] = IFFT[hl(k) * Sl(k)] + zl(k) \tag{4.23}$$

$$rl(t) = \frac{1}{N}\sum_{k=0}^{N-1} hl(k) * Sl(k).\, e^{j2\pi(k+\varphi)(n+\theta)/N} + zl(t)\,, \qquad zl(t) = IFFT(zl(k)$$

Where $hl(k)$ denotes the channel's impulse response, $Sl(k)$ denotes the transmitted OFDM signal and $zl(k)$ denotes the additive noise.

4.5.1 Effects of STO and CFO Errors

Substantial frequency and timing offset errors in an OFDM system cause severe ISI and ICI levels that lead to a large degradation of the system performance. By supposing that the receiver's local oscillator frequency fc is not perfectly synchronized with the transmitter local oscillator frequency. Therefore, the received baseband OFDM signal is defined by:

$$rl(t) = Sl(t).\, e^{j2\pi f_{error} t} + zl(n) \tag{4.24}$$

Where f_{error} denotes the errors of frequency offset. After demodulation and filtration the subcarrier lm can be defined by:

$$rlm(t) = \left[Sl(t).\, e^{j2\pi f_{error} t} + zl(t)\right].\, e^{j2\pi fmt} \otimes h(t) \tag{4.25}$$

$$rlm(t) = \left[\sum_{i=-\infty}^{\infty}\sum_{n=0}^{N-1} d(n,i)g(t - iTs).\, e^{-j2\pi\left(\frac{n-m}{Ts}\right)}.\, e^{j2\pi f_{error} t}\right] \otimes h(t) + zl'(t)$$

Where $zl'(t)$ denotes the filtered noise. By supposing that the sampling timer has a consistent error T_{error}. Thus the sample at the value lTs at the lm subcarrier of the received OFDM signal is defined by:

$$rlm(lTs + T_{error}) = d(m,i).Am(T_{error}).e^{j2\pi f_m lTs} + ISI(m,l) + ICI(m,l) \quad (4.26)$$

$$+zl'(lTs + T_{error})$$

Where the first part represents the transmitted data $d(m,i)$ and the second and the third parts represent the ISI and ICI, respectively. Which are identified by:

$$ISI(m,i) = \sum_{i=-\infty, i\neq l}^{\infty} d(m,i).Am[(l-i)Ts + T_{error}].e^{j2\pi f_{error} iTs} \quad (4.27)$$

$$ICI(m,i) = \sum_{i=-\infty}^{\infty} \sum_{n=0, n\neq m}^{\infty} d(n,i).An[(l-i)Ts + T_{error}].e^{j2\pi f_{error} iTs} \quad (4.28)$$

Where $An(t)$ is defined by:

$$An(t) = \left[g(t).e^{j2\pi f_{error} t}.e^{j2\pi \frac{(n-m)t}{Ts}}\right] \otimes h(t) \quad (4.29)$$

Where $g(t)$ denotes the transmitter's filter impulse response and $An(lTs)$ denotes the samples after convolution process. As a consequence, the OFDM system is highly sensitive to frequency and time synchronization errors. Therefore, to make the performance degradation lower than $(0.5 - 1\ dB)$ the occurred errors after synchronization process must be below these limits:

$$\begin{Bmatrix} T_{error}/Ts < 0.01 \\ f_{error}.Ts < 0.02 \end{Bmatrix} \quad (4.30)$$

The STO synchronization has to be achieved to recognize each OFDM symbol start after removing the CP. The effect of STO is varied according to the position of the OFDM symbol initial point

Table 4.4: Effects of STO on the OFDM received signal

Type	Received OFDM signal	STO (θ)
Frequency Representation	$rl(k)$	$Sl(t+\theta)$
Time Representation	$rl(t)$	$e^{j2\pi k\theta/N}.Sl(k)$

On the other hand, the CFO is caused by the shifting of Doppler frequency fd. By supposing that the fc and fc' represent the transmitter and the receiver local oscillator's frequencies respectively.

And $f_{shift} = fc - fc'$ represents the difference between them. Thus, the fd is identified by:

$$fd = \frac{ve.fc}{c} \tag{4.31}$$

Where c denotes the speed of light and ve denotes the velocity of the receiver. The CFO (φ) is defined by:

$$\varphi = \frac{f_{shift}}{subcarrier\ spacing\ \Delta f} \tag{4.32}$$

For instance, a carrier frequency of 2Ghz with a subcarrier spacing of 15Khz at the speed of 120Km produces approximately 222.22Hz of Doppler frequency offset and about a CFO of 0.0148.

4.5.2 Time Synchronization

The timing synchronization process estimates two things. The first is to estimate the window positioning of FFT, and the second is the ADC sampling rate estimation. The time synchronization is performed in two types fine and coarse STO synchronization [50].

4.5.2.1 Coarse time synchronization

In coarse symbol timing the power of the received OFDM signal is observed before implementing the FFT operation. Several coarse timing techniques are performed for estimating the initial part of the transmitted OFDM symbol.

Detection by using CP-based technique:

In this method the correlation of the CP extension is exploited to estimate the time synchronization in time domain. Furthermore, the ADC sampling rate can also be estimated by implementing this correlation method. The two equivalent samples of B and B' are separated by $Nsub$ samples. B and B' are implemented as sliding windows $w1$ and w2 [48]. These windows have the ability of calculating the similarity of samples located inside these windows. This similarity is maximized when the OFDM symbol CP falls into the initial window $w1$. This peaked point is exploited to estimate STO. When the similarity between samples in both windows is maximized this leads to the minimum difference between them. The STO is estimated by looking for the minimum difference point between both blocks of NG samples in $w1$ and w2. The STO is calculated by:

$$\hat{\theta} = \arg\min \theta \left\{ \sum_{i=\theta}^{NG-1+\theta} |yl(t+i) - yl(t+N+i)| \right\} \tag{4.33}$$

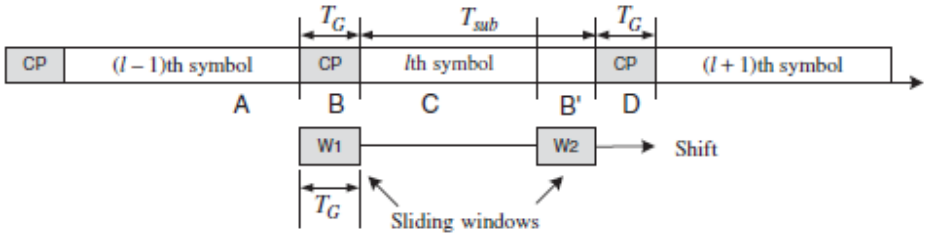

Figure 4.10: CP coarse time synchronization using sliding windows [48]

Figure 4.10 shows the CP time synchronization using sliding windows. Another STO estimator minimizes the squared difference between both blocks of samples in $w1$ and $w2$ by:

$$\hat{\theta} = \arg\min \theta \left\{ \sum_{i=\theta}^{NG-1+\theta} [|yl(t+i)| - |yl^*(t+N+i)|]^2 \right\} \tag{4.34}$$

Another method can be used to estimate the STO by considering the correlation between both blocks of samples in $w1$ and $w2$ [48]. This is achieved by applying the estimation of maximum likelihood ML by:

$$\hat{\theta}_{ML} = \arg\max \theta \left\{ \sum_{i=\theta}^{NG-1+\theta} |yl(t+i) - yl^*(t+N+i)| \right\} \tag{4.35}$$

The STO is estimated by maximizing the correlation between the two NG blocks of samples.

4.5.2.2 Fine time synchronization

In this technique reference symbols are transmitted with the OFDM signal. Many methods apply this principle. One method estimates the channel impulse response $h(t)$. The received signal without AWGN $rl(t) = Sl(t) \otimes h(t)$. After applying the FFT in the frequency domain leads to achieve $rl(f) = Sl(f) \otimes h(f)$. By applying training symbols of reference, such as CAZAC sequences, the $SL(f)$ is recognized by the receiver. Therefore, after splitting the $rl(f)$ by IFFT

operation and $Sl(f)$, the $h(t)$ is estimated and a precise time synchronization can be obtained. If the window of FFT is not perfectly located the received OFDM signal turns into:

$$rl(t) = Sl(t - t0) \otimes h(t) \tag{4.36}$$

$$rl(f) = Sl(f).h(f).e^{-j2\pi ft0}$$

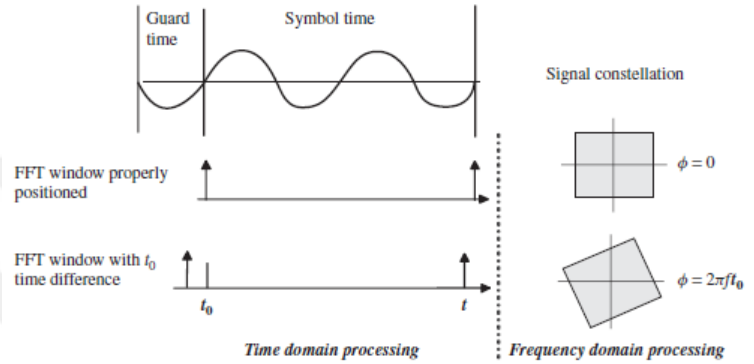

Figure 4.11: Fine time synchronization using channel impulse response estimation [50]

After implementing the FFT operation the OFDM receiver achieves $h(t - t0)$. Thus, a delayed FFT window is obtained by the fine synchronization. The STO estimation can be performed in frequency domain by the difference of phase between neighbor subcarrier parts. Thus, the STO $\hat{\theta}$ estimation is calculated by:

$$\hat{\theta} = \frac{N}{2\pi} arg\left\{\sum_{k=1}^{N-1} yl(k).y^*(k-1)\right\} \tag{4.37}$$

Figure 4.11 shows the fine time synchronization using channel impulse response estimation.

4.5.3 Frequency Synchronization

The CFO is caused by the difference between the transmitter and the receiver local oscillators. Also shifting of Doppler frequency and phase noise lead to CFO. And therefore, the CFO reduces the amplitude of the transmitted signal and also causes the shifting of SINC pulse shaping functions. Subsequently, the orthogonality between subcarriers is lost which generates ICI. Several methods are used to estimate the frequency offset.

4.5.3.1 Coarse frequency synchronization

By supposing that the frequency offset is larger than the half of the Δf and therefore the frequency errors are defined by:

$$f_{error} = \frac{2z}{Ts} + \frac{\emptyset}{\pi Ts} \tag{4.38}$$

Where the first part refers to the frequency offset which is consisting of multiple Δfs, z is an integer and the last part refers to the extra frequency offset and $\emptyset$ must be lower than π. The main objective of coarse frequency synchronization is the estimation of z value. Various techniques of coarse frequency estimation are performed.

Detection by using CP-based technique:

The difference of phase caused by CFO between the rear part of the OFDM symbol and the CP is $2\pi n\varphi/N = 2\pi\varphi$. Therefore, the CFO within the CP interval can be calculated in time domain by:

$$\hat{\varphi} = \frac{1}{2\pi} arg\left\{\sum_{t=-NG}^{-1} yl^*(t)yl(t+N)\right\} \tag{4.39}$$

Where the arg is calculated by tan^{-1} function. The limits of CFO that can be estimated by this method is located between $[-0.5, +0.5]$ which is equal to $[-\pi, +\pi]/2\pi$. By supposing that L denotes the averaging number of samples. Thus, the estimation of errors is identified by:

$$Error_{\varphi} = \frac{1}{L}\left\{\sum_{t=1}^{L} Imag\{yl^*(t)yl(t+N)\}\right\} \tag{4.40}$$

Detection by using CP-based training symbol:

As the CP-based technique is only limited to below 0.5 CFO ranges. Thus, the estimation of CFO range can be extended by decreasing the space between the two correlated blocks of samples [48]. This is achieved by implementing repeated periods of training symbols. By supposing D is an integer that represents the ratio between the length of the OFDM symbol and the length of the repeated period. Thus, the transmitter sends the training symbols with the repeated periods of D in

time domain, that can be produced by applying the IFFT of a comb form in the frequency domain. The receiver estimates the CFO by:

$$\hat{\varphi} = \frac{D}{2\pi} tan^{-1}\left\{\sum_{t=0}^{N/D-1} [yl^*(t).yl(t+N/D)]\right\} \tag{4.41}$$

The estimated CFO is only limited to $\{|\varphi| \leq D/2\}$. Therefore, can be extended by increasing the value of D. Unfortunately, the MSE performance is degraded as D increases. This can be fixed by computing the average of the estimation with the repeated periods have the short period by:

$$\hat{\varphi} = \frac{D}{2\pi} tan^{-1}\left\{\sum_{m=0}^{D-2}\sum_{t=0}^{N/D-1} [yl^*(t+mN/D).yl(t+(m+1)N/D)]\right\} \tag{4.42}$$

4.5.3.2 Fine frequency synchronization

Detection by using Moose preamble window:

The CFO can be estimated by transmitting two equivalent training reference symbols. The signals of φ CFO are related to each other by:

$$rl2(t) = rl1(t).e^{j2\pi\varphi/N}, \qquad rl2(k) = rl1(k).e^{j2\pi\varphi} \tag{4.43}$$

The CFO estimation can be calculated by:

$$\hat{\varphi} = \frac{1}{2\pi} tan^{-1}\left\{\sum_{k=0}^{N-1} imag[y1^*(k).y2(k)] \Big/ \sum_{k=0}^{N-1} real[y1^*(k).y2(k)]\right\} \tag{4.44}$$

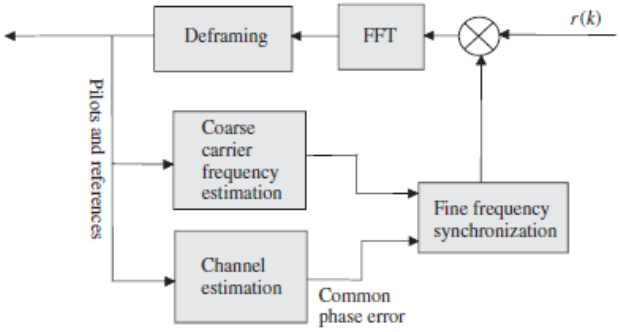

Figure 4.12: Fine frequency synchronization using reference symbols [50]

This technique requires a period that is called preamble period in which the training symbols are used. In this period the OFDM symbols are not transmitted. The range of CFO estimation is $|\varphi| \leq \frac{\pi}{2\pi} = 1/2$, which can be expanded by D times and D repeated periods. Figure 4.12 shows the fine frequency synchronization using reference symbols.

Detection by using Classen pilot tones:

In this technique the OFDM symbols can be transmitted when performing the CFO estimation. Where a pilot tones are added in frequency representation and are transmitted in each data symbol for monitoring CFO. After the estimation of CFO of the addition of pilot tones. The signal compensation is done in time domain by the estimated CFO. Two modes of estimation are performed, tracking and acquisition [48]. In acquisition mode an integer CFO is calculated by:

$$\hat{\varphi}_{acq} = \frac{1}{2\pi Tsub} \max(\varphi) \left\{ \left| \sum_{j=0}^{L-1} yl + D[p(j), \varphi].yl^*[p(j), \varphi].Sl^* + D[p(j)]Sl[p(j)] \right| \right\} \quad (4.45)$$

Where $L, p(j), Sl[p(j)]$ represent the pilot tones count, the position of the jth pilot tone and the frequency domain located pilot tone at $p(j)$ at the symbol period of lth. In tracking mode, the fine CFO is calculated by:

$$\hat{\varphi}_{fine} = \frac{1}{2\pi Tsub.D} \arg \left\{ \sum_{j=1}^{L-1} yl + D\left[p(j), \hat{\varphi}_{acq}\right].yl^*\left[p(j), \hat{\varphi}_{acq}\right].Sl^* + D[p(j)]Sl[p(j)] \right\} \quad (4.46)$$

5. PAPR AND PAPR REDUCTION METHODS

The peak to average power ratio PAPR is one of the most problematic issues encountering OFDM transmission systems where the amplitude of the signal that is transmitted using OFDM system can be considerably peaked highly than the amplitude of the averaged signal measurement. These peaked values are constructed in time domain representation since the fact that several parallel subcarriers are processed using IFFT operation. Therefore, according to the nature of the process of the IFFT the combination of multiple carriers produces the PAPR peaked values. The PAPR degrades the transmitter's power amplifier efficiency while reducing the noise ration of the signal quantization SQNR of both the DAC and ADC converters [48] [53]. The main reason for the construction of the PAPR is the substantial dynamic range of OFDM symbols which are modulated on N subcarriers and converted in time domain form using IFFT. As a result, the PAPR is observed in the transmitted OFDM signal. In time domain the high varied amplitude can be observed as a Gaussian waveform [7].

5.1 PAPR IN OFDM SYSTEMS

Generally high power amplifiers with linearity cause a nonlinear distortion in the transmitted signal that is because these HPAs have saturation characteristics [48]. By considering the input power Pin and output power $Pout$ of a high power amplifier. Therefore, according to the saturation characteristics, the produced power is limited by the $(Pmaxout)$ where the input power is measured as $(Pmaxin)$. Thus, to work in the linear area the power input has to be firstly backed off [48]. Regarding that operation, the area with nonlinearity can be determined by the output power back off or input power back off and that can be described by:

$$IPBO = 10log_{10}\left(\frac{Pmaxin}{Pin}\right), \qquad OPBO = 10log_{10}(\frac{Pmaxout}{Pout}) \tag{5.1}$$

Therefore, the nonlinearity of HPAs cause distortion on the received OFDM signal. In practice, the RF circuit HPA of the OFDM transmitter operates in linearity only in a limited dynamic domain. Thus, the clipping of the transmitted OFDM signal cause severe distortion [7]. To prevent this distortion from occurrence. The HPA needs to be designed in an expensive complexity to work on substantial back offs. Figure 5.1 illustrates the characteristics of the high power amplifier.

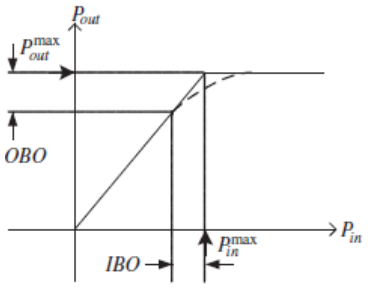

Figure 5.1: High power amplifier characteristics [48]

Obviously, if the number of subcarriers are quite large the amplitudes of the inphase and quadrature parts are Gaussian distributed with a standard deviation of value $\alpha = 1/\sqrt{2}$ and therefore the absolute amplitude is distributed by Rayleigh distribution method [3]. Regarding Gaussian and Rayleigh distributions the PAPR is produced on the transmitted OFDM signal.

5.1.1 Mathematical Representation of PAPR

By considering a PAM baseband signal for a complex modulated symbols ($Sy(k)$) which is calculated by:

$$Xk(t) = \sum_{l=0}^{N-1} Sy(k)g(t - lT), \qquad 0 \le t \le T \tag{5.2}$$

Where T is the transmitted symbol duration and $g(t)$ is the pulse shaping for every transmitted symbol. The passband modulated signal is calculated by:

$$Sk(t) = \sqrt{2}.Re\{(XkI(t) + jXkQ(t))e^{j2\pi fct}\} \tag{5.3}$$

Where $XkI(t)\ and\ XkQ(t)$ refers to the inphase and quadrature parts of the baseband signal.

The PAPR represents the value of the ratio between the maximum power of the OFDM passband signal $Sk(t)$ and the average power of the same OFDM passband signal $Sk(t)$. The PAPR for continuous time representation is defined by:

$$PAPR\big(Sk(t)\big) = \frac{max\left[Re\{Xk(t).e^{j2\pi fct}\}\right]^2}{Ev[Re\{Xk(t).e^{j2\pi fct}\}]^2} = \frac{max[Sk(t)]^2}{Ev[Sk(t)]^2} \tag{5.4}$$

By considering the produced OFDM signal from the IFFT in discrete time domain which is calculated by:

$$Sk(n) = \frac{1}{\sqrt{N}} \sum_{i=0}^{N-1} Sy(k).e^{j2\pi i(\frac{n}{N})} \ , \qquad 0 \leq n \ and \ i \ \leq N-1 \tag{5.5}$$

Where k denotes the index of the OFDM symbols. The PAPR for discrete time representation is calculated from the (L) period of oversampled OFDM signal by:

$$PAPR\big(Sk(n)\big) = \frac{max\ n[Sk(n)\}]^2}{Ev[Sk(n)\}]^2} \ , \qquad 0 \leq n \leq NL \tag{5.6}$$

The PAPR in DB can be calculated by:

$$PAPR\big(Sk(n)\big) in\ DB = 10log_{10}\left[\frac{maxn[Sk(n)\}]^2}{Ev[Sk(n)\}]^2}\right] , \qquad 0 \leq n \leq NL \tag{5.7}$$

Where N represents the number of subcarriers. And the characteristics of the power can be expressed in magnitude rather than power by using the crest factor (CF) which is representing the ratio between the maximum amplitude of the transmitted OFDM signal and the RMS of the wave form [54]. The CF is calculated by:

$$CF = \sqrt{PAPR} \tag{5.8}$$

In most situations the peaked value of the signal $Sk(t)$ is equal to the value of its envelope $|SK(t)|$ and therefore, the maximum value of $|SK(t)|$ is not used to form the peaked value in the practical applications because it is rarely occurred [48].

5.1.2 Oversampling and PAPR

The PAPR treats the passband OFDM signal $Sk(t)$ which uses in continuous time representation a carrier frequency of fc that is always greater than $1/T$. Thus, in continuous time range the baseband OFDM signal $Xk(t)$ with a data symbol of T period and the related passband OFDM signal $Sk(t)$ possess approximately the same PAPR levels. In discrete time representation the passband OFDM signal $Sk(n)$ has a PAPR level different from the continues time passband

OFDM signal $Sk(t)$ where PAPR level for $Sk(n)$ is less than that occurred in $Sk(t)$ [48]. To achieve an identical PAPR level for both $Sk(t)$ and $Sk(n)$ if the discrete time signal $Sk(n)$ is oversampled by $L \geq 4$ times as shown in figure 5.2.

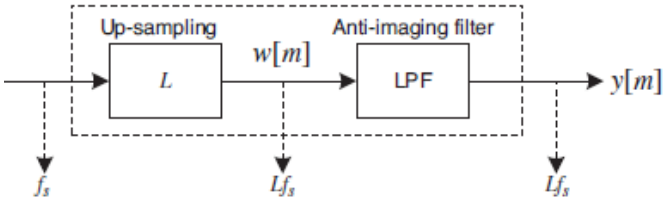

Figure 5.2: IFFT output oversampled by L times [48]

The $Sk(n)$ over-sampler adds zeros of $(L-1)$ between the taken samples of $Sk(n)$ and this process obtains:

$$W(m) = \begin{Bmatrix} Sk[\frac{m}{L}] & where\ m = 0, \pm L, \pm 2L, \dots \dots \\ 0 & otherwise \end{Bmatrix} \quad (5.9)$$

The LPF with an impulse response of $h(m)$ is used to rebuild the oversampled version of $Sk(n)$ from the $W(m)$. Therefore, the over-sampler produces an output which is calculated by:

$$y(m) = \sum_{i=-\infty}^{\infty} h(i)W(m-i) \quad (5.10)$$

Therefore, the oversampled version can be expressed as:

$$SK'(m) = \frac{1}{\sqrt{L-N}} \sum_{i=0}^{L.N-1} Sk'(i).e^{j2\pi m\Delta f i/L-N}, m = 0,1,2, \dots \dots, NL-1 \quad (5.11)$$

Where $SK'(i)$ equals to:

$$SK'(i) = \begin{Bmatrix} Sy(i) & where\ 0 \leq i \leq \frac{N}{2}\ and\ NL - N/2 < i < NL \\ 0 & otherwise \end{Bmatrix} \quad (5.12)$$

Where $Sy(i)$ refers to a complex symbol with subcarrier i and Δf is the sub channel spacing of N sub channels. Thus, the PAPR level is calculated by:

$$PAPR(SK'(m)) = \frac{max[SK'(m)\}]^2}{Ev[SK'(m)\}]^2}\ , 0 \leq m \leq NL \tag{5.13}$$

5.1.3 PAPR Distribution Principle

To achieve an efficient method for decreasing PAPR levels the PAPR distribution must be precisely defined in OFDM transmission systems. In which it can be used to determine the efficient output back off of the high power amplifier to decrease the system performance degradation [55]. In OFDM transmission system, by assuming that the input data sequence is independent and statistically distributed equivalently. Therefore, for a great number of subcarriers N both inphase and quadrature signal components of $Sk(n)$ are Gaussian distributed and they are unrelated and orthogonal. These Gaussian variables with variance and zero mean are given by:

$$\sigma^2 = Ev[|Sk(n)|^2]/2 \tag{5.14}$$

The distribution probability of complex OFDM symbols with substantial number of subcarriers N is a complex Gaussian distributed function that is expressed by the following relation:

$$P[Sk(n)] = \frac{1}{\sqrt{2\pi\sigma^2}}.e^{\left(-\frac{Sk^2(n)}{2\sigma^2}\right)} \tag{5.15}$$

Where σ^2 is the varied value of $Sk(n)$ and the amplitude of the transmitted OFDM signal is Rayleigh distributed and has a function of density probability PDF which is calculated by:

$$P[Sk(n)] = \frac{2|Sk(n)|}{\sigma^2}.e^{\left(-\frac{|Sk(n)|^2}{\sigma^2}\right)} \tag{5.16}$$

The OFDM signal power has a property of Chi-Square distribution and the distribution of PAPR is always determined by using CCDF function. According to statistic and probability theory the CCDF expresses the probability that a random variable X of real value with a distributed probability has to be distinguished at a value larger or identical to x. The cumulative distributed function CDF of the PAPR amplitude of the OFDM signal samples is calculated by:

$$F(REFPAPR) = 1 - e^{REFPAPR} \tag{5.17}$$

The CCDF function of the PAPR of the data sequence is required to make a comparison of the results of various PAPR decreasing methods. Which is identified by:

$$P(PAPR > REFPAPR) = 1 - P(PAPR \leq REFPAPR) \tag{5.18}$$

$$P(PAPR > REFPAPR) = 1 - F(REFPAPR)^N$$

$$P(PAPR > REFPAPR) = 1 - (1 - e^{-REFPAPR})^N$$

Where $REFPAPR$ refers to the used PAPR reference range.

5.1.4 Power Efficiency and PAPR

By considering a RF high power amplifier with a substantial dynamic range. The efficiency of power through that HPA is extremely low. In order to increase the efficiency of power a particular way must be performed by obtaining the required output power average [56] [57]. By assuming a HPA with linear properties, the efficiency of its power can be calculated by:

$$\eta = \frac{1/2}{PAPR} \quad , \qquad \eta = Poave/Podc \tag{5.19}$$

Where η denotes the efficiency of power of the HPA, $\{Poave\}$ denotes the output power average and $\{Podc\}$ denotes a constant value of power without respecting its power input. For instance, by assuming a transmitted OFDM signal with the N size of subcarriers equals to 256 sub channels which require a value of IBO equivalent to PAPR at the range of probability less than $\{0.01\%\}$. Consequently, the transmitted OFDM signal PAPR must be reduced to avoid this inefficiency of HPA power.

5.2 CLASSIFICATION OF OFDM PAPR REDUCTION TECHNIQUES

Various PAPR decreasing methods are deeply studied and analyzed for decreasing the PAPR of the transmitted OFDM signal. Despite the fact that no specific method is selected for the LTE downlink OFDM signal creation, many PAPR reduction techniques can be implemented at the eNodeB. The determination of the PAPR reduction technique depends on both the complexity and cost of the configuration. On the other hand, no such method is applied at the user equipment transmitter due to the limited power of the mobile station. In general, PAPR decreasing techniques

can be classified into two main sub-divisions distorted relating techniques and pre-distortion relating techniques [53]. In distortion related techniques the non-linearity of the transmitted OFDM signal is distorted or can be called regrowth of spectrum and this distortion can be fixed to some level by the process of filtration [58]. Many PAPR decreasing methods apply this approach such as clipping and filtering technique, peak windowing and companding techniques. And these techniques are implemented after the construction of the OFDM by the IFFT process before RF amplification [59]. On the other hand, the pre-distortion methods that have the ability for compensating the high power amplifier non-linearity region in OFDM transmission systems [58]. These methods spreading the OFDM symbols energy before performing the IFFT process. These techniques also capable of coping of the time varied of the nonlinearity of HPA. One of these techniques the spreading of DFT method where the input signal is spread with DFT that can be afterwards implemented by IFFT. As a consequence, the PAPR of the transmitted OFDM signal can be reduced to the range of one carrier transmission. This method is suitable for mobile user uplink transmission which is employed by the 3GPP LTE-OFDM system and it is called SC-FDMA [48]. Multiple PAPR decreasing methods are combined together to achieve better results rather than using standalone versions with slight complexity. These combined methods are called hybrid methods. There are various versions of these hybrid techniques such as clipping combined with companding.

5.3 DIFFERENT PAPR DECREASING METHODS

Various PAPR decreasing methods are proposed in the literature. These methods are studied mathematically and are analyzed deeply for the produced OFDM transmission system output. Each method is tested individually to monitor the performance degradation of the system.

5.3.1 Clipping and Filtering Method

Input signal amplitude clipping is considered as the simplest method decreasing PAPR of the transmitted OFDM signal which limits the high peak of the source signal envelope to a fixed and previously defined threshold. This method is relatively simple to implement by clipping the amplitude of the signal that is located outside the permitted limits. For instance, by supposing a high power amplifier has a saturation range lower than the input signal envelope span. As a result, the exceeded input signal envelope outside the reference region will be clipped automatically. By

supposing an OFDM system with N subcarriers and L oversampling factor. The clipping is done regarding the sampling rate of Nyquist in discrete time representation. The clipping is carried out for the oversampled OFDM symbols where $\{L \geq 4\}$. The oversampled signal with L-times $Sk'(n)$ is produced from the IFFT operation and after that it is modulated by a carrier frequency of fc to generate the passband signal $Sk^p(n)$. The clipping and filtering PAPR reduction method is shown in figure 5.3. By supposing the clipped signal is expressed as $Sk_c^p(n)$ which can be calculated by:

$$Sk_c^p(n) = \begin{Bmatrix} -A & Sk^p(n) \leq -A \\ Sk^p(n) & |Sk^p(n)| < A \\ A & Sk^p(n) \geq A \end{Bmatrix} \quad \text{Or} \tag{5.20}$$

$$Sk_c^p(n) = \begin{Bmatrix} Sk^p(n) & ,if\ |Sk^p(n)| < A \\ \dfrac{Sk^p(n)}{|Sk^p(n)|} & ,elsewhere \end{Bmatrix}$$

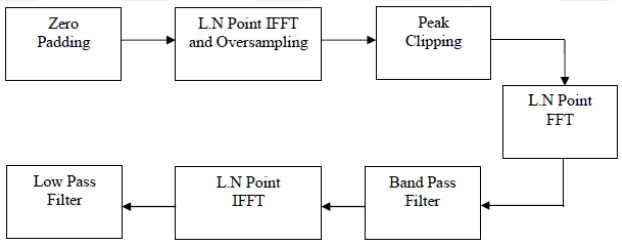

Figure 5.3: Clipping and filtering PAPR decreasing method [60]

Where A is the previously defined threshold limit. When the clipping threshold A is normalized by RMS value of the OFDM signal σ the clipping rate CR is defined by:

$$CR = \frac{A}{\sigma} \tag{5.21}$$

Where $\sigma = \sqrt{N}$ and $\sigma = \sqrt{N/2}$ for the baseband and passband transmitted OFDM signals respectively [48]. Typically, the clipping is performed at the OFDM transmitter. Whereas the OFDM receiver has to estimate the occurred clipping and compensate the received OFDM signals. Generally, one clipping event occurs per one OFDM symbol. As a result, the receiver has to estimate two values the clipping size and the clipping location [57]. In practice, it is difficult to retrieve these values and thus, the clipping method produces both in band noise and out of band noise within an OFDM signal. Which cause a performance degradation of the system in both

efficiency spectrum and BER [21]. Consequently, the filtration process is required which has the ability of reducing the out of band distortion. Unfortunately, it cannot decrease the in band noise. The clipping and filtering can be iterated to reach the required PAPR level but with more complexity of the system.

5.3.1.1 Clipping and filtering types

These are two types of the clipping and filtering process:

1. Iterated clipping and filtering technique RCF. In which the input signal amplitude is clipped if it exceeds a previously defined limit and after that it is filtered. When the process of clipping and filtering is repeated many times the produced result is better than using a single clipping and filtering method. The repeated clipping and filtering method minimizes the peaked value regrowth that is generated during the filtration process.

2. Iterated filtering and clipping technique RFC. In which the input signal is filtered and then clipped if it exceeds a previously defined limit. When the process of filtering and clipping is repeated many times the produced result is better than using a single filtering and clipping method. The repeated filtering and clipping method performs better than the clipping and filtering technique RCF.

5.3.2 Companding PAPR Decreasing Techniques

The companding technique as shown in figure 5.4 with no linearity is considered as the special clipping method provides an acceptable PAPR reduction level, no complex configuration and reasonable performance in terms of BER. The contrast between the companding and clipping techniques is that in the clipping approach the peaked amplitude of the transmitted OFDM signal is clipped. However, the signal cannot be retrieved exactly at the OFDM receiver. On the contrary, in the companding technique the source signals are companded by applying the increasing function of the strict monotone. Therefore, the transmitted OFDM signals can be retrieved perfectly at the OFDM receiver by implementing the corresponding companding transform inversion. The companding method enlarges the tiny signals and compresses the peaked signals [61]. Whereas clipping method does not alter the tiny signals. The principle of the companding techniques is changing the Rayleigh distributed OFDM signal to a uniform distributed output. There are many

companding techniques can be performed in reducing PAPR of the transmitted OFDM signal, but the literature only concentrates on the exponential companding and the rooting hyperbolic tangent $tanhR$ techniques. Since it offers better performance rather than other companding techniques.

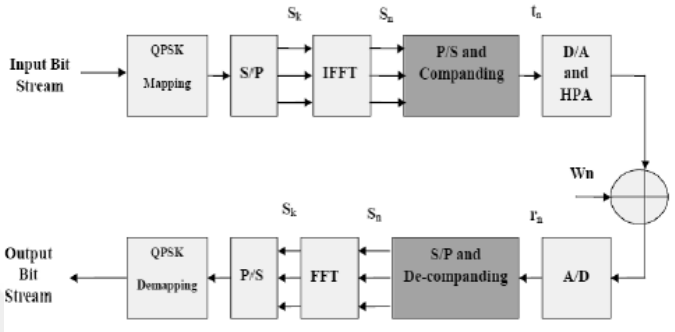

Figure 5.4: Companding technique of PAPR decreasing

5.3.2.1 Exponential companding PAPR decreasing technique

The nonlinear exponential companding technique implements a special algorithm to decease PAPR of the transmitted OFDM signal. This technique modifies the original signal in both the tiny and peaked parts of the signal and the average power is kept at the same range. The exponential method transforms the Rayleigh distributed signal into a signal that is uniformly distributed. Therefore, the PAPR is decreased to an acceptable level. By supposing $|PAn|^i$ is the i^{th} power of the companded signal amplitude A which is uniformly distributed between the interval range $[0, \alpha]$. A particular exponential companding technique degree is represented by the α exponent. The CDF function of the $|PAn|^i$ is calculated by:

$$F_{|PAn|^i}(x) = \frac{x}{\alpha}, \qquad 0 \le x \le \alpha \tag{5.22}$$

The companded signal amplitude of $|PAn|$ possess a CDF function which is identified by:

$$F_{|PAn|}(x) = P(|PAn| \le X) \tag{5.23}$$

$$F_{|PAn|}(x) = P\big(\ |PAn|^i \le x^i\big)$$

$$F_{|PAn|}(x) = \frac{x^i}{\alpha}, \quad 0 \le x \le x^i$$

The inversion function of $PA|n|(x)$ is calculated by:

$$F^{-1}_{|PAn|}(x) = \sqrt[i]{\alpha.x}, \qquad 0 \le x \le 1 \tag{5.24}$$

Subsequently, resulting that the companding transform function $h(x)$ is strictly monotonic. Thus, that is obtaining the following:

$$F_{|Sn|}(x) = P(|Sn| \le x) \tag{5.25}$$

$$F_{|Sn|}(x) = P(h(|Sn|) \le h(x))$$

$$F_{|Sn|}(x) = F_{|PAn|}(h(x)), \;\; 0 \le x \le h^{-1}(\sqrt[i]{\alpha})$$

The companding function $h(x)$ after consideration of the phase of the source signals it is calculated by:

$$h(x) = sgn(x).F^{-1}_{|PAn|}.F_{|Sn|} \tag{5.26}$$

$$h(x) = sgn(x).\sqrt[i]{\alpha\left[1 - e^{\left(-\frac{|x|^2}{\sigma^2}\right)}\right]}$$

Where the sign function is expressed as $sgn(x)$, i is the companding technique degree and σ^2 refers to the source signal variance that is applied for the process of companding. And the average power of the produced signals is identified by the fixed positive factor α. In order to make the source and produced signals equal in an average power. The following operation is applied:

$$\alpha = \left(\frac{Ev[|x|^2]}{Ev\sqrt[i]{\left[1 - e^{\left(\frac{|x|^2}{\sigma^2}\right)}\right]^2}}\right)^{\frac{i}{2}} \tag{5.27}$$

Conversely, at the OFDM receiver side the function inversion $h^{-1}(x)$ is performed for the decompanding process which is calculated by:

$$h^{-1}(x) = sgn(x).\sqrt{-\sigma^2 log_e\left(1 - \frac{x^{\frac{2}{\bar{l}}}}{\alpha}\right)} \tag{5.28}$$

5.3.2.2 Tangent of hyperbolic (tanh) companding PAPR decreasing technique

The companding function of the hyperbolic tangent $(tanh)$ is calculated by:

$$ht(x) = i1.\tanh(i2.x) \tag{5.29}$$

Where $i1\ and\ i2$ are positive numbers that are used to adjust the applied companding range to the envelope of the signal x.

5.3.3 DFT Spreading of Discrete Fourier Transform PAPR Decreasing Technique

The principle of the spreading of DFT method is to spread the source data signal with DFT and therefore, the spread signal is fed to the IFFT process. As a result, PAPR can be reduced to the single carrier transmission level due to that the DFT and IDFT omit each other [48] [62]. The DFT spreading method is implemented at the user's equipment for uplink transmission. It is called the SC-FDMA single carrier FDMA or OFDMA. This method is standardized by 3GPP as the transmission method of uplink connection. By assuming that M denotes the number of subcarriers which are assigned for each user. By implementing the spreading DFT method, the spreading is done by M-DFT points and the produced result of the DFT is allocated to the IFFT subcarriers with N size. Thus, the reduction of PAPR will be based on how the subcarriers are allocated for each terminal [48]. Two approaches are used for allocating subcarriers among different users, localized FDMA and distributed FDMA [62]. Where D-FDMA distributes M-DFT outputs to the total of N subcarriers and the remaining $(N - M)$ subcarriers are zero padded. On the contrary, L-FDMA distributes M consecutive subcarriers DFT outputs in N size of IFFT subcarriers. When N/M equals the factor of bandwidth spreading S, this method is called interleaved FDMA. In I-FDMA the source data $x(m)$ is the spreading DFT for producing $X(i)$ and after that, allocated as:

$$X'(k) = \begin{Bmatrix} X\left(\frac{k}{S}\right) & ,k = S.m1 & ,m1 = 0,1,\ldots\ldots,M-1 \\ 0 & & ,else\ where \end{Bmatrix} \tag{5.30}$$

The production of IFFT $x'(n)$ where $n = M.s + m$ where $m = 0,1,2,3, \dots \dots, M-1$ and the value of $s = 0,1,2, \dots \dots, S-1$ is defined by:

$$x'(n) = \frac{1}{N}\sum_{k=0}^{N-1} X'(k).e^{j2\pi\frac{n}{N}K} \tag{5.31}$$

$$x'(n) = \frac{1}{S}.x(m)$$

In the interleaved FDMA the mapping of subcarriers is initialized by the l^{th} subcarrier $\{l = 0,1, \dots \dots, S-1\}$. Therefore, the spreading DFT symbol is calculated by:

$$X'(k) = \begin{Bmatrix} X\left(\frac{k-l}{S}\right) & , k = S.m1 + l \quad , m1 = 0,1, \dots \dots, M-1 \\ 0 & , else\ where \end{Bmatrix} \tag{5.32}$$

Therefore, the related production of IFFT is defined by:

$$x'(n) = x'(Ms + m) = \frac{1}{N}\sum_{k=0}^{N-1} X'(k).e^{j2\pi\frac{n}{N}K} \tag{5.33}$$

$$x'(n) = \frac{1}{S}.e^{j2\pi\frac{n}{N}l}.x(m)$$

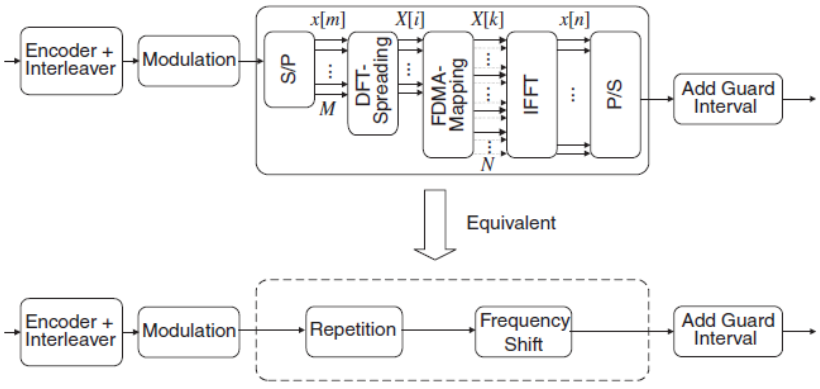

Figure 5.5: DFT spreading technique of interleaved FDMA [48]

By comparing (5.33) with (5.31) it can be obvious that the subcarrier assigning with an initial point by l subcarriers is offset by $e^{j2\pi\frac{n}{N}l}$ in interleaved FDMA as shown in figure 5.5.

6. OFDM PERFORMANCE ANALYSIS SIMULATIONS & RESULTS

6.1 LTE CONSTELLATION MAPPING BER PERFORMANCE

When signals of the source data bits are transmitted by the communication transmitter over the channel of communication several bit errors are occurred in the signals that are received at the communication receiver. These errors are occurred due to different reasons such as noise, fading of multipath reception, noise caused by phase offset and synchronization errors. Therefore, the BER of the communication system is defined mathematically by:

$$BER_s = \frac{Total\ Number\ Of\ Errors}{Total\ Number\ Of\ Transmitted\ Bits} = \frac{No_{errors}}{No_{trans-bits}} \tag{6.1}$$

The BER can be expressed in the measurement of dB by:

$$BER_s(dB) = 20Log_{10}\left(\frac{No_{errors}}{No_{trans-bits}}\right) \tag{6.2}$$

6.1.1 BPSK Mapping BER Performance Through Different Channels

6.1.1.1 BPSK BER performance analysis simulation in AWGN channel

The Matlab model simulates the performance of BPSK mapping technique through an AWGN transmission channel. In BPSK mapping technique the source data stream of bits 0s and 1s is generated in which 1 volt represents the ones and -1 volt represents the zeros. BPSK implements only the inphase component of the signal. The communication channel in BPSK is identified by:

$$Yk = A.SK + n \tag{6.3}$$

Where Yk denotes the received signal by the BPSK receiver, Sk denotes the transmitted modulated signal and A denotes the scaling parameter of the channel amplitude for the transmitted modulated signal. And finally, the AWG noise is identified by n with the variation of β^2 and a mean of zero. The β^2 regarding to the spectral density of noise power No is calculated by:

$$\beta^2 = \frac{No}{2} \tag{6.4}$$

For M-PSK mapping techniques including BPSK the energy of the symbol power is defined by:

$$Esy = R.Ebit \tag{6.5}$$

Where $R = Log_2(M)$ which equals to 2 in BPSK and $Ebit$ represents a particular bit energy. By supposing that Esy is normalized to one. The $SNR\ or\ \frac{Ebit}{No}$ is calculated by:

$$\frac{Ebit}{No} = \frac{Esy}{R.No} = \frac{Esy}{R.2\beta^2} = \frac{1}{2R.\beta^2} \tag{6.6}$$

Therefore, β^2 can be expressed as:

$$\beta^2 = \left(2R.\frac{Ebit}{No}\right)^{-1} \tag{6.7}$$

The receiver of BPSK mapping technique receives the signal as zeros or ones according to a determined threshold that has been setup. The probability theory for BPSK mapping technique is calculated by:

$$P_{bit} = \frac{1}{2}erfc\left(\frac{Ebit}{No}\right) = Q\left(\sqrt{\frac{2Ebit}{No}}\right) \tag{6.8}$$

Input parameters:

The following parameters are used by BPSK mapping system:

Table 6.1: BPSK mapping input parameters over AWGN channel

Parameter	Value
Source Data Bits Count	1000000
$Ebit/No$(dB)	-6 to 10
M	2
$R = Log_2(M)$	1

Simulation results:

The BPSK performance is illustrated as the form of the BER vs the measured SNR ($EBIT/No$). Moreover, the received BPSK signal errors are computed at each SNR level.

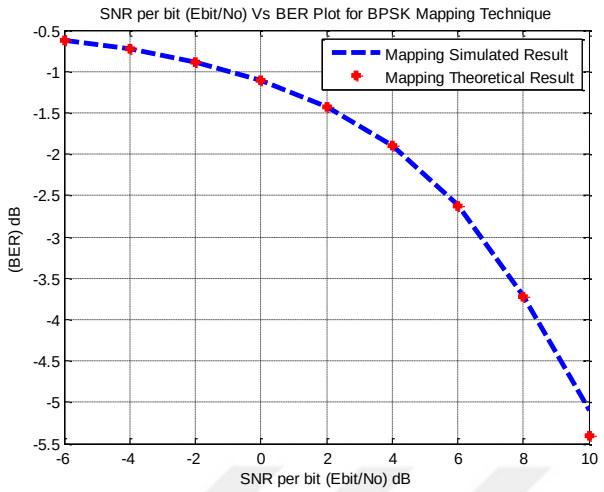

Figure 6.1: BPSK mapping BER performance over AWGN channel

Table 6.2 BPSK mapping over AGWN channel simulation results

Ebit/No(DB)	BER	No. of Errors	Total bits
-6	0.2392	239166	1000000
-2	0.1311	131116	1000000
2	0.0375	37496	1000000
6	0.0025	2459	1000000
10	8.0000e-06	8	1000000
14	0	0	1000000
18	0	0	1000000
22	0	0	1000000
26	0	0	1000000

From the simulation results in table 6.2 and the simulation graph in figure 6.1. It is obvious that while the SNR increases both the bit errors and the BER of the BPSK system are decreased. Initially, when the SNR is -6, the number of bit errors shows 239166. Whereas, the SNR is increased to 2, the bit errors gradually reach 37496. After that, when the SNR reaches 10, the total number of occurred bit errors, becomes only 8 bit errors. Finally, the produced bit errors equal to zero while the level of SNR is increased to 14.

6.1.1.2 BPSK BER performance analysis simulation in Rayleigh & AWGN channels

The Matlab model simulates the BPSK mapped and transmitted signal over both AWGN and Rayleigh Channels. Where the received signal is coherently detected at the receiver side. Where

the flat fading channel of Rayleigh distribution is modelled as a singular tap equalizer and filter an impulse response h_{ray} that contains the complex value. The received BPSK modulated signal YK is identified by:

$$Yk = h_{ray}.Sk + n \tag{6.9}$$

Where n denotes the distributed AWG noise, h_{ray} denotes the Rayleigh distributed scaling parameter of the complex channel amplitude and Sk denotes the BPSK modulated signal. The receiver detects the signal coherently and knows the impulse response of the channel perfectly. Where methods of channel estimation are implemented to estimate the impulse response of the channel or the scaling parameter of the channel amplitude h_{ray} at receiver side. Initially, prior actual data transmission occurrence. By supposing that h_{ray} approximation is accurately known at the BPSK receiver. Therefore, the transmitted signal symbols Sk can be detected coherently by the operation of equalization from the received signal YK which is calculated by:

$$Yk' = \frac{Yk}{h_{ray}} = \frac{h_{ray}.Sk + n}{h_{ray}} = Sk + z \tag{6.10}$$

Where z represents the distributed AWG noise but only for the scaling parameter $1/h_{ray}$. Therefore, the retrieving of Sk is carried out according the same process that is applied in the case of AWGN channel. The source binary bits Sy of the BPSK mapping technique are recovered by:

$$re = real[Yk'] = real[Sk + z], \begin{cases} Sy = 1 & ,if\ re > 0 \\ Sy = 0 & ,if\ re < 0 \end{cases} \tag{6.11}$$

The probability theory of BPSK mapping technique through Rayleigh and AWGN distributed channel is calculated by:

$$P_{bit} = \frac{1}{2}\left(1 - \sqrt{\frac{Ebit/No}{1 + Ebit/No}}\right) \tag{6.12}$$

Input parameters:

The following parameters are used by BPSK mapping system:

Table 6.3: BPSK mapping input parameters over AWGN & Rayleigh channels

Parameter	Value
Transmitted BPSK source data bits	$10^{\wedge 6}$ =1000000 bits
$Ebit/No$ (dB)	-6 to 26
M	2
$R = Log_2(M)$	1

Simulation results:

The BPSK transmission through AWGN and Rayleigh channels performance is demonstrated by plotting the BER against the correlated SNR ($Ebit/No$).

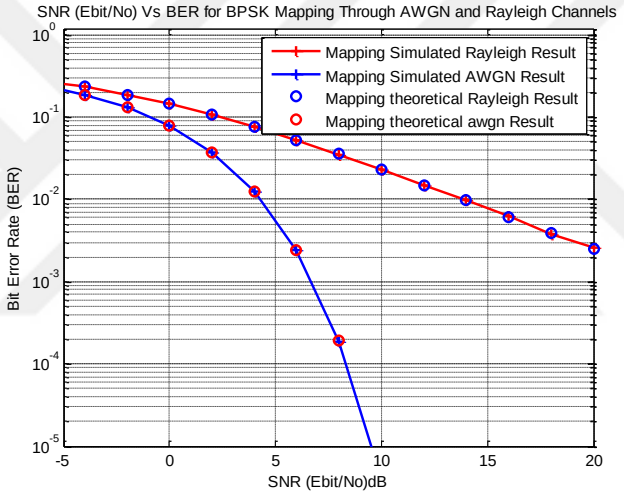

Figure 6.2: BPSK mapping BER performance over Rayleigh & AWGN

Table 6.4: BPSK mapping BER over Rayleigh & AWGN simulation results

Ebit/No(DB) (DB)	BER AWGN	No. of Errors AWGN	BER Rayleigh	No. of Errors Rayleigh	Total Bits
-6	0.2392	239156	0.2764	276402	1000000
-2	0.1310	130960	0.1887	188715	1000000
2	0.0373	37265	0.1085	108537	1000000
6	0.0024	2394	0.0528	52835	1000000
10	4.0000e-06	4	0.0234	23352	1000000
14	0	0	0.0097	9675	1000000
18	0	0	0.0038	3826	1000000
22	0	0	0.0016	1608	1000000
26	0	0	6.2000e-	620	1000000

From the simulation results. It can be seen that in the case of AWGN channel when the SNR increases both the BER and the total number of errors of the BPSK system are decreased. Firstly, while the SNR is -6, the number of bit errors counts 239156. After that, while the SNR reaches 14, the total number of the found bit errors, gives zero-bit error. On the other hand, in the case of Rayleigh distributed fading channel. Both bit errors and BER are reduced when SNR level is increased. Initially, the SNR is set to -6 which gives about 276402 bit errors. Next, the SNR is increased to 6 which produces approximately 52835 bit errors. Lastly, when the SNR level is peaked to 26. Subsequently, the total number of bit errors gives only 620. In comparison of the BPSK system performance of both AWGN and Rayleigh channels. It is clear that the performance of AWGN channel gives better results than Rayleigh channel.

6.1.1.3 BPSK BER performance analysis simulation in Rician & AWGN channel

The Matlab program simulates the BPSK mapped and transmitted signal over both AWGN and Rician Channel. Where the received signal is coherently detected at the receiver side. Where the Rician distribution channel is modelled by implementing two factors the first factor is the total power of both the line of sight path and multiple scattered non LOS paths $P_T = {S_T}^2 + 2.\beta^2$. The second factor is the K Rician factor. The simulation model applies both parameters as inputs to the system. therefore, from the K Rician factor it is necessary to form the Gaussian distribution variation. The value of S_T is calculated by:

$$S_T = \frac{k}{k+1}.P_T \tag{6.13}$$

And the variation of Gaussian distribution β is calculated by

$$\beta = \frac{P_T}{\sqrt{2(k+1)}} \tag{6.14}$$

The Rician distributed channel simulation requires the calculation of the standard deviation and mean of the Gaussian random variables by using the Rician K parameter and the components of both LOS way and non LOS ways. Two Gaussian random variables (x, y) are generated. Where x is produced with a standard deviation equals to β and a mean equals to S_T. On the contrary, the y is generated by using the identical standard deviation β and a mean that equals to zero. By the

Matlab simulation software the $(randn)$ function produces Gaussian random variables with a standard deviation $\beta = 1$ and a mean equals to zero. In order to produce x with a standard deviation $= \beta$ and a mean equals to S_T the result of $(randn)$ function is multiplied by β and combined with S_T.

Input parameters:

The following parameters are implemented by the BPSK system:

Table 6.5: BPSK mapping input parameters over AWGN & Rician channel

Parameter	Value
Transmitted BPSK Source Data Bits	$10^{\wedge 6}$ =1000000 bits
$Ebit/No$ (dB)	-6 to 26
M	2
$R = Log_2(M)$	1
K Rician Factor	1, 10, 20, 30

Simulation results:

The BPSK transmission system through AWGN and Rician channel BER performance is demonstrated by graphing the BER against the related SNR ($Ebit/No$). Thus, the received BPSK modulated signal errors are calculated at every SNR level that is applied.

Table 6.6: BPSK mapping BER performance over Rician & AWGN channel

SNR (DB)	BER k=1	Errors k=1	BER k=10	Errors k=10	BER k=20	Errors k=20	BER k=30	Errors k=30
-6	0.2691	269096	0.2470	246956	0.2430	243020	0.2416	241632
-2	0.1793	179336	0.1418	141792	0.1370	137009	0.1349	134942
2	0.0970	97035	0.0516	51554	0.0449	44888	0.0428	42770
6	0.0441	44122	0.0089	8895	0.0053	5270	0.0042	4222
10	0.0181	18132	7.0000e-	700	1.3700e-	27	6.5000e-	65
14	0.0074	7415	4.6000e-	46	1.0000e-	1	0	0
18	0.0029	2923	4.0000e-	4	0	0	0	0
22	0.0011	1122	2.0000e-	2	0	0	0	0
26	4.7300e-	473	0	0	0	0	0	0

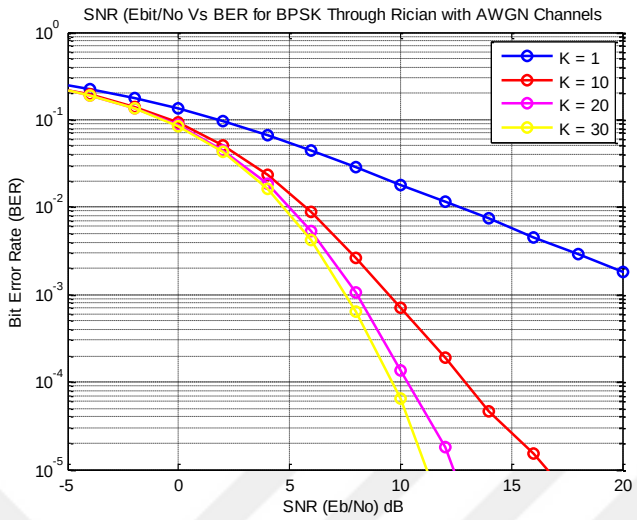

Figure 6.3: BPSK mapping BER performance over Rician & AWGN channel

From the simulation results that it is shown in figure 6.3 and table 6.6. It can be observed that in the case of Rician distributed fading channel with k=1 both the BER and the number of bit errors are minimized when the SNR level is raised up. At first, the SNR initiates to -6 which produces about 269096 bit errors. At last, when the SNR level is peaked up to 26. As a consequence, the number of bit errors counts only 473. After that, when k is raised up to 10. The BER and bit errors are minimized as well when the SNR level is increased. At the initial process, the SNR is set to -6 and the resulted signal generates 246956 bit errors. And at the end of the process a level of SNR equal to 26 is used which produces zero bit errors. In the case that k=20 and the SNR level equals to -6 the bit errors of the output signal are equivalent to 243020. On the other hand, when the SNR level is increased to 18 which generates an output signal with zero bit errors. Finally, while k parameter reaches 30, the BER and bit errors of the received signal are decreased as the SNR level is minimized. At -6 SNR the produced bit error calculation computes 241632. Fortunately, at SNR level of 14 the calculated bit errors are equal to zero value. To sum up, the performance of the BPSK transmission system through Rician fading channel is increased and gives less bit errors as the k factor is raised up.

6.1.2 QPSK Mapping BER Performance in AWGN Channel

The Matlab model simulates the performance of QPSK mapping technique through an AWG noise transmission channel. In QPSK the transmission symbol is constructed of two bits. Therefore, the

produced source data bits are modulated according to the construction of two bits. The QPSK constellation mapping is calculated by:

Table 6.7: QPSK constellation mapping

QPSK Symbol	Calculation Value
00	1+j (phase offset of 45°)
01	-1+j (phase offset of 135°)
10	-1-j (phase offset of 225°)
11	1-j (phase offset of 315°)

After the QPSK symbols are mapped the QPSK modulated signal is applied by a normalization factor $1/\sqrt{2}$. The QPSK transmission AWGN channel is modelled as the applied model in BPSK mapping. The channel model uses the ($randn$) Matlab function to produce the complex channel noise as the QPSK modulated signal is represented in the form of complexity due to the sin and cosine components. The QPSK receiver has two coherent detectors, one is used for retrieving the real inphase component, and the other for retrieving the imaginary quadrature component. The two parts are combined by Matlab reshape function which works as a parallel to serial inverter. The BER performance for QPSK is similar to BPSK due to that the QPSK mapper comprises of two BPSK mappers with a satisfaction of orthogonality between them. Therefore, the probability of bit error is identical to the BPSK mapping system.

6.1.2.1 Input parameters

The following parameters are used by the QPSK system model:

Table 6.8: QPSK mapping input parameters over AWGN channel

Parameter	Value
Source Data Bits Count	1000000
$Ebit/No$(dB)	-6 to 10 step 2
M	4
$R = Log_2(M)$	2

6.1.2.2 Simulation results

The QPSK performance is shown as the graph of the BER vs the measured SNR ($EBIT/No$). Finally, the received QPSK signal bit errors are calculated for each SNR level.

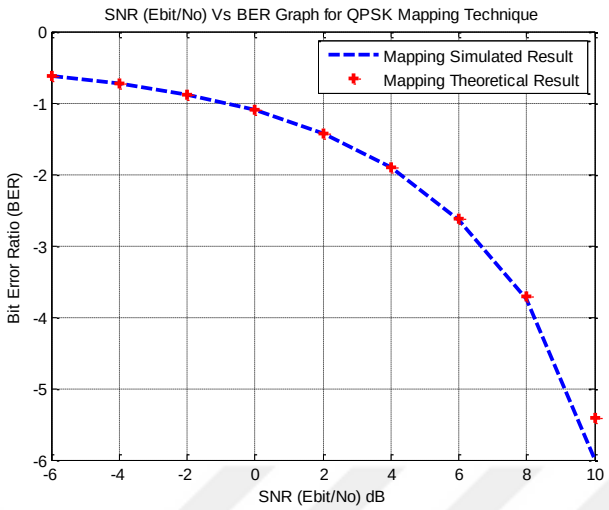

Figure 6.4: QPSK mapping BER performance over AWGN channel

Table 6.9 QPSK mapping over AGWN channel simulation results

Ebit/No(DB)	BER	No. of Errors	Total bits
-6	0.2394	239358	1000000
-2	0.1308	130816	1000000
2	0.0375	37505	1000000
6	0.0023	2305	1000000
10	1.0000e-06	1	1000000
14	0	0	1000000

From the simulation results of QPSK mapping in table 6.9 and the simulation plot in figure 6.4. It is clearly seen that while the SNR rises both the number of bit errors and the BER of the QPSK system are minimized. Firstly, when the SNR is -6, the number of bit errors shows 239358. After that, when the SNR rises to 10, the number of generated bit errors, becomes only one. Lastly, the resulted bit errors equal to zero when the level of SNR is increased to 14. Consequently, the BER performance of QPSK is approximately identical to BPSK.

6.1.3 16-QAM Mapping BER Performance in AWGN Channel

M-QAM mapping technique which combines both M-ASK and M-PSK mapping methods to modulate the source signal in phase and amplitude variations. In the Matlab simulation a rectangular M-QAM mapper is simulated due to its implementation simplicity. The M-QAM mapping is performed either in gray coded type or binary coded type. The gray coded type is

performed in a way in which the source data symbols are subdivided into quadrature and inphase bits which are then mapped into the constellation of M-QAM. Therefore, the M-QAM constellation points are constructed by:

$$MQAM_{(K,L)} = K + jL\ , (k, L) \in \{\pm 1, \pm 3, \dots, (\lceil \sqrt{M} \rceil - 1)\} \tag{6.15}$$

The constellation points $MQAM(N)_{(K,L)}$ total energy for N points is identified by:

$$E_{(K,L)} = \sum_{n}^{N} (S_{I,n}^2 + S_{Q,n}^2) \tag{6.16}$$

Where $S_{I,n}$ and $S_{Q,n}$ are the inphase and quadrature components for a particular constellation point of N points. 16-QAM constellation mapping consists of 16 points. Four points for each quadrant. Since the constellation has four identical quadrants. Thus, power normalization of single quadrant is processed by:

$$Normalization\ Factor = \frac{1}{\sqrt{E_{avg(K,L)}}} = \frac{1}{\sqrt{10}} \tag{6.17}$$

Where $E_{avg(K,L)} = \frac{E_{(K,L)}}{4} = \frac{40}{4} = 10$ and $E_{(K,L)}$ is the total power for each quadrant. The bit error probability of M-QAM mapping is calculated by:

$$P_{bit} = 4/k\left(1 - 1/\sqrt{M}\right) Q\left(\sqrt{3k/M - 1}\right) \tag{6.18}$$

And the probable symbol error calculation is identified by:

$$P_{sy} = 1 - \left(1 - \left(1 - \frac{1}{\sqrt{M}}\right).erfc\left(\sqrt{\frac{3k.Ebit}{2(M-1)No}}\right)\right)^2 \tag{6.19}$$

6.1.3.1 Input parameters

The following parameters are implemented by the 16-QAM system model:

Table 6.10: 16-QAM mapping input parameters over AWGN channel

Parameter	Value
Source Data Bits Count	100000
$Ebit/No$(dB)	-6 to 14 step 2
M	16
$R = Log_2(M)$	4

6.1.3.2 Simulation results

The 16-QAM performance is illustrated in the graph of the BER vs the measured SNR ($EBIT/No$). After that, the received 16-QAM mapped signal bit errors are computed for each SNR level.

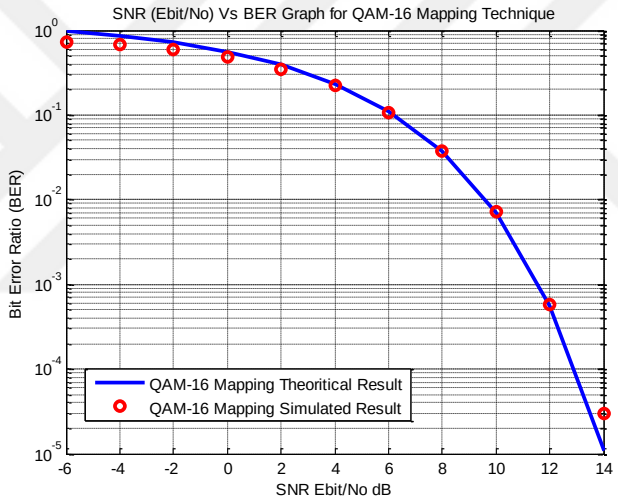

Figure 6.5: 16-QAM mapping BER performance over AWGN channel

Table 6.11 16-QAM mapping over AGWN channel simulation results

Ebit/No(DB)	BER	No. of Errors	Total bits
-6	0.7380	73801	100000
-2	0.5873	58725	100000
2	0.3520	35200	100000
6	0.1080	10801	100000
10	0.0073	730	100000
14	3.0000e-05	3	100000
18	0	0	100000

From the simulation results of 16-QAM mapping in table 6.11 and the simulation plot in figure 6.5. It is obviously illustrated that while the SNR increases both the bit errors and the BER of the

16-QAM system are reduced. At first, when the SNR is -6, the number of bit errors shows 73801. After that the bit errors are decreased gradually until the SNR level equals to 6. Next the bit errors are reduced sharply until they are reached only 3 where SNR equals to 14. At last, the generated bit errors equal to zero when the level of SNR is raised to 18.

6.1.4 64-QAM Mapping BER Performance in AWGN Channel

64-QAM mapping technique is similar to 16-QAM except that the constellation points equal to 64 and each modulated symbol consists of 6 bits which is higher than the 4 bits per symbol rate in 16-QAM. 64-QAM constellation mapper consists of 64 points. 16 points for each quadrant. Since the constellation has four identical quadrants. Thus, power normalization of single quadrant is processed by:

$$Normalization\ Factor = \frac{1}{\sqrt{E_{avg(K,L)}}} = \frac{1}{\sqrt{42}} \tag{6.20}$$

Where $E_{avg(K,L)} = \frac{E_{(K,L)}}{16} = \frac{672}{4} = 42$ and $E_{(K,L)}$ is the total power for each quadrant. The bit error probability of 64-QAM mapper is similar to the calculation of 16-QAM mapper.

6.1.4.1 Input parameters

The following parameters are entered to the 64-QAM system model:

Table 6.12: 64-QAM mapping input parameters over AWGN channel

Parameter	Value
Source Data Bits Count	100000
$Ebit/No$(dB)	-6 to 18 step 2
M	64
$R = Log_2(M)$	6

6.1.4.2 Simulation results

The 64-QAM performance is demonstrated in the plotting of the BER against the measured SNR ($EBIT/No$). Lastly, the received 64-QAM mapped signal is analyzed for bit errors for each SNR level. From the simulation results of 64-QAM mapper in table 6.13 and the simulation plot in figure 6.6. It is can be seen that when the SNR increases both the bit errors and the BER of the 64-

QAM system are decreased. Initially, the SNR is set to -6 which gives a number of bit errors of 90265. Then the bit errors are minimized gradually unless the SNR level becomes 10. After that the bit errors are decreased sharply until they become only 4 when the SNR equals to 18. Finally, the generated bit errors give zero when the level of SNR is increased to 20.

Table 6.13: 64-QAM mapping over AGWN channel simulation results

Ebit/No(DB)	BER	No. of Errors	Total bits
-6	0.9026	90265	100000
-2	0.8275	82752	100000
2	0.6818	68185	100000
6	0.4370	43697	100000
10	0.1527	15272	100000
14	0.0130	1303	100000
18	4.0000e-05	4	100000

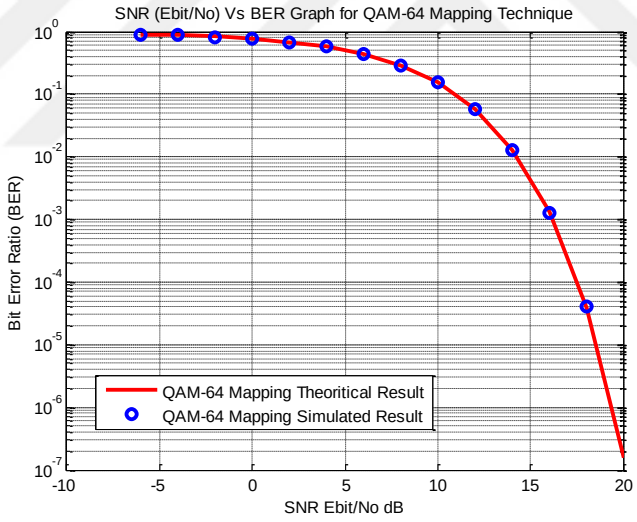

Figure 6.6: 64-QAM mapping BER performance over AWGN channel

6.1.5 Performance Comparison of LTE Constellation Mapping Types

In this simulation several constellation mapping techniques which are used in LTE networks are theoretically evaluated during transmission through AWG noise channel. The spectral efficiency of linear mapping technique that has M constellation points is identified by:

$$\eta = log_2(M)\ bits/s/Hz \tag{6.21}$$

Which identifies the rate of bits per transmitted symbol R and by applying a raised cosine filter pulse shaping with a roll-off factor of β. The lowest bandwidth is calculated by:

$$BW_{min} = 1 + \beta(R/\eta) \tag{6.22}$$

Therefore, the capacity of the system over AWG noise is calculated by the Shannon's equation:

$$C = BWlog\left(1 + \frac{C}{BW}.\frac{Ebit}{No}\right) \tag{6.23}$$

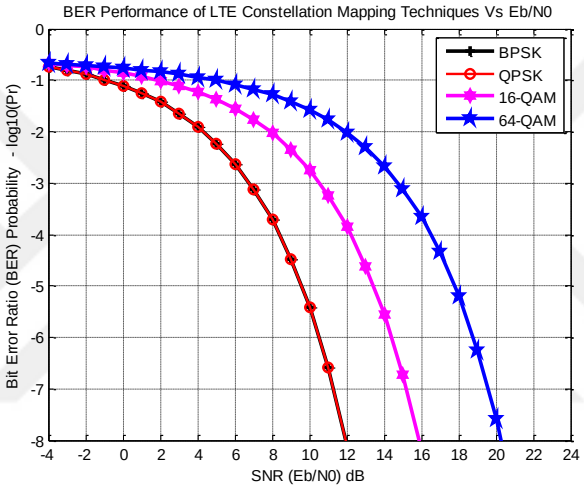

Figure 6.7: BER performance of LTE constellation mapping techniques

From the simulation graph in figure 6.7. it is distinguished that both BPSK and QPSK produce better results than 16-QAM and 64-QAM mapping schemes. Furthermore, 16-QAM performs well in comparison with 64-QAM modulation. To sum up, as the rate of bits per symbol increases the number of bit errors increases.

6.2 OFDM BER PERFORMANCE SIMULATION

The analysis of OFDM transmission system and the simulation of its various functions are implemented using Mathworks Matlab simulation software. The evaluation of the OFDM system is carried out according to several constellation mapping techniques. The output results are analyzed for the transmission performance regarding to the BER factor. Initially, the source binary data sequence is randomly generated using a Matlab function. After that the produced data bits are mapped into several symbols in terms of the constellation mapping bits per every symbol rate. In

the next stage, the mapped symbols are modulated according to one of the constellation mapping techniques such as BPSK, QPSK and QAM. The serial modulated symbols are subdivided by Matlab reshape function into parallel sub sequences of N orthogonal subcarriers (from 0 to $N-1$). After that channel estimation pilot addition takes place which is used for synchronization process at an OFDM receiver. The parallel N mapped symbols with pilot bits feed an IFFT algorithm.

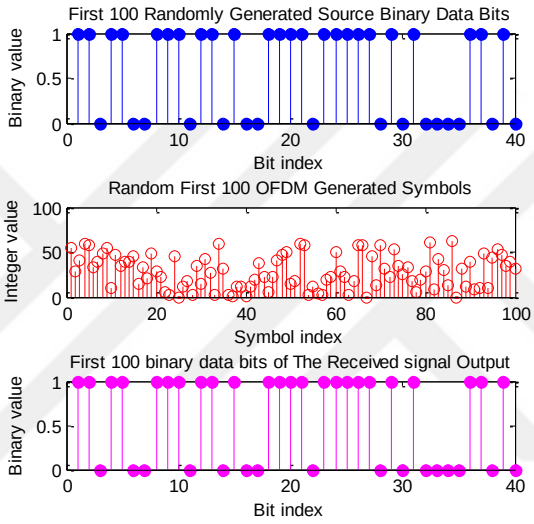

Figure 6.8: OFDM input bits, generated symbols & output bits graph

The IFFT alters the frequency domain representation to a time domain representation by multiplying the signal with a series of sine waves. This process splits the signal into various bins of frequency. The complex result of the IFFT process is added a guard interval which is named cyclic prefix CP. The produced parallel complex values with CP addition are inversed back to a series form. Then the resulted series values are inversed by DAC to an analogue waveform. After that the RF circuit transmits the signal by the transmission antenna. In RF circuit N parallel oscillators are tuned to independent frequencies of N size $(f1, f2, f3, f4, \dots \dots fN-1)$. At the OFDM receiver the received signal is altered to digital waveform by ADC and then the cyclic prefix is eliminated and avoided. After that the series values are inversed to parallel values that are used as an input to the FFT algorithm where the received signal is transformed back to frequency representation format. After that the parallel frequency domain symbols are inversed into a series

form. Then the series form symbols are demodulated using the same constellation mapping that is implemented at the OFDM transmitter. Finally, the original binary bits are retrieved.

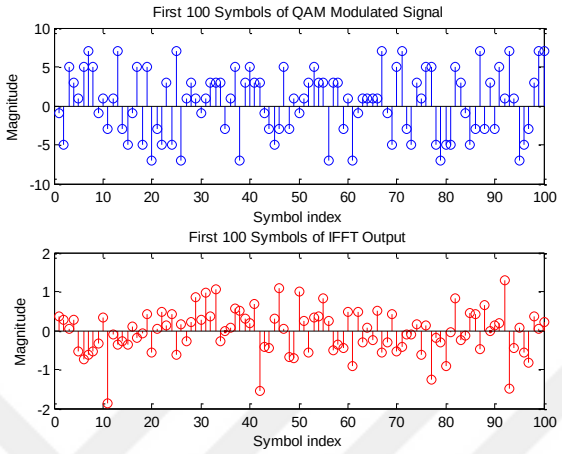

Figure 6.9: OFDM 16-QAM mapping output & IFFT operation output

In practice, not all of the IFFT size N subcarriers are exploited for data transmission. Some are used as pilot additives for channel estimation. Moreover, OFDM transmission operations do not implement subcarriers that are located at the start and at the end for data transmission.

6.2.1 OFDM Using BPSK Mapping BER Performance Simulation

To design an OFDM transmission system with BPSK constellation mapping. the design parameters are considered as the important stage of the design process. The transmission channel is modelled as Gaussian noise AWGN which is generated using ($randn$) Matlab function. The required generated noise is identified by:

$$Required\ noise = 10^{\frac{Esy}{No}\cdot\frac{1}{20}} * noise \tag{6.24}$$

By the addition of CP the power energy of each OFDM symbol is distributed within ($N + N\_CP$) bits and the relationship between them is identified by:

$$Esy(N + N\_CP) = N.Ebit \tag{6.25}$$

$$Esy.N = N_{Used\ Subcarriers}.Ebit$$

Therefore, the effects of inserted CP on the value of Esy/No is defined by:

$$\left(\frac{Esy}{No}\right)_{dB} = \left(\frac{N}{N + N\_CP}\right)_{dB} + \left(\frac{N_{Used\ Subcarriers}}{N}\right)_{dB} + \left(\frac{Ebit}{No}\right)_{dB} \quad (6.26)$$

The produced signal of the inversion of parallel to series after inserting the CP must be scaled to compensate the lost energy of the addition of CP. The Matlab model scales the signal for final transmission by:

$$Scaled\ OFDM\ Signal = \sqrt{\frac{N_{CP} + N}{N}}\, OFDM\ Signal_{After\ Parrallel\ to\ Serial} \quad (6.27)$$

6.2.1.1 Input parameters

The following parameters are entered to the BPSK-OFDM system model:

Table 6.14: OFDM using BPSK mapping over AWGN channel input parameters

Parameter	Value
Source Data Bits Count	521040 bits
$Ebit/No$(dB)	-10 to 10 step 2
$R = Log_2(M)$ Bits Per Symbol for BPSK	1
IFFT size of N Subcarriers	64
No of Subcarriers for Data Transmission	48
No of Subcarriers for Pilot Insertion	4
No of Unused Zero Padded Subcarriers	12
OFDM System BW	20 MHz =20*10^6
Δf Frequency Spacing	BW/N=20 MHz/64= 0.3125 MHz
T_FFT IFFT/FFT Period	1/Δf=1/0.3125=3.2μs
T_CP Cyclic Prefix Period	T_FFT/4
T_Signal Signal Period	T_FFT+T_CP
CP_Length	16
N_CP Cyclic Prefix Symbols	N*T_CP/T_FFT
Symbols_Subcarrier symbols Per N Subcarrier	52
N_Symbols Symbols Count	10020

6.2.1.2 Simulation results

The OFDM system with BPSK mapping technique performance is demonstrated in the graph of BER against various measured SNR levels ($EBIT/No$). finally, the received OFDM modulated signal is evaluated for bit error computation for each measured SNR level.

Table 6.15 OFDM with BPSK mapping over AGWN channel simulation results

Ebit/No(DB)	BER	No. of Errors	Total bits
-10	0.3274	170601	521040
-6	0.2395	124778	521040
-2	0.1302	67838	521040
2	0.0373	19427	521040
6	0.0024	1263	521040
10	5.7577e-06	3	521040
11	0	0	521040

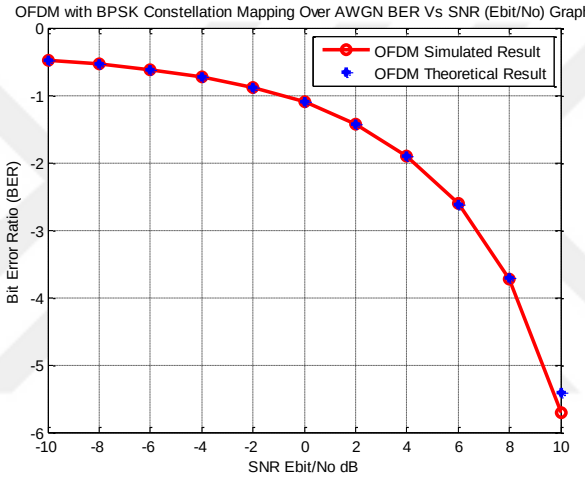

Figure 6.10: OFDM with BPSK mapping BER performance over AWGN

From the simulation results of OFDM with BPSK constellation mapper in table 6.15 and the simulation graph in figure 6.10. It is obvious that whenever the SNR level increases both the bit errors and the BER of the BPSK-OFDM system are decreased. firstly, the SNR initiates to -10 which generates bit errors of 170601. Then bit errors are minimized slowly up to 19427 when SNR level approaches 2. After that the bit errors go down deeply until they count only 3 bit errors. where the SNR equals to 10. Finally, the bit errors compute zero as the level of SNR is raised approximately up to 11.

6.2.2 OFDM Using (16-64)-QAM Mapping BER Performance Simulation

6.2.2.1 Input parameters

The following parameters are configured as inputs to the OFDM with (16-64)-QAM constellation mapping simulation model:

Table 6.16: OFDM using (16-64)-QAM mapping over AWGN input parameters

Parameter	Value
Source Data Bits Count	521040 bits
$Ebit/No$(dB)	-10 to 20 step 2
M	16 For 16-QAM, 64 For 64-QAM
$R = Log_2(M)$ Bits Per Symbol	4 For 16-QAM, 6 For 64-QAM
IFFT size of N Subcarriers	64
No of Subcarriers for Data Transmission	52
No of Subcarriers for Pilot Insertion	4
No of Unused Zero Padded Subcarriers	12
OFDM System BW	20 MHz =20*10^6 Hz
Δf Frequency Spacing	BW/N=20 MHz/64= 0.3125 MHz
T_FFT IFFT/FFT Period	$1/\Delta f$=1/0.3125=3.2μs
T_CP Cyclic Prefix Period	T_FFT/4
T_Signal Signal Period	T_FFT+T_CP
CP_Length	N/4 =16
N_CP Cyclic Prefix Symbols	N*T_CP/T_FFT
Symbols_Subcarrier symbols Per N Subcarrier	52
N_Symbols Symbols Count	10020

6.2.2.2 Simulation results

The OFDM system with (16-64)-QAM constellation mapping technique performance is shown in the graph of BER vs various measured SNR levels ($EBIT/No$). eventually, the received OFDM QAM modulated signal is analyzed for bit error calculation for each given SNR level.

Table 6.17: OFDM with (16-64)-QAM mapping over AWGN simulation results

Ebit/No (DB)	16-QAM BER	16-QAM No. of Errors	64-QAM BER	64-QAM No. of Errors	Total Bits
-10	3.711327e-01	193375	3.924900e-01	204503	521040
-6	2.863062e-01	149177	3.293336e-01	171596	521040
-2	1.876862e-01	97792	2.454303e-01	127879	521040
2	9.773914e-02	50926	1.562932e-01	81435	521040
6	2.783088e-02	14501	8.400123e-02	43768	521040
10	1.779134e-03	927	2.639912e-02	13755	521040
14	1.919238e-06	1	2.187932e-03	1140	521040
16	0	0	1.900046e-04	99	521040
18	0	0	5.757715e-06	3	521040
19	0	0	0	0	521040

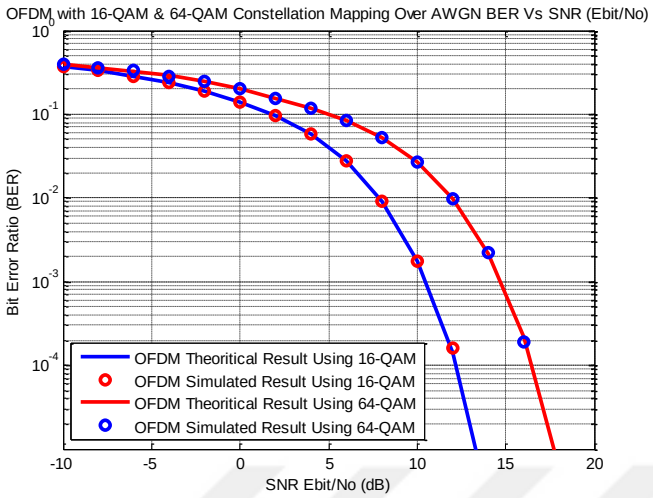

Figure 6.11: OFDM with (16-64)-QAM mapping BER performance over AWGN

From the Matlab model results of OFDM with (16-64)-QAM constellation mapper in table 6.17 and the simulation graph in figure 6.11. It can be seen obviously that whenever the SNR level rises up both bit errors and BER of the OFDM with (16-64)-QAM system increase. In the case of OFDM with 16-QAM, the SNR initiates to -10 which produces bit errors of 193375. This number of bit errors decreases gradually to 50926 when SNR level reaches 2. After that bit errors decrease rapidly unless they show only one-bit error. when SNR measures 14. Finally, bit errors count zero as the level of SNR reaches up to 16. On the other hand, in the case of OFDM system with 64-QAM. When SNR is set to -10 the system produces 204503 of bit errors. These bit errors decrease slowly until SNR becomes 10. After that bit errors go down sharply unless they count zero at 19 SNR level. To sum up, the OFDM system performance is degraded as the modulation order is increased.

6.3 OFDM PERFORMANCE AFTER ENCODING & DECODING SIMULATION

The OFDM modulated signal is encoded at the transmitter and decoded at the receiver. These encoding and decoding processes are performed to minimize bit errors and provide the ability for bit error recovery. The source binary bits are encoded before the constellation mapping at the transmitter. Inversely, the decoding process is applied at the receiver after the constellation de-mapping. The Matlab simulations simulate the performance of Turbo coding technique as it is the primary method that is employed by LTE networks.

6.3.1 16QAM-OFDM BER Performance of Turbo Encoding Simulation

This Matlab model simulates the process of coding using a turbo coding block. Which encodes source binary data stream by implementing a coding technique applying a parallel concatenating process. This process exploits convolutional coding method by a single interleaver and double of equal convolutional encoders. Each encoder is stopped by tail bits independently. The result of the turbo encoder comprises of three sequences. Two sequences of the first encoder, parity sequence and systematic sequence. And only parity bit sequence of the other encoder. The turbo encoder uses an input of a column vector of size $(S * 1)$ and generates an output of a column vector of size $K * 1)$. For a particular trellis L and M has the following relationship:

$$A = B.(2.n - 1) + 2.tails\_no) \tag{6.28}$$

$$B = \frac{(A - 2.tails\_no)}{(2.n - 1)}$$

Where:

$$n = log_2(trellis.Symbols_{out}), when\ n = 2, gives\ a\ rate\ of\ ½$$

And:

$$tails_{no} = log_2(trellis.states_{no}) * n$$

This simulation implements the Trellis structure parameter of $poly2trellis(4, [13\ 15], 13)$ for 64 bits input and 204 bits output. Where the initial 192 bits refer to three sequences of 64 bits constructed by ($X_k^{systematic}$ and Z_k^{parity} bit sequences from the initial encoder and Z_k^{parity} bit sequence of the final encoder). The remains of 12 bits refer to the tail bits from both encoders. Unfortunately, because of the tail bits the coding rate is lower than $1/3$. The simulation uses (comm. TurboEncoder) and (comm. TurboDeccoder) Matlab functions. The transmitter, generates the random source binary data and then generates interleaver indices randomly. After that the bit sequence is encoded using $1/3$ turbo encoder and then mapped by 16-QAM modulator. The receiver demodulated the received signal using 16-QAM de-mapper and finally the data sequence is decoded using a turbo decoder with the same coding type at the transmitter.

6.3.1.1 Input parameters

The following parameters are configured as inputs to the OFDM uses 16-QAM constellation mapping with turbo encoding simulation model:

Table 6.18: 1/3 Turbo encoding of 16-QAM over AWGN input parameters

Parameter	Value
Data Packet Length	521040 bits
$Ebit/No$(dB)	2 to 6 Step 0.25
M	16
$R = Log_2(M)$ Bits Per Symbol	4
InterleaverIndices	521040
Turbo Encoder Type	Trilles Structure
Trilles Structure Parameter	$poly2trellis(4, [13\ 15], 13)$
$NumIterations$, Number of Iteration	4

6.3.1.2 Simulation results

The OFDM system with 16-QAM constellation mapping technique and $1/3$ turbo encoder performance is shown in the graph of coded and un-coded signal BER vs various measured SNR levels ($EBIT/No$). Eventually, the system is analyzed for bit errors.

From the Matlab simulation model of 16-QAM constellation mapper with $1/3$ turbo encoder in table 6.19 and the simulation plot in figure 6.12. It can be distinguished that the coded modulated signal provides a high BER performance in comparison with the un-coded signal. Subsequently, bit errors are lower because that the coding process avoids occurrence of bit errors by encoding the source bits into a code word. The receiver decodes the signal and retrieve the original sequence with less errors due to that the occurrence of errors is happened on the extra coded bits instead of on the original bits. On the one hand, the coded 16-QAM modulated signal generates approximately 22000 bit errors as the SNR measures 2. The bit errors go down rapidly until they show only 3 errors at 3 SNR level. And produce zero bit errors since the SNR measures 3.5. on the other hand, in the case of un-coded signal the BER performance shows a degradation and bit error probability is extremely high if it is compared with the coded signal. At first, the SNR initiates to 2 in which the bit error probability gives about 25500 bit errors. After that it is observed that figure is gradually lowered as the quality of signal is increased. At SNR level of 6 the modulated signal computes only 721 bit errors.

Table 6.19: OFDM with 16-QAM & turbo encoding over AWGN simulation results

Ebit/No (DB)	16-QAM Coded BER	16-QAM Coded No. of Errors	16-QAM Uncoded BER	16-QAM Uncoded No. of Errors	Total Bits
2	0.0422	21984	0.0491	25569	521040
2.5	0.0090	4684	0.0367	19110	521040
3	2.5910e-04	135	0.0259	13504	521040
3.25	3.8385e-06	3	0.0219	11436	521040
3.5	0	0	0.0183	9525	521040
4	0	0	0.0120	6273	521040
4.5	0	0	0.0077	4014	521040
5	0	0	0.0046	2405	521040
5.5	0	0	0.0027	1386	521040
6	0	0	0.0014	721	521040

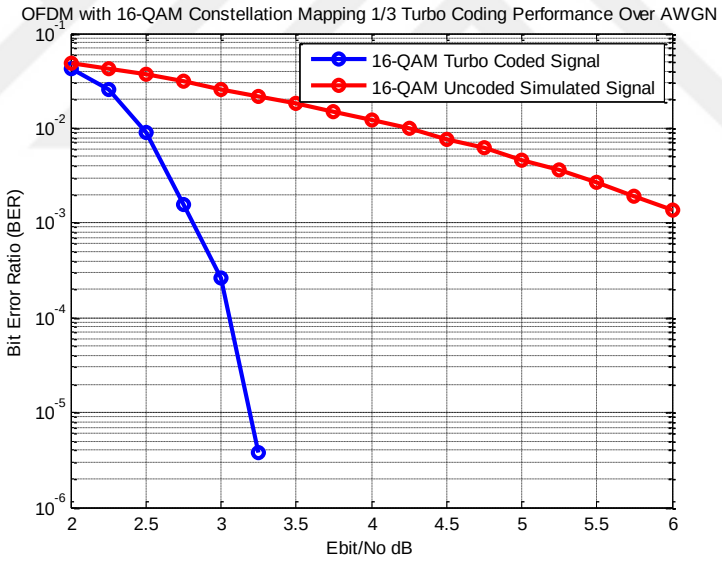

Figure 6.12: 1/3 Turbo encoder with 16-QAM mapper BER performance

6.4 OFDM PAPR DECREASING PERFORMANCE ANALYSIS SIMULATION

The PAPR is considered as the important key factor when designing an OFDM transmission system. However, high PAPR degrades the performance in the case of utilizing a high power amplifier works in the regain of non-linearity. Therefore, several PAPR decreasing techniques are proposed and evaluated for better performance using Matlab simulation models.

6.4.1 PAPR of OFDM with QPSK Mapper Simulation

The simulation model statistically analyzes PAPR by implementing the CCD function which is used to compute the increasing of PAPR probability above a predefined PAPR reference point $[CCDF(PAPR > PAPR\_REF)]$. The PAPR of the transmitted OFDM signal is calculated by:

$$PAPR_{Sk} = 10.log_{10}\frac{max|Sk|^2}{Ev|Sk|^2} \quad (6.29)$$

Initially, the OFDM simulation model evaluates the BER performance without employing any of PAPR decreasing techniques. The achieved results are then compared with other PAPR decreasing methods simulations to distinguish the effects of PAPR on BER. The modulated signal is transmitted over a Rayleigh channel consists of 6 multipath delays.

6.4.1.1 Input parameters

The following parameters are initiated as inputs to the OFDM system that uses QPSK constellation mapper for PAPR computation simulation model:

Table 6.20: PAPR calculation of OFDM with QPSK mapper input parameters

Parameter	Value
FFT Size of N Subcarriers	128
Δf Spacing Frequency (Khz)	15
OFDM_BW Bandwidth (Mhz)	1.25
CP Cyclic Prefix	¼ N=32
Frequency of Sampling Fsa (Mhz)	192
Number of Symbols Per Subcarrier	1000
Sampling Period Tsa	$1/Fsa$
$Ebit/No$ SNR Range	-6 to 14 step 2
Total of Transmitted Symbols	127744
Bits Per Symbol for QPSK	2
Source Data Binary Bits	2 x 127744=255488

6.4.1.2 Simulation results

The BER simulation results of the OFDM system with QPSK mapper without processing any of PAPR decreasing methods are shown in figures 6.13, 6.14 and table 6.21. finally, the received OFDM modulated signal is analyzed for error computation for each measured SNR level.

Table 6.21: QPSK-OFDM without PAPR decreasing over Rayleigh simulation results

Ebit/No(DB)	BER	No. of Errors	Total Bits
-6	0.3662	93564	255488
-2	0.2741	70040	255488
2	0.1436	36677	255488
6	0.0348	8899	255488
10	0.0013	323	255488
14	0	0	255488

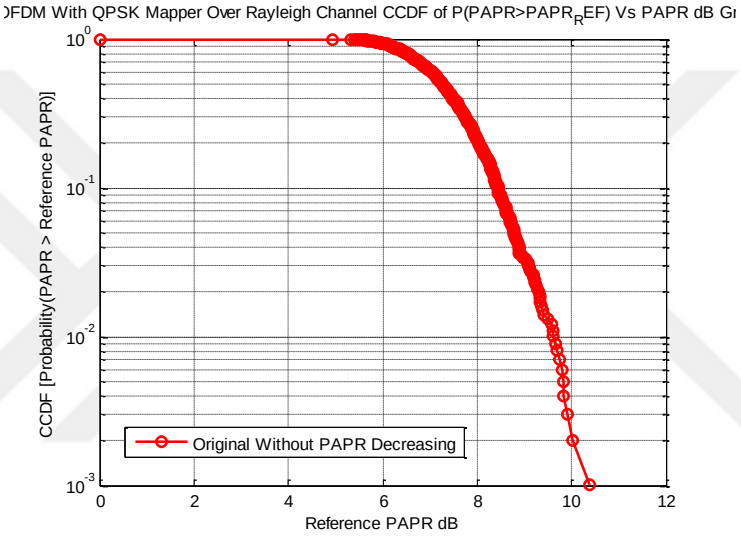

Figure 6.13: CCDF of PAPR without any PAPR decreasing technique

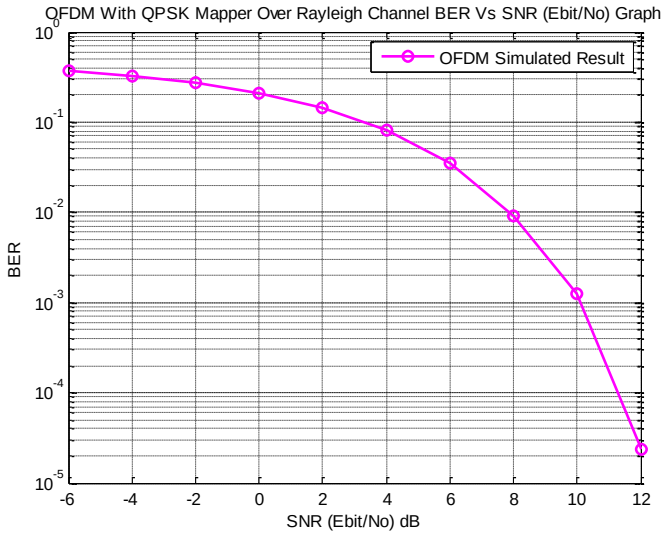

Figure 6.14: OFDM BER VS SNR (Ebit/No) over Rayleigh channel

The BER performance at the variation of the SNR decreases since the SNR increases. When SNR equals to zero the computed errors equal to 93564. At last, whereas SNR is set to 14 the calculation of errors gives zero. The simulation model calculates about 10.37 dB reference PAPR of the CCD function of PAPR and generates a value of PAPR in dB of the transmitted signal approximately equals to 25 dB.

6.4.2 QPSK-OFDM Simulation with RCF PAPR Decreasing Technique

The iteration of clipping RC is applied in time domain on the amplitude of the IFFT operation output complex values and filtering F is used to avoid out of band noise. Whereas the in band noise cannot be recovered. By using L factor of oversampling the vector of input is expanded in the center by zeros of $(L-1)$. This process interpolates the signal. Then the clipping process is carried out on the output of the IFFT operation. The clipped signal can be defined by:

$$C_{SIGNAL} = \begin{cases} \sqrt{CR.Ev[|Sk|^2]}.\dfrac{Sk}{|Sk|} & |Sk|^2 > C_{ref} \\ Sk & |Sk|^2 \leq C_{ref} \end{cases} \tag{6.30}$$

Where CR represents the clipping rate which describes the ratio between the clipping range and mean power of the original baseband signal without clipping. And C_{ref} represents the predefined clipping threshold. $|Sk|^2$ represents the power of Sk and $Ev[|Sk|^2]$ represents the mean power. After clipping process, the signal is filtered to eliminate the out of band noise that is produced due to the clipping process. The filtration process contains one FFT followed by IFFT. The clipped signal is inversed back to frequency domain by FFT operation. The out of band noise is avoided and the in band noise is entered the second IFFT operation. This process is iterated according to the defined number of iteration (1 to 4 as usual). In LTE-OFDM system. in order to decrease PAPR of the downlink signal a variation of CR and L factor values are applied in RCF technique. The best results of BER and PAPR are accepted.

6.4.2.1 Input parameters

The input parameters are set to the QPSK-OFDM system over Rayleigh channel which uses RCF PAPR decreasing technique constellation mapper for PAPR computation simulation model:

Table 6.22: RCF PAPR calculation of OFDM with QPSK input parameters

Parameter	Value
FFT Size of N Subcarriers	128
Δf Spacing Frequency (Khz)	15
OFDM_BW Bandwidth (Mhz)	1.25
CP Cyclic Prefix	¼ N=32
Frequency of Sampling Fsa (Mhz)	192
Number of Symbols Per Subcarrier	1000
Sampling Period Tsa	$1/Fsa$
$Ebit/No$ SNR Range	-6 to 20 step 2
Total of Transmitted Symbols	127744
Bits Per Symbol for QPSK	2
Source Data Binary Bits	2 x 127744=255488
CR Rate of Clipping	[1.5, 2, 3, 4]
Factor of Oversampling L	[1.5, 2, 3, 4]
Iteration count	4

6.4.2.2 Simulation results

The BER performance and PAPR calculation simulation results of RCF PAPR decreasing method are shown in figures 6.15, 6.16 and tables 6.23, A.1. finally, the received OFDM modulated signal is analyzed for error computation for each measured SNR level. The counted errors go down since the SNR increases. When SNR shows -6 the generated errors count 55118. Whereas the SNR is equal to 10 the occurred errors count zero. The simulation model implements a clipping rate of 3 and an oversampling factor of 4. The model calculates about 5.78 dB reference PAPR of the CCD function after four clipping operations. And generates a PAPR level of the transmitted signal equals to 13.5 dB. Which is lower than the level obtained from OFDM system without any PAPR decreasing method.

Table 6.23 QPSK-OFDM with RCF PAPR decreasing simulation results

Ebit/No(DB)	BER	No. of Errors	Total Bits
-6	0.2157	55118	255488
-2	0.0859	21944	255488
2	0.0110	2814	255488
6	1.8788e-04	48	255488
10	0	0	255488

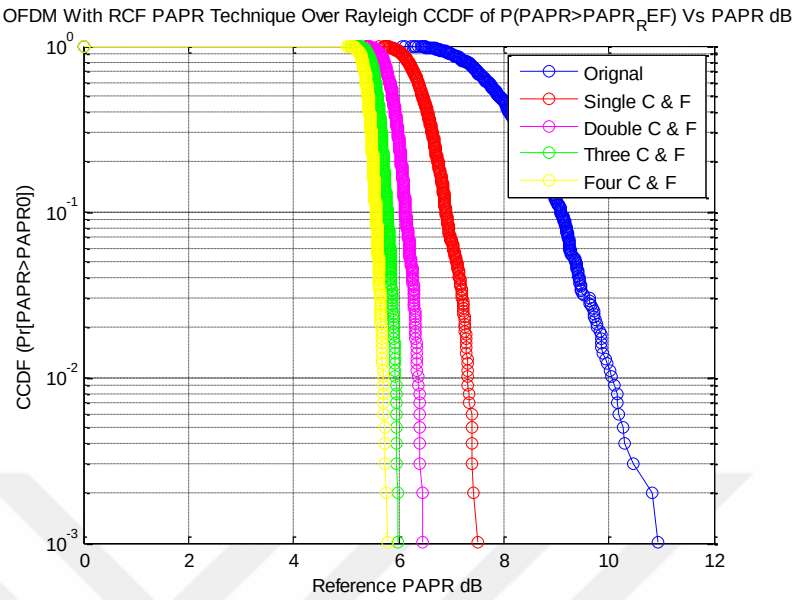

Figure 6.15: CCDF of PAPR (CR=3, L=4) of RCF PAPR decreasing technique

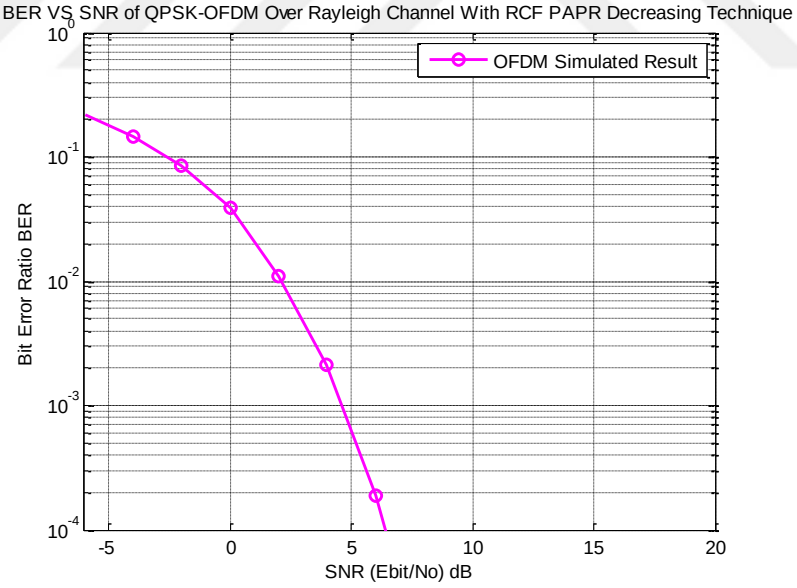

Figure 6.16: OFDM with (CR=3, L=4) RCF BER VS SNR (Ebit/No)

When CR=3 and L=4 the CCDF of PAPR of one RCF gives about 7.5 dB, two RCF produces 6.4 dB, three RCF generates 6 dB and finally four RCF iterations introduces about 5.78 dB. Whenever the clipping rate CR and oversampling factor L increase the PAPR increases as well. But fortunately the bit errors decrease in the meanwhile. The RCF performs better than [21].

6.4.3 QPSK-OFDM Simulation with RFC PAPR Decreasing Technique

The repeating process of filtering and clipping RFC works as the same principle of RCF process except that the filtering is processed in frequency domain prior clipping in time domain. In this technique the filtering enhances the BER performance, whereas the clipping enhances the effects of PAPR. The output of IFFT operation is filtered in frequency domain by implementing FFT operation followed by IFFT operation. The filtered signal is then clipped in time domain according to the clipping rate CR. The out of band noise is avoided and the in band noise is entered the second IFFT operation. This process is iterated according to the defined number of iteration (1 to 4 as usual). In LTE-OFDM system. in order to decrease PAPR of the downlink signal several values CR and L factor are entered in RFC technique. The best results of BER and PAPR are approved.

6.4.3.1 Input parameters

The following input parameters are initiated to the QPSK-OFDM system over Rayleigh channel which uses RFC PAPR decreasing technique for PAPR calculation simulation model:

Table 6.24: RFC PAPR calculation of OFDM with QPSK input parameters

Parameter	Value
FFT Size of N Subcarriers	128
Δf Spacing Frequency (Khz)	15
OFDM_BW Bandwidth (Mhz)	1.25
CP Cyclic Prefix	¼ N=32
Frequency of Sampling Fsa (Mhz)	192
Number of Symbols Per Subcarrier	1000
Sampling Period Tsa	$1/Fsa$
$Ebit/No$ SNR Range	-6 to 20 step 2
Total of Transmitted Symbols	127744
Bits Per Symbol for QPSK	2
Source Data Binary Bits	2 x 127744=255488
CR Rate of Clipping	[1.5, 2, 3, 4]
Factor of Oversampling L	[1.5, 2, 3, 4]
Iteration count	4

6.4.3.2 Simulation results

The BER performance and PAPR decreasing simulation results of RFC PAPR decreasing method are illustrated in figures 6.17, 6.18 and tables 6.25, A.2. The received OFDM modulated signal is

evaluated for error counting for every measured SNR level. The bit errors decrease since the SNR increases. When SNR shows -6 the generated errors give 54590. Whereas the SNR is equivalent to 9 the produced errors count zero. The simulation model implements a clipping rate of 3 and an oversampling factor of 4. The model calculates about 4.8451 dB reference PAPR of the CCD function after four filtering and clipping operations. And generates a PAPR level of the transmitted signal equals to 11.7533 dB. Which is lower than the level that is obtained from the OFDM system without any PAPR decreasing method and also better than the RCF technique.

Table 6.25: QPSK-OFDM (CR=3, L=4) of RFC PAPR decreasing simulation results

Ebit/No(DB)	BER	No. of Errors	Total Bits
-6	0.2137	54590	255488
-2	0.0864	22079	255488
2	0.0109	2796	255488
6	1.2525e-04	32	255488
9	0	0	255488

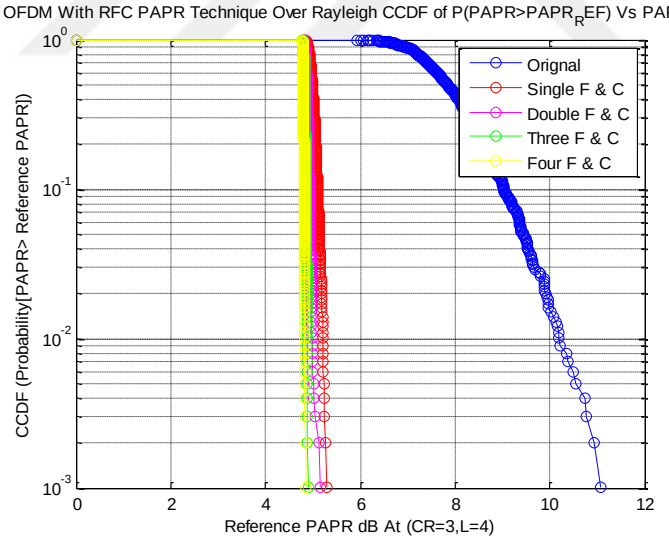

Figure 6.17: CCDF of PAPR (CR=3, L=4) of RFC PAPR decreasing technique

While CR=3 and L=4 the CCDF of PAPR of one RFC gives about 5.2829 dB, two RFC produces 5.1693 dB, three RFC generates 4.8949 dB and finally, four RFC iterations introduces about 4.8451 dB. Whenever the clipping rate CR increases the PAPR increases as well. But fortunately the bit errors decrease in the meanwhile. On the other hand, while L is raised up the bit errors are minimized and the calculation of PAPR is approximately the same.

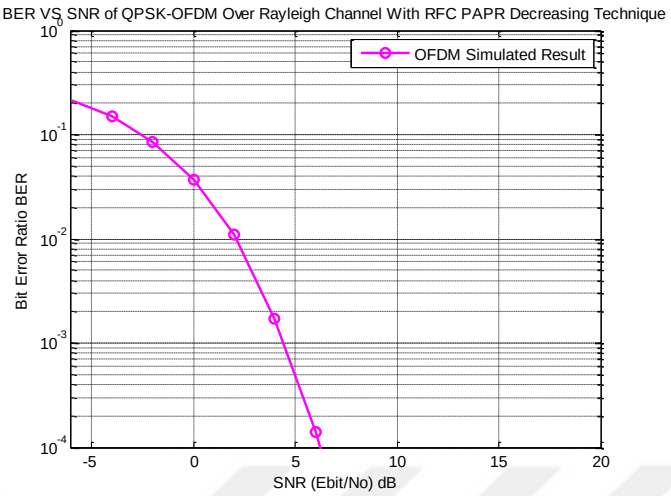

Figure 6.18: OFDM with RFC BER VS SNR (Ebit/No)

6.4.4 QPSK-OFDM Simulation with Companding PAPR Decreasing Techniques

The companding process is performed in discrete time domain and it comprises of two operations. The first compresses the signal at the transmitter and the second expands the signal at the receiver. The companding processes the signal in a range greater than the noise level. While the source signal is low, increasing the SNR is the main benefit of the companding process which minimizes the effects of noise of source. Different companding techniques are configured to reduce PAPR. Such as the popular A-Law and u-Law. Bur this thesis proposes new techniques that give better results. These techniques implement the exponential method and the $tanhR$ method.

6.4.4.1 QPSK-OFDM simulation with AEXP companding technique

The AEXP companding technique is performed by applying the absolute value of the exponential companding result which is defined by:

$$AEXP(Sk) = sgn(Sk).\left|\sqrt[i]{\alpha\left[1 - e^{\left(-\frac{|Sk|^2}{\sigma^2}\right)}\right]}\right| \tag{6.31}$$

The produced signal of the EXP exponential companding is extremely distorted as the square root of the EXP companding represents an imaginary complex value. Subsequently, of taking the absolute value of that square root phase distortion can be avoided. Where $sgn(Sk)$ denotes the

sign function and α indicates to the output signal average power which is always positive. In order to maintain that the input average power equals the output average power this should be satisfied:

$$\alpha = \left(\frac{Ev[|Sk|^2]}{Ev \sqrt[i]{\left[1 - e^{\left(\frac{|Sk|^2}{\sigma^2}\right)}\right]^2}} \right)^{\frac{i}{2}} \tag{6.32}$$

The inversion $AEXP^{-1}(Sk)$ is performed at the receiver where the signal is de-companded by:

$$AEXP^{-1}(Sk) = sgn(Sk).\left| \sqrt{-\sigma^2 log_e \left(1 - \frac{Sk^{\frac{2}{i}}}{\alpha}\right)} \right| \tag{6.33}$$

Where i represents the AEXP constant. The compressing is performed after the insertion of CP at the transmission and the expanding is carried out before the removing of CP at the reception side.

Input parameters:

The following input parameters are setup into the QPSK-OFDM system over Rayleigh channel which uses AEXP PAPR decreasing technique for PAPR calculation simulation model:

Table 6.26: AEXP PAPR calculation of OFDM with QPSK input parameters

Parameter	Value
FFT Size of N Subcarriers	128
Δf Spacing Frequency (Khz)	15
OFDM_BW Bandwidth (Mhz)	1.25
CP Cyclic Prefix	¼ N=32
Frequency of Sampling Fsa (Mhz)	192
Number of Symbols Per Subcarrier	1000
Sampling Period Tsa	$1/Fsa$
$Ebit/No$ SNR Range	-6 to 20 step 2
Total of Transmitted Symbols	127744
Bits Per Symbol for QPSK	2
Source Data Binary Bits	2 x 127744=255488
AEXP_Coefficient	0.2 to 1.8 step 0.4

Simulation results:

The BER performance and PAPR decreasing simulation results of AEXP PAPR decreasing method are demonstrated in figures 6.19, 6.20 and tables 6.27, A.3. The OFDM modulated signal is analyzed for bit error counting for each SNR range. The bit errors minimize since the SNR maximizes. When SNR measures -6 the generated errors show 96058. Whereas the SNR is measuring 19 the generated errors count zero. The simulation model implements the AEXP technique depending on the AEXP constant. The model calculates about 3.3878 dB reference PAPR of the CCD function when the AEXP constant equals to 1. And produces a PAPR level of the transmitted signal of 7.3001 dB. Which is better than the PAPR level that is obtained from the OFDM system without any PAPR decreasing method.

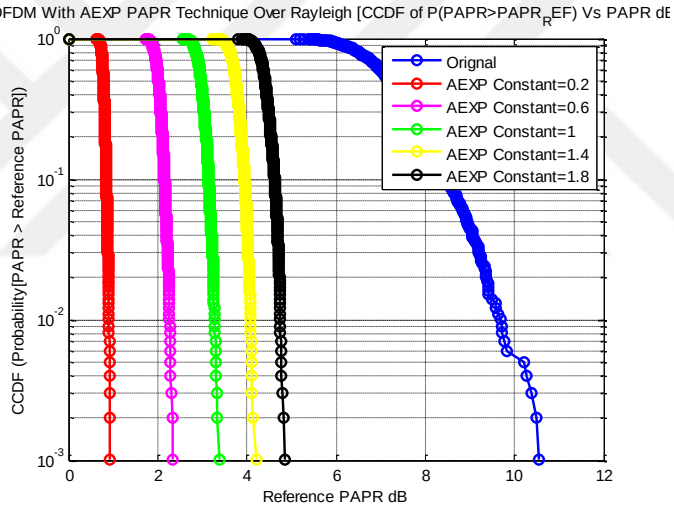

Figure 6.19: CCDF of PAPR with AEXP PAPR decreasing technique

Table 6.27: QPSK-OFDM (AEXP constant=1) of AEXP PAPR decreasing simulation

Ebit/No(DB)	BER	No. of Errors	Total Bits
-6	0.3760	96058	255488
-2	0.2910	74358	255488
2	0.1739	44442	255488
6	0.0614	15698	255488
10	0.0083	2113	255488
14	2.8181e-04	72	255488
18	1.1742e-05	1	255488
19	0	0	255488

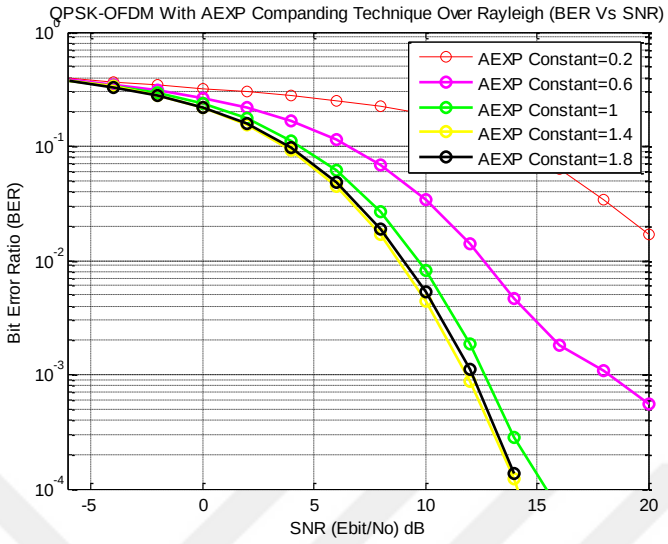

Figure 6.20: OFDM with AEXP BER VS SNR (Ebit/No)

While AEXP constant equals to 0.2 the CCDF of PAPR shows about 0.9295 dB and gives a total of PAPR equals to 1.8448 dB which is better than both RCF and RFC methods. But unfortunately the bit errors are significantly higher than RCF and RFC methods. As the AEXP constant increases the PAPR increases and the bit errors decreases. Finally, when the AEXP constant is set to 1.8 the CCDF of PAPR generates about 4.860 dB and gives a total of PAPR equals to 11.587 dB. But fortunately the bit errors decrease in the same period.

6.4.4.2 QPSK-OFDM simulation with tanhR companding technique

The tanhR companding technique is performed according the tanh algorithm which is mathematically identified by:

$$f_{tanhR}(Sk) = [(|Sk| * X)^{Y}] * sgn(Sk) \tag{6.34}$$

Where X and Y represent positive constants which is maintaining the level of companding of the signal Sk. The absolute value of SK and $sgn(Sk)$ are controlling the OFDM modulated signal phase. The de-companding process at the reception side is identified by:

$$f^{-1}_{tanhR}(Sk) = \left| \left(atanhR\left(\frac{|Sk|}{X}\right)\right)^{1/Y} \right| * sgn(Sk) \tag{6.35}$$

Input parameters:

The following input parameters are configured for the QPSK-OFDM system over Rayleigh channel which uses tanhR PAPR decreasing technique for PAPR calculation simulation model:

Table 6.28: tanhR PAPR calculation of OFDM with QPSK input parameters

Parameter	Value
FFT Size of N Subcarriers	128
Δf Spacing Frequency (Khz)	15
OFDM_BW Bandwidth (Mhz)	1.25
CP Cyclic Prefix	¼ N=32
Frequency of Sampling Fsa (Mhz)	192
Number of Symbols Per Subcarrier	1000
Sampling Period Tsa	$1/Fsa$
$Ebit/No$ SNR Range	-6 to 20 step 2
Total of Transmitted Symbols	127744
Bits Per Symbol for QPSK	2
Source Data Binary Bits	2 x 127744=255488
X_Coefficient	1 to 20 step 5
Y_Coefficient	1 to 0.2 step -0.2

Simulation results:

The BER performance and PAPR decreasing simulation results of tanhR PAPR decreasing technique are shown in figures 6.21, 6.22, 6.23, 6.24 and tables 6.29, A.4. The OFDM modulated signal is analyzed for bit error counting for each measured SNR level.

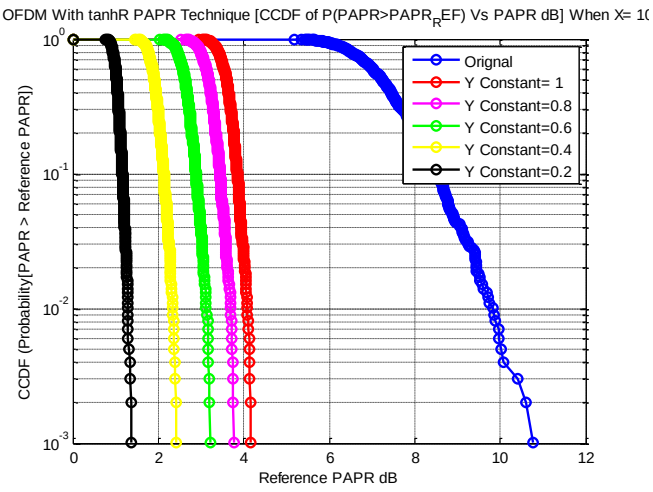

Figure 6.21: CCDF of PAPR with X=10 tanhR PAPR decreasing technique

Table 6.29: QPSK-OFDM (X=10, Y=0.2) of tanhR PAPR decreasing simulation results

Ebit/No(DB)	BER	No. of Errors	Total Bits
-6	0.4497	114895	255488
-2	0.4255	108700	255488
2	0.3937	100584	255488
6	0.3410	87113	255488
10	0.2476	63249	255488
14	0.1229	31387	255488
18	0.0298	7601	255488
20	0.0096	2463	255488

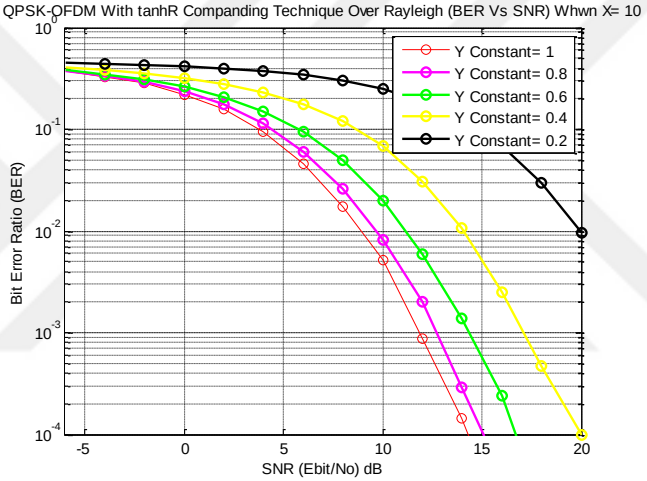

Figure 6.22: OFDM with X=10 tanhR BER VS SNR (Ebit/No)

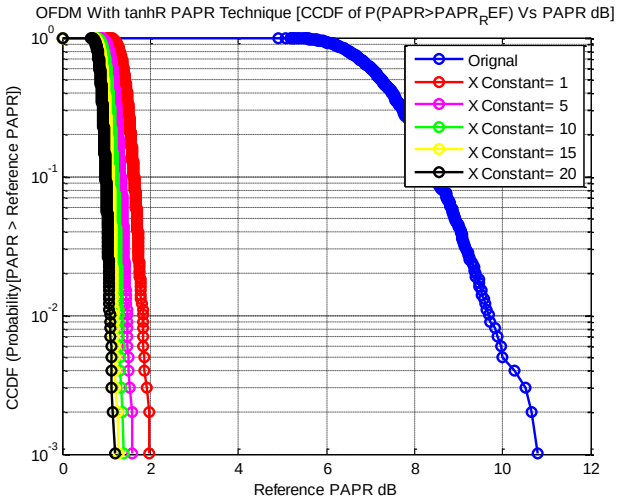

Figure 6.23: CCDF of PAPR with Y=0.2 tanhR PAPR decreasing technique

The bit errors minimize since the SNR maximizes. While X=10 and Y=0.2 the -6 SNR measurement generates 114895 bit errors. Whereas the SNR is measuring 20 the generated errors count 2463. The simulation model implements the tanhR technique depending on the X and Y constants. The model calculates about 1.2889 dB reference PAPR of the CCD function when the X=10 and Y=0.2. And produces a PAPR level of the transmitted signal of 2.9116 dB. Which is better than the PAPR value that is provided by the OFDM system without any PAPR decreasing technique.

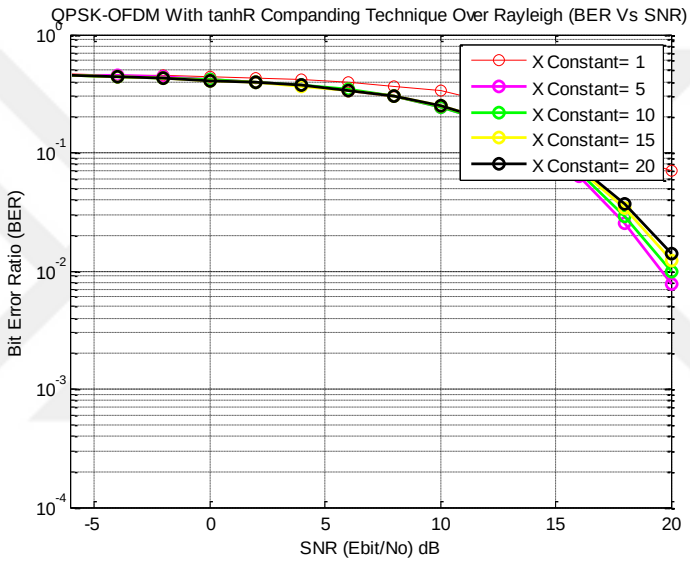

Figure 6.24: OFDM with Y=0.2 tanhR BER VS SNR (Ebit/No)

While X=10 and Y=1 the CCDF of PAPR shows about 4.1583 dB and generates a PAPR equals to 8.8102 dB and the bit errors count zero when SNR equals to 17. As Y decreases the PAPR decreases as well and inversely, when Y increases the bit errors decrease in the meanwhile. When Y=0.2 the PAPR equals to 2.9116 dB. Whereas the bit errors count about 2463 when SNR equals to 20 dB. Which is better than both RCF and RFC methods in terms of PAPR. But unfortunately the bit errors are significantly higher than RFC, RCF and AEXP techniques. On the other hand, while X increases the PAPR decreases. But unfortunately, the performance has a slight degradation. To sum up, $tanhR$ decreasing method performs better than RCF and RFC methods, and lower than AEXP method in terms of PAPR. While its performance is lower than RFC, RCF and AEXP in terms of BER. The tanhR performs slightly better than [18].

6.4.5 QPSK-OFDM Simulation with Pre-distortion PAPR Decreasing Techniques

The pre-distortion methods are performed according to the principle of data symbol energy spreading before applying the IFFT operation. The Matlab simulation model simulates the discrete Fourier transform DFT PAPR decreasing technique as it is performing better than the traditional pre-distortion methods such as tone reservation, tone injection and pulse shaping.

6.4.5.1 QPSK-OFDM simulation with DFT spreading PAPR decreasing technique

The principle of DFT method is positioning a FFT block before the IFFT block at the transmission side and positioning an IFFT block after the FFT block at the reception side. The produced PAPR of this technique is lower than the traditional OFDM system because the extra FFT operation spreads data symbol energy into various subcarriers. As a result, PAPR can be reduced to the single carrier transmission level due to that the DFT and IDFT omit each other [48] [62].

Input parameters:

The following input parameters are initiated to the QPSK-OFDM system over Rayleigh channel which uses DFT spreading PAPR decreasing technique for PAPR calculation simulation model:

Table 6.30: DFT spreading PAPR calculation of OFDM with QPSK input parameters

Parameter	Value
FFT Size of N Subcarriers	128
Δf Spacing Frequency (Khz)	15
OFDM_BW Bandwidth (Mhz)	1.25
CP Cyclic Prefix	¼ N=32
Frequency of Sampling Fsa (Mhz)	192
Number of Symbols Per Subcarrier	1000
Sampling Period Tsa	$1/Fsa$
$Ebit/No$ SNR Range	-6 to 20 step 2
Total of Transmitted Symbols	127744
Bits Per Symbol for QPSK	2
Source Data Binary Bits	2 x 127744=255488

Simulation results:

The BER performance and PAPR decreasing simulation results of DFT spreading PAPR decreasing method are shown in figures 6.25, 6.26 and table 6.31. The OFDM modulated signal is

evaluated for bit error counting for each SNR level. The bit errors decrease since the SNR increases. When SNR measures -6 the produced bit errors count 93996. Whereas the SNR is measuring 13 the generated errors count zero. The simulation model implements the DFT spreading technique. The model calculates about $6.7503e-15\ dB$ reference PAPR of the CCD function. And generates a PAPR level of the transmitted signal of $0.020\ dB$. Which is better than the PAPR level that is obtained from the OFDM system without any PAPR decreasing method.

Table 6.31: QPSK-OFDM with DFT spreading PAPR decreasing simulation results

Ebit/No(DB)	BER	No. of Errors	Total Bits
-6	0.3679	93996	255488
-2	0.2748	70215	255488
2	0.1444	36883	255488
6	0.0339	8654	255488
10	0.0011	284	255488
13	0	0	255488

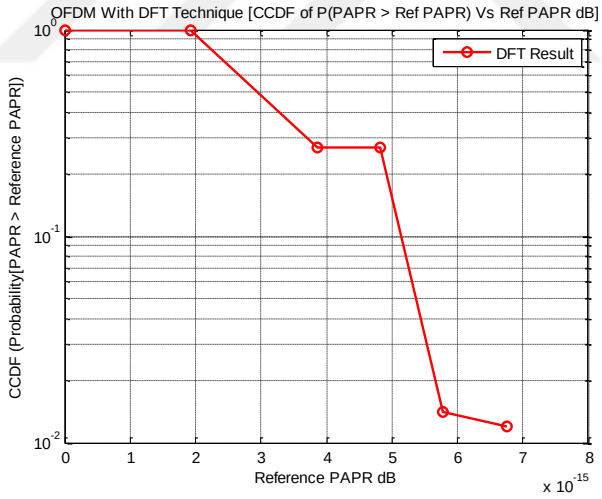

Figure 6.25: CCDF of PAPR with DFT spreading PAPR decreasing technique

The DFT spreading PAPR decreasing technique generates a level of PAPR that is lower than RCF, RFC, AEXP and tanhR techniques. Moreover, the DFT spreading technique obtains a reasonable BER performance. This technique is usually implemented by uplink transmission by mobile terminals as a process called SC-FDMA. Since mobile devices has a limitation of power. As a result, high consumption power amplifiers are not desirable by mobile terminals and low PAPR level is required and DFT spreading technique achieves this goal. The main drawback of DFT

spreading technique is that the transmission rate is extremely low and therefore, it cannot be performed in downlink transmission.

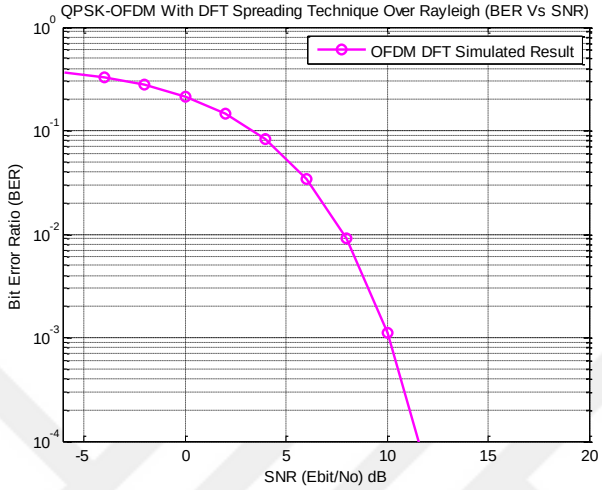

Figure 6.26: OFDM with DFT spreading BER VS SNR (Ebit/No)

6.4.6 QPSK-OFDM Simulation with RFC & AEXP PAPR Decreasing Technique

In this technique two methods RFC and AEXP are combined together to represent a hybrid technique. The combination is performed by applying the RFC and then followed by the AEXP.

6.4.6.1 Input parameters

The following input parameters are configured into the QPSK-OFDM system over Rayleigh channel which uses a hybrid RFC & AEXP PAPR decreasing technique for PAPR calculation simulation model:

Table 6.32: Hybrid RFC & AEXP PAPR calculation of OFDM with QPSK input parameters

Parameter	Value
FFT Size of N Subcarriers	128
Δf Spacing Frequency (Khz)	15
OFDM_BW Bandwidth (Mhz)	1.25
CP Cyclic Prefix	¼ N=32
Frequency of Sampling Fsa (Mhz)	192
Number of Symbols Per Subcarrier	1000
Sampling Period Tsa	$1/Fsa$

$Ebit/No$ SNR Range	-6 to 20 step 2
Total of Transmitted Symbols	127744
Bits Per Symbol for QPSK	2
Source Data Binary Bits	2 x 127744=255488
AEXP_Coefficient	0.2 to 1.8 step 0.4
Oversampling Factor L	4
Rate of Clipping CR	1.5 to 4

6.4.6.2 Simulation results

The BER performance and PAPR decreasing simulation results of the hybrid RFC and AEXP PAPR decreasing technique are illustrated in figures 6.27, 6.28 and tables 6.33, A.5. The OFDM modulated signal is evaluated for bit errors for each SNR level. The bit errors minimize since the SNR maximizes. The simulation results while the oversampling factor L equals to four, the clipping rate CR equals to 3 and the AEXP constant equals to 1 are shown in figure 6.33. When SNR calculates -6 the counted errors show 58969. Whereas the SNR is measuring 13 the produced errors count zero. The simulation model performs the hybrid technique depending on the AEXP constant, the oversampling factor L and the clipping rate CR. The model calculates about 2.8436 dB reference PAPR of the CCD function after four filtering and clipping iterations and followed by AEXP method. And produces a PAPR level of 6.2796 dB. Which is better than the PAPR level that is obtained from the OFDM system without any PAPR decreasing technique.

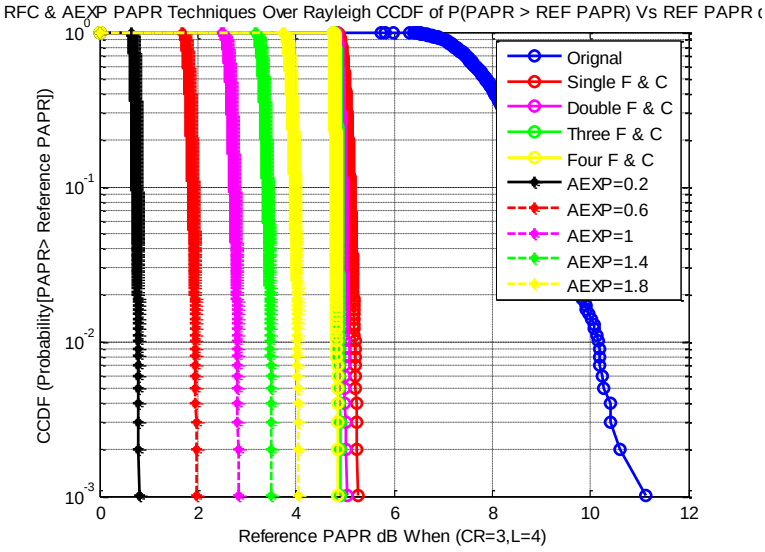

Figure 6.27: CCDF of PAPR with hybrid RFC & AEXP PAPR decreasing technique

The produced PAPR level and the BER performance of the hybrid RFC and AEXP are better than both the RFC method alone and AEXP method alone. The RFC enhances both the BER and the PAPR and the AEXP improves the PAPR level reduction. When applying only the RFC method while L=4 and CR=3 the generated PAPR level is 11.7533 dB. On the contrary, when applying only the AEXP method while AEXP constant equals to 1, the produced PAPR computes about 7.3001 dB. To sum up, the hybrid RFC and AEXP improves the performance of the OFDM system and performs better than [16], but unfortunately increases the system complexity.

Table 6.33: QPSK-OFDM (L=4, CR=3, AEXP constant=1) RFC & AEXP PAPR decreasing

Ebit/No(DB)	BER	No. of Errors	Total Bits
-6	0.2308	58969	255488
-2	0.1062	27121	255488
2	0.0222	5682	255488
6	0.0013	244	255488
10	3.9141e-05	10	255488
13	0	0	255488

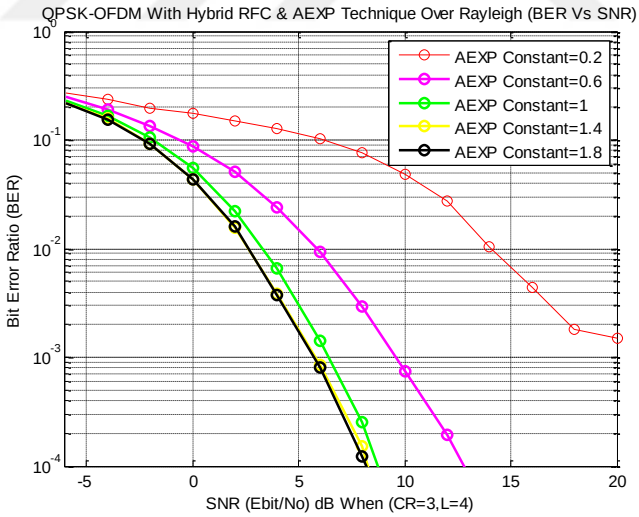

Figure 6.28: OFDM with hybrid RFC & AEXP BER VS SNR (Ebit/No)

6.5 QPSK MAPPING OVER FADING CHANNEL PERFORMANCE ANALYSIS

The Matlab simulation model simulates the performance of QPSK modulator over both flat fading and frequency selective fading channels. The model passes the transmitted QPSK modulated signal over a Rayleigh multipath delayed channel. The signal bandwidth is altered to evaluate the effects

that are caused by multipath delayed channel. The channel delay consists of four delays. The first delay refers to zero delay. Where one micro second represents 300 meters delayed path. Initially, the data is generated using a random generation function. Then, the data is mapped using QPSK mapper. After that the data is transmitted over a Rayleigh multipath channel with four delays. The transmitted signal also passed through an AWG noise. Initially, the system bandwidth is set to 500 bps symbol rate. Finally, the symbol rate is raised up to 500 kbps.

6.5.1 Input Parameters

The following input parameters are entered into the QPSK-OFDM system over Rayleigh multipath delayed channel:

Table 6.34: QPSK modulator over Rayleigh multipath channel input parameters

Parameter	Value
Symbol Rate in Bit Per Second (bps)	500 to 500000
Number of Data Symbols	10000
$Ebit/No$ SNR Level	25
M	4
Bits Per Symbol for QPSK	2
Number of Delayed Paths	4
Delayed paths Period (Micro Seconds)	[0 3 10 20] * 1e-6
Average of Delayed Path Gains (dB)	[0 -3 -6 -9]
Number of Data Bits	20000

6.5.2 Simulation Results

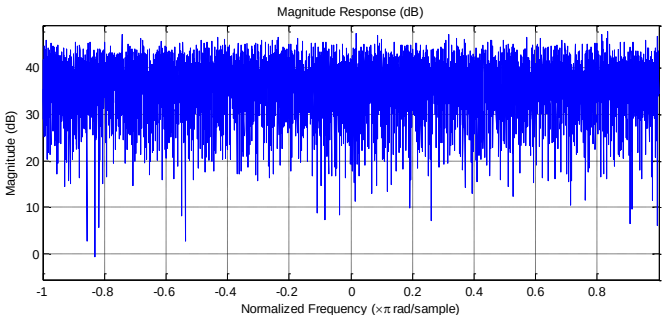

Figure 6.29: Amplitude response of QPSK over flat fading channel at 500 bps

At the first stage when the system bandwidth is initiated to a symbol rate of 500 bps. From figures 6.29 and 6.30, the amplitude and impulse response of the transmitted signal indicate that the

channel performs as a flat fading one. This happened due to that the 500 Hz signal bandwidth is much lower than the 50 KHz coherence bandwidth. Therefore, the channel delay length of 20 micro seconds is smaller than 2 milliseconds of the QPSK symbol duration. As a consequence, the channel acts as a flat fading channel and generates low bit errors.

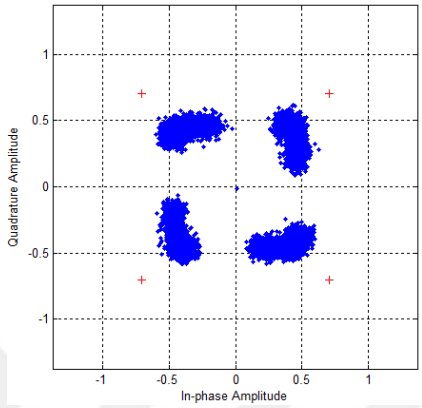

Figure 6.30: Constellation of QPSK over flat fading channel at 500 bps

After increasing the bandwidth of the symbol rate to 500 Kbps. From figures 6.31 and 6.32 it can be seen that the transmitted signal is severely distorted due to the time dispersion which causes the ISI interference. The channel delay of 20 micro seconds is higher than the QPSK symbol duration of 2 micro seconds. Therefore, the signal bandwidth is much larger than the 50 KHz coherence bandwidth. Subsequently, the channel acts as a frequency selective channel.

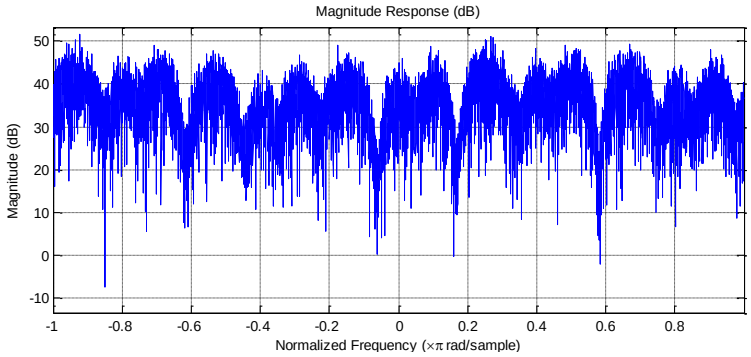

Figure 6.31: QPSK Amplitude response via frequency selective fading channel at 500 Kbps

From table 6.35, in the case of 500 bps bandwidth the system generates about 3485 bit errors. On the other hand, in the case of 500 Kbps symbol rate the system produces approximately 9550 bit errors.

Table 6.35: QPSK Mapper over Rayleigh delayed multipath channel simulation results

Symbol Rate	BER	No. of Errors	Delays	Total Bits
500 bps	0.1742	3485	4 delays	20000
500 Kbps	0.4775	9551	4 delays	20000

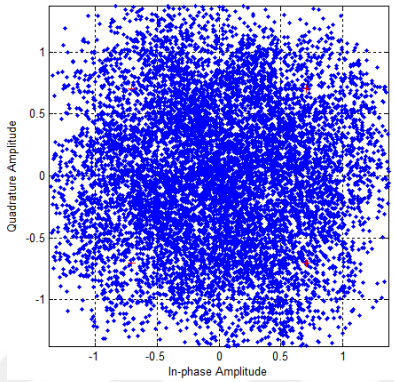

Figure 6.32: QPSK Constellation via frequency selective fading channel at 500 Kbps

6.6 OFDM PERFORMANCE AGAINST SYNCHRONIZATION ERRORS

6.6.1 OFDM Performance with The Presence of CFO

6.6.1.1 BPSK-OFDM performance with the presence of CFO noise

This Matlab model simulates the BER performance of OFDM system with BPSK mapper with the existence of CFO noise. The simulation is performed with the variation of CFO noise levels. The BPSK mapper is selected for the simulation as it causes less errors than other high order mapping schemes such as QAM-16 and QAM-64. The CFO noise leads to a severe signal distortion due to the produced ISI and ICI.

Input parameters:

The following input parameters are configured into the BPSK-OFDM system over AWGN channel which are implemented within the variation of CFO noise:

Table 6.36: CFO sensitivity of OFDM with BPSK input parameters

Parameter	Value
FFT Size of N Subcarriers	128
Δf Spacing Frequency (Khz)	15

OFDM_BW Bandwidth (Mhz)	1.25
CP Cyclic Prefix	¼ N=32
Frequency of Sampling Fsa (Mhz)	192
Number of Symbols Per Subcarrier	1000
Sampling Period Tsa	$1/Fsa$
$Ebit/No$ SNR Range	0 to 16 step 1
Total of Transmitted Symbols	128000
Bits Per Symbol for BPSK	1
Source Data Binary Bits	128000
CFO Noise	0 to 0.15 step 0.05
M	2

Simulation results:

The BER performance of BPSK-OFDM with the noise of CFO simulation results are shown in figure 6.33 and table 6.37. The OFDM modulated signal is evaluated for bit errors for each SNR level at the variation of CFO noise. The bit errors minimize since the SNR maximizes. Firstly, in the case of CFO equals to zero, When the SNR measures zero the generated errors count 10117. Whereas the measured SNR reaches 12 the produced errors show zero. Then when the CFO is increased to 0.075, the produced bit errors give 12570 at the zero measurement of SNR. As the SNR increases the bit errors decrease until it counts zero at 14 SNR measurement. Finally, while the CFO is raised up to 0.15. the generated bit errors give about 20044 errors at zero SNR level. The bit errors gradually decrease as the SNR increases, until they show only zero errors at 18 SNR measurement.

Table 6.37: BPSK-OFDM with CFO variation BER performance simulation results

Ebit/No (DB)	BER CFO=0	Errors CFO=0	BER CFO=0.075	Errors CFO=0.075	BER CFO=0.15	Errors CFO=0.15
0	0.0790	10117	0.0982	12570	0.1566	20044
2	0.0373	4770	0.0539	6895	0.1080	13819
4	0.0130	1663	0.0218	2788	0.0671	8589
6	0.0024	307	0.0068	874	0.0360	4613
8	2.1094e-04	27	0.0012	154	0.0164	2099
10	7.8125e-06	1	1.1719e-04	15	0.0069	877
12	0	0	7.8125e-06	1	0.0025	218
14	0	0	0	0	8.9844e-04	115
16	0	0	0	0	1.9531e-04	25

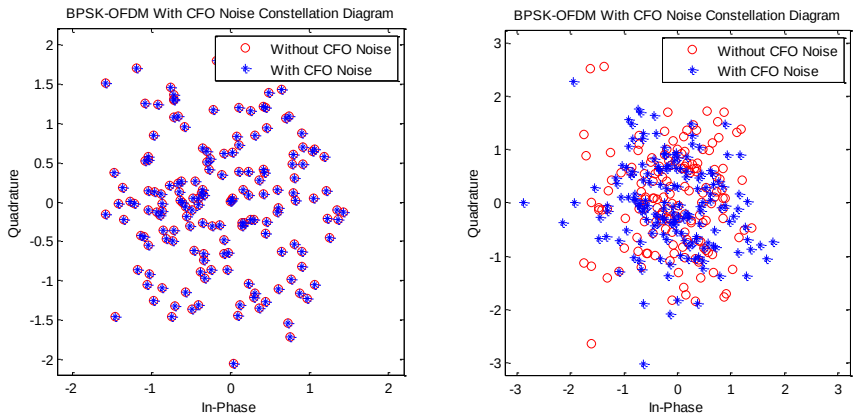

Figure 6.33: BPSK-OFDM with CFO=0 and CFO=0.15 at Ebit/No=16 scatter plots

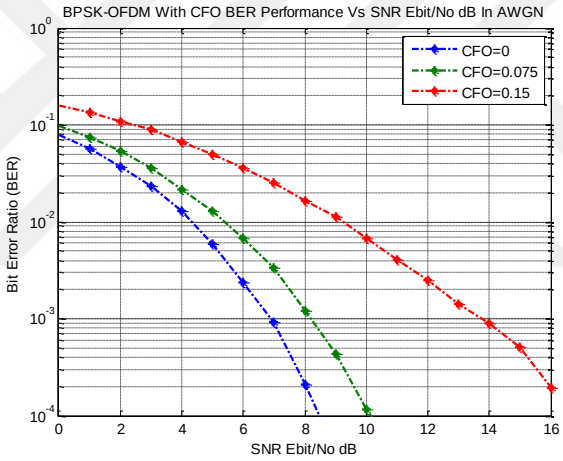

Figure 6.34: BPSK-OFDM sensitivity of CFO BER Vs SNR Ebit/No in AWGN

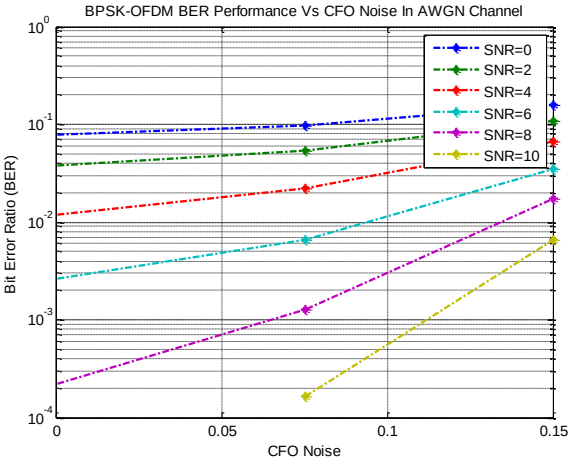

Figure 6.35: BPSK-OFDM CFO Vs BER at varied SNR levels in AWGN

Therefore, from figure 6.34 and 6.35 the increment of CFO noise level degrades the OFDM system in terms of BER. As well as the high levels of CFO noise destroy the orthogonality of the transmitted subcarriers and thus, lead to the occurrence of ICI and ISI.

6.6.1.2 QAM16-OFDM with CFO noise estimation simulation

This model of the 16QAM-OFDM system estimates the CFO compensation by applying several techniques. The CFO is added to the transmitted OFDM signal. The CFO estimation is calculated as well as the MSE mean square error is measured to analyze the degradation of performance. The estimation process is iterated 100 times. Three Estimation methods are used to estimate the CFO which are the CP-based training symbol, preamble and pilot tones. In the cyclic prefix training symbol technique, the CFO estimation is calculated by the phase difference between CP intervals:

$$\hat{\varphi} = \frac{D}{2\pi} tan^{-1} \left\{ \sum_{t=0}^{N/D-1} [yl^*(t).yl(t+N/D)] \right\} \tag{6.36}$$

Whereas, the preamble Moose technique estimates the CFO by using phase difference between two repeated preamble windows:

$$\hat{\varphi} = \frac{1}{2\pi} tan^{-1} \left\{ \sum_{k=0}^{N-1} imag[y1^*(k).y2(k)] \,/\, \sum_{k=0}^{N-1} real[y1^*(k).y2(k)] \right\} \tag{6.37}$$

And the pilot tones technique computes the CFO estimation by using the difference of phase between several pilot tones:

$$\hat{\varphi}_{acq} = \frac{1}{2\pi.Tsub} \max(\varphi) \left\{ \left| \sum_{j=0}^{L-1} yl + D[p(j),\varphi].yl^*[p(j),\varphi].Sl^* + D[p(j)]Sl[p(j)] \right| \right\} \tag{6.38}$$

In every used technique the MSE mean square error for each iteration is calculated by:

$$MSE_{iteration} = \hat{\varphi} - \varphi^2 \tag{6.39}$$

Finally, the total MSE after 100 iterations is computed by:

$$MSE_{Total} = MSE_{iteration}/100 \quad (6.40)$$

Input parameters:

The following input parameters are used by the 16QAM-OFDM system over AWGN channel which are implemented with several CFO estimation techniques:

Table 6.38: CFO estimation of OFDM system with 16QAM input parameters

Parameter	Value
FFT Size of N Subcarriers	128
Δf Spacing Frequency (Khz)	15
OFDM_BW Bandwidth (Mhz)	1.25
CP Cyclic Prefix	¼ N=32
Frequency of Sampling Fsa (Mhz)	192
Number of Symbols Per Subcarrier	1000
Sampling Period Tsa	$1/Fsa$
$Ebit/No$ SNR Range	0 to 30 step 5
Total of Transmitted Symbols	128000
Bits Per Symbol for 16-QAM	4
Number of Source Data Symbols	128000
CFO Noise	0 to 0.15 step 0.025
M	16
Number of Estimation Iterations	100

Simulation results:

The MSE performance of 16QAM-OFDM with 0.15 noise of CFO simulation results are shown in figures 6.36, 6.37, 6.38 and table 6.39. The OFDM modulated signal is evaluated for mean square errors for each SNR level for every used estimation technique. The MSE gradually minimizes as the SNR maximizes. Firstly, in the case of CP estimator, When the SNR measures zero the MSE gives 0.0013 and estimates about 0.1472 CFO. Whereas the measured SNR reaches 30 the produced MSE counts 6.7409e-07 and produces 0.1502 CFO estimation. After that, in the case of preamble CFO estimator the produced MSE gives 2.5212e-04 and the generated estimation of CFO equals to 0.1244 at the zero measurement of SNR. As the SNR increases the MSE gradually decreases until it counts only 2.0898e-07 and produces about 0.1496 CFO estimation at

14 SNR measurement. Finally, with the pilot tones CFO estimator. the generated MSE gives about 1.5606e-04 and the estimated CFO shows about 0.1345 at zero SNR level. The MSE gradually decreases as the SNR increases, until it shows only 1.3826e-07 and the estimation of CFO gives approximately 0.1496 at 30 SNR measurement.

Table 6.39: 16QAM-OFDM (CFO=0.15) of CFO estimation performance simulation results

Ebit/No (DB)	MSE CP	CFO CP Estimation	MSE Preamble	CFO Preamble Estimation	MSE Pilot Tones	CFO Pilot Tones Estimation
0	0.0013	0.1472	2.5212e-04	0.1244	1.5606e-04	0.1345
5	2.6993e-04	0.1505	6.5746e-05	0.1390	4.5369e-05	0.1419
10	7.3429e-05	0.1510	2.0118e-05	0.1448	1.3981e-05	0.1456
15	2.1993e-05	0.1507	6.4164e-06	0.1474	4.3864e-06	0.1476
20	6.8167e-06	0.1505	2.0560e-06	0.1486	1.3838e-06	0.1487
25	2.1388e-06	0.1503	6.5666e-07	0.1493	4.3729e-07	0.1492
30	6.7409e-07	0.1502	2.0898e-07	0.1496	1.3826e-07	0.1496

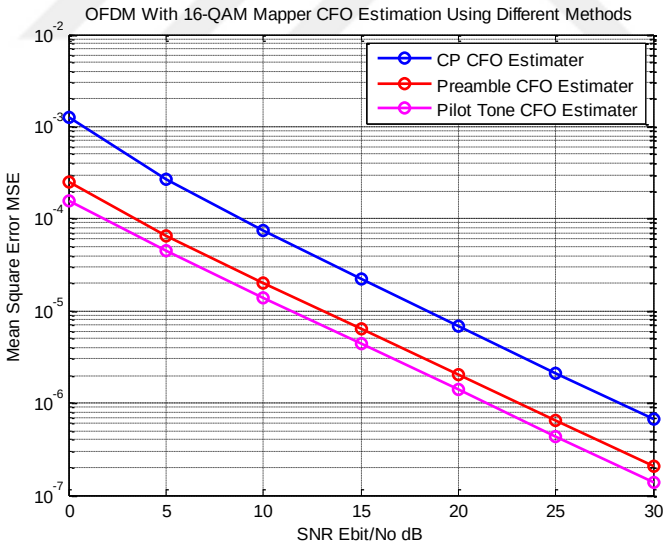

Figure 6.36: 16QAM-OFDM sensitivity (CFO=0.15) MSE Vs SNR Ebit/No dB in AWGN

From figure 6.38 it can be seen that the estimation of CFO has better values in the using of CP-based CFO estimator than those values estimated by both preamble and pilot tones techniques. Furthermore, pilot tone performs better than the preamble method at the low measurements of SNR.

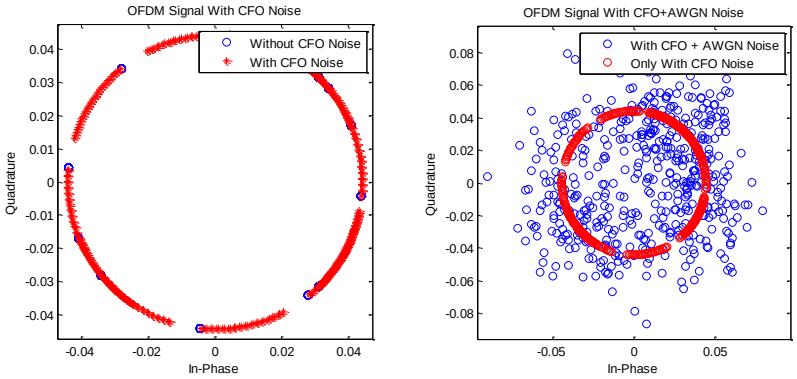

Figure 6.37: 16-QAM-OFDM with CFO=0.025 at Ebit/No=5 scatter plots

But unfortunately, the MSE performance of CP-based estimator is lower than the preamble and pilot tone methods. Moreover, the MSE degradation by using preamble method is higher than using the pilot tone method. To sum up the performance of these CFO estimation methods is varied according to the number of samples of CP and preamble windows and also depending on the number of pilot tones.

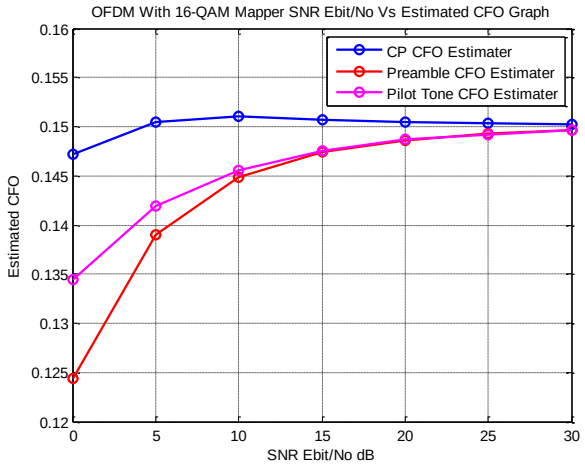

Figure 6.38: 16QAM-OFDM sensitivity (CFO=0.15) of estimated CFO Vs SNR Ebit/No

6.6.2 OFDM Performance with The Presence of STO

6.6.2.1 16QAM-OFDM with STO noise estimation simulation

This Matlab model of the OFDM system with 16-QAM mapping scheme estimates the STO compensation by applying several techniques. The CFO and STO are added to the transmitted

OFDM signal. The estimation of the STO is calculated to analyze the degradation of performance that is caused by the STO noise. The estimation process is iterated 100 times. Two Estimation methods are used to estimate the STO which are the CP-based with maximizing the correlation between blocks of samples in $w1$ and $w2$ windows. And the CP-based with minimizing the squared difference between samples in $w1$ and $w2$ windows. In the cyclic prefix based technique with maximizing the correlation, the estimation of STO is calculated by:

$$\hat{\theta} = \arg\max \theta \left\{ \sum_{i=\theta}^{NG-1+\theta} |yl(t+i).yl^{*}(t+N+i)| \right\} \tag{6.41}$$

Whereas, the CP-based technique with minimizing the squared difference estimates the STO by:

$$\hat{\theta} = \arg\min \theta \left\{ \sum_{i=\theta}^{NG-1+\theta} [|yl(t+i)| - |yl^{*}(t+N+i)|]^{2} \right\} \tag{6.42}$$

Input parameters:

The following input parameters are used by the 16QAM-OFDM system over AWGN channel which are implemented with several STO estimation techniques:

Table 6.40: STO estimation of OFDM system with 16QAM input parameters

Parameter	Value
FFT Size of N Subcarriers	128
Δf Spacing Frequency (Khz)	15
OFDM_BW Bandwidth (Mhz)	1.25
CP Cyclic Prefix	¼ N=32
Frequency of Sampling Fsa (Mhz)	192
Number of Symbols Per Subcarrier	1000
Sampling Period Tsa	$1/Fsa$
$Ebit/No$ SNR Range	0 to 30 step 5
Total of Transmitted Symbols	128000
Bits Per Symbol for 16-QAM	4
Number of Source Data Symbols	128000
STO Noise	0 to 0.15 step 0.025
M	16
Number of Estimation Iterations	100

Simulation results:

The maximum magnitude correlation CP based and the minimum magnitude squared difference CP based simulation results are shown in figures 6.39, 6.40 and table 6.41. they demonstrate the performance of 16QAM-OFDM with 0.15 noise of CFO and a variation of STO from 3 to -3 at varied SNR measurement. As the SNR increases the maximum magnitude correlation and the minimum magnitude squared difference decrease in the meanwhile.

Table 6.41: 16QAM-OFDM (STO=-3, CFO=0.15) STO estimation simulation results

Ebit/No (DB)	Max Magnitude Correlation	Min Magnitude Squared Difference
0	2.2888	1.2290
5	2.0090	0.6115
10	1.9506	0.2146
15	1.9543	0.0643
20	1.9859	0.0235
25	1.9793	0.0073
30	1.9615	0.0022

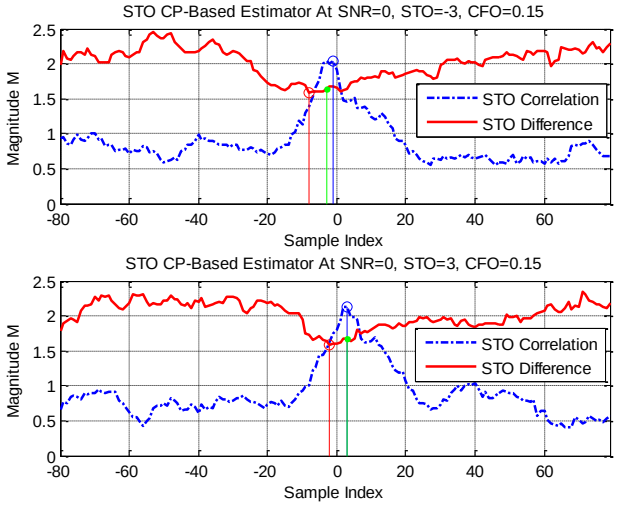

Figure 6.39: 16-QAM-OFDM with CP-based max correlation Vs min difference at SNR=0

From the simulation results, it is obvious that the maximum correlation method performs better than the minimum squared difference method in bad channel conditions. As it can be seen in figure 6.39 the difference between the original STO with the green color almost the same with the estimated STO by correlation method. While there is a shift in the case of squared difference.

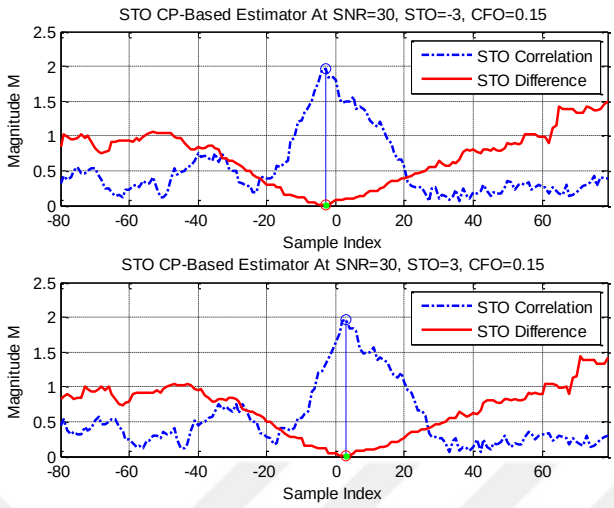

Figure 6.40: 16-QAM-OFDM with CP-based max correlation Vs min difference at SNR=30

On the other hand, in figure 6.40 both methods perform almost the same in good channel conditions at 30 dB SNR measurement.

6.7 16QAM-OFDM WITH PILOT CHANNEL ESTIMATION SIMULATION

This Matlab model of the OFDM system with 16-QAM mapping scheme estimates the propagation channel by implementing various techniques. The estimation of the channel is simulated to analyze the degradation of OFDM performance that is caused by the communication channel effects. The estimation process is performed by two estimation methods. The LS least squares pilot insertion channel estimator and the MMSE minimum mean square error pilot insertion channel estimator. The LS estimator estimates the channel by inserting pilot symbols with the OFDM transmitted symbols. At the receiver, the initial step in computing the least squares estimate is removing the pilot symbols as their locations are already known. The least squares estimate is used to determine the channel response. The calculation of LS estimate is provided by dividing the number of received pilots by their predicted value as the following:

$$R(k,l) = H(k,l).S(k,l) + N(k,l) \tag{6.43}$$

Where $R(k,l)$ represents the complex received symbol, $H(k,l)$ represents the channel gain affected a particular symbol, $S(k,l)$ represents the transmitted symbol and $N(k,l)$ represents the noise. The already known pilots are transmitted to estimate the channel by:

$$\widehat{H}_p(k,l) = \frac{R_p(k,l)}{S_p(k,l)} = H_p(k,l) + N(k,l) \tag{6.44}$$

Where $R_p(k,l)$ represents the received pilot, $S_p(k,l)$represents the known transmitted pilot, $\widehat{H}_p(k,l)$ represents the channel response for the pilot symbol. Finally, interpolation can be used to estimate the lost values of the channel estimation response.

In the MMSE estimator, the same process of inserting reference pilots within the transmitted OFDM symbols. By supposing that the received OFDM signal is defined by:

$$R(k,l) = S(k,l).H(k,l) + N(k,l) \tag{6.45}$$

Where k represents the subcarrier index and l represents the OFDM symbol index. By assuming that the locations of pilots are represented by $P_{(m,n)}$ with the related subcarrier index m and the related OFDM symbol index n $(m,n) \ni P)$.

By calculating the normalized received signals at P pilot locations as the following:

$$norm(m,n) = R_p(m,n)/S_p(m,n) \tag{6.46}$$

$$norm(m,n) = H_P(m,n) + v(m,n)$$

The main objective of the channel estimation process is to estimate the channel response $H_P(k,l)$ by observing the pilot locations:

$$\widehat{H}_p(k,l) = \sum_{(m,n)\ni P} c(k,l,m,n).norm(m,n) \tag{6.47}$$

Where $c(k,l,m,n)$ represents the time-frequency filter coefficients which can be calculated by implementing the minimum mean squared error as the following:

$$MMSE_{c(k,l,m,n)} = \arg\min E\left[\left|H_P(k,l) - \widehat{H}_p(k,l)\right|^2\right] \tag{6.48}$$

6.7.1 Input Parameters

The following input parameters are used by the 16QAM-OFDM system which are implemented with several channel estimation techniques:

Table 6.42: Channel estimation of OFDM system with 16QAM input parameters

Parameter	Value
FFT Size of N Subcarriers	128
Δf Spacing Frequency (Khz)	15
OFDM_BW Bandwidth (Mhz)	1.25
CP Cyclic Prefix	¼ N=32
Frequency of Sampling Fsa (Mhz)	192
Number of Symbols Per Subcarrier	1000
Sampling Period Tsa	$1/Fsa$
$Ebit/No$ SNR Range	-6 to 40 step 2
Total of Transmitted Symbols	12800
Bits Per Symbol for 16-QAM	4
Number of Channel Delays	6
Number of Inserted Pilots	FFT Size /4 = 32
M	16
Channel Estimation Methods	LS Pilot & MMSE Pilot

6.7.2 Simulation Results

The LS and MMSE channel estimation simulation results are shown in figures 6.41 and table 6.43. They demonstrate the performance of 16QAM-OFDM with LS and MMSE channel estimators with a prorogation channel with 6 delays of multipath to make the worst condition of the communication channel. As well as the simulation of OFDM system without any channel estimation while the channel has 6 delays of multipath.

Table 6.43: 16QAM OFDM with LS & MMSE channel estimation simulation results

Ebit/No (DB)	BER LS Estimation 6 Delays	Errors LS Estimation 6 Delays	BER MMSE Estimation 6 Delays	Errors MMSE Estimation	BER No Estimation 6 Delays	Errors No Estimation 6 Delays
-6	0.6635	84934	0.6550	83837	0.9228	118115
-2	0.6247	79959	0.6145	78650	0.9126	116807
2	0.5558	71144	0.5462	69911	0.9031	115599

6	0.4444	56884	0.4313	55206	0.8973	114854
10	0.2980	38138	0.2839	36338	0.8926	114249
14	0.1645	21059	0.1525	19520	0.8939	114414
18	0.0765	9794	0.0696	8912	0.8951	114577
22	0.0336	4296	0.0297	3805	0.8947	114523
26	0.0138	1770	0.0122	1564	0.8955	114629
30	0.0068	866	0.0063	800	0.8957	114646
34	0.0034	435	0.0031	393	0.8942	114455
40	0.0015	195	0.0015	189	0.8940	114429

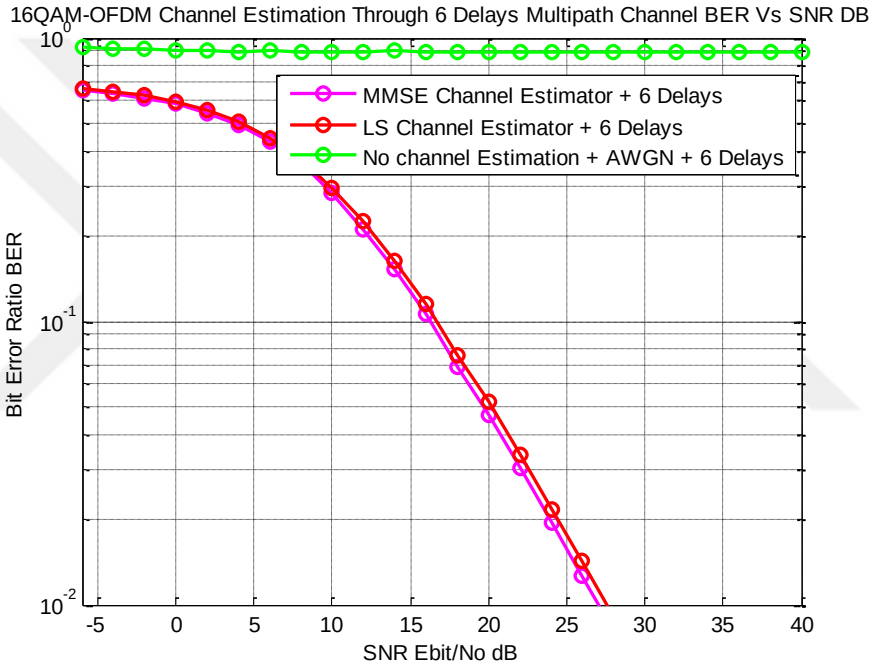

Figure 6.41: 16QAM-OFDM with LS & MMSE channel estimation BER Vs SNR Ebit/No

As the SNR increases the BER performance increases in the meanwhile. In the case of LS estimator when initially the SNR is set to -6 the number of produced errors count about 84934 and they are gradually decrease until they finally reach only 195 bit errors at 40 SNR measurement. On the other hand, in the case of MMSE the generated bit errors show approximately 83837 when the SNR initiates to -6, after that the bit errors are minimized gradually unless they count only 189 bit errors at the measurement of 40 of the SNR. Unfortunately, in the case of the simulation without any channel estimation process the received signal is almost completely distorted. From the simulation results, it is obvious that the MMSE channel estimation method performs slightly better than the LS channel estimation method. Both LS and MMSE performs slightly better than [22] and [23].

7. CONCLUSION

Initially, the impacts of various wireless communication channels are evaluated in implementing several constellation mapping schemes that are adopted in the OFDM system of LTE network. The simulation results of these evaluation processes show that the best results of performance are achieved through the AWGN channel as shown in figure 7.1. The assessment shows that the AWGN gives better BER and less bit errors in comparison with the multipath flat fading and frequency selective fading channels such as Rayleigh and Rician channels. Since, the investigation of simulation results demonstrate that they are less efficient. On the other hand, the Rician channel provides better performance than Rayleigh multipath channel. The Rician channel performs well when the *K* Rician facto increases. The degradation of performance in fading channels is based on several factors that cause more bit errors and sometimes destroy the transmitted signal thoroughly. For instance, the number of delayed paths of the signal, the environment of the location and the constellation mapping scheme that is used for modulation. Therefore, in fading channels the fading is caused by delay spread or by Doppler spread. Thus, the simulation results investigate the effects of these fading channels and illustrates the signal output distortions that are occurred during the simulations.

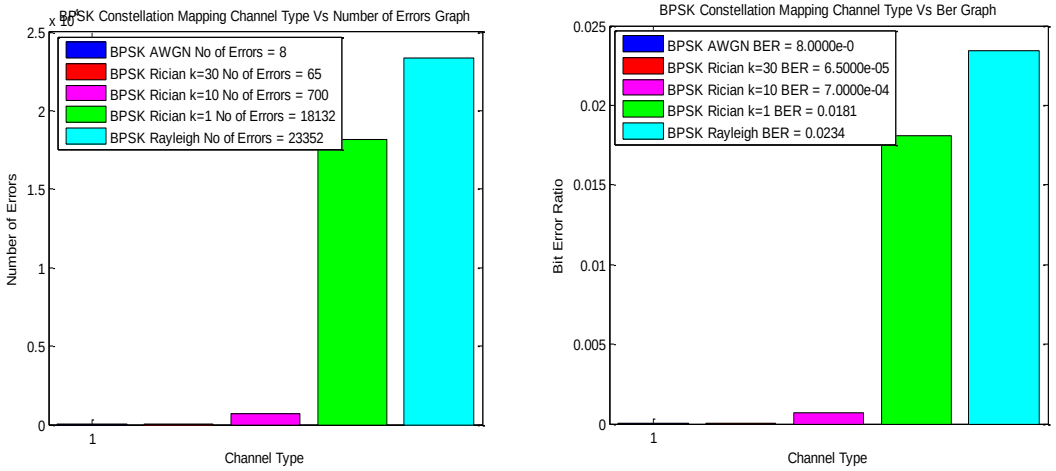

Figure 7.1: Comparison of BPSK performance over different channels at 10 DB SNR

In LTE OFDM network four mapping schemes are employed for the mapping process. BPSK, QPSK, 16-QAM and 64-QAM. The simulations of those techniques are implemented in different communication channels as shown in figure 7.2 and they are investigated for BER performance.

The simulation results show that when the number of transmitted bits per symbol is increased the system performance is degraded in the meanwhile. As a result, the best results are obtained by BPSK mapping scheme where the transmitted symbol only consists of one bit. The QPSK has won the second rank. After that 16-QAM and finally 64-QAM. The high order mapping schemes increase the transmission rate of the system but their throughputs have large number of bit errors. The simulation results show that the number of bit errors is dependent to the channel conditions. Therefore, LTE network adopts a mechanism of adaptive modulation in which if the channel condition is good a higher order mapping scheme is used. Otherwise low order schemes are used instead.

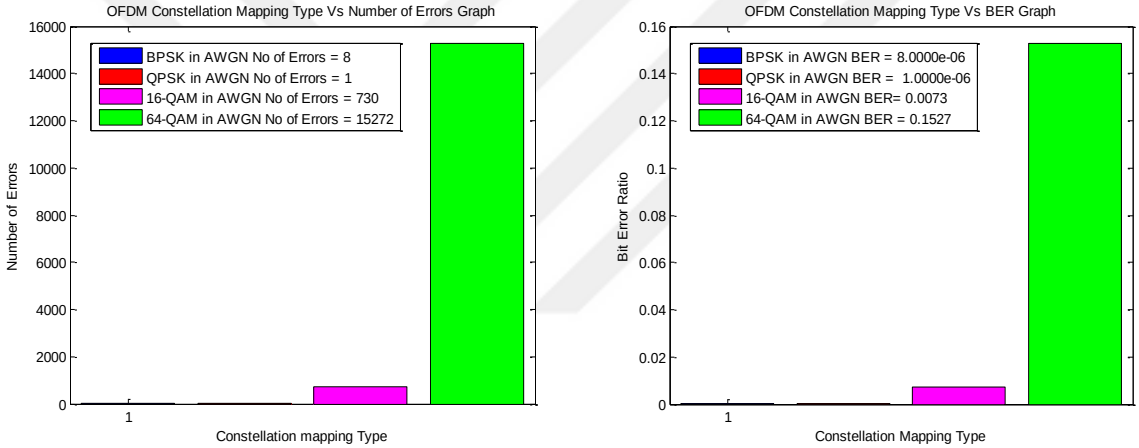

Figure 7.2: Comparison of LTE Constellation mappers at 10 DB SNR

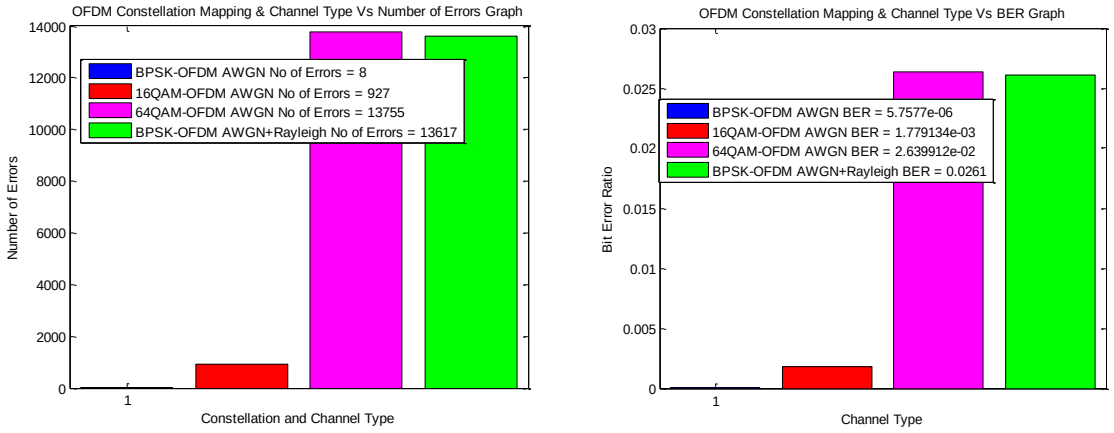

Figure 7.3: Comparison of different OFDM simulations at 10 DB SNR

After that a Matlab model simulates the performance of the multicarrier LTE-OFDM system. the model simulates the modulation process steps. As shown in figure 7.3 the simulation results show that the BER performance is quite reasonable and gives better results than single carrier transmission. Furthermore, OFDM with low order BPSK mapping scheme performs better than the high order 16-QAM and 64-QAM. The simulated output signal has bit errors that is caused by several factors. But the main issues that lead to these signal distortions is the PAPR that is occurred during the modulation process. And to be precise the output of the IFFT is effected by this issue. Another important issues facing OFDM system are the noises of STO and CFO.

Bit error detection and bit error correction are necessary to achieve best results of the transmitted signals. Thus, coding and decoding is extremely important in LTE-OFDM systems. The 3GPP adopts the turbo coding technique. Therefore, a Matlab model simulates the performance of the 16-QAM transmission system with and without encoding. The simulation results as illustrated in figure 7.4 show that the BER performance is substantially improved by implementing a $1/3$ turbo encoder. For instance, at $3dB$ SNR the coded signal has 135 errors. While the non-coded signal has 13504 bit errors. The simulation results also show that if encoding process is iterated many times this leads to better results.

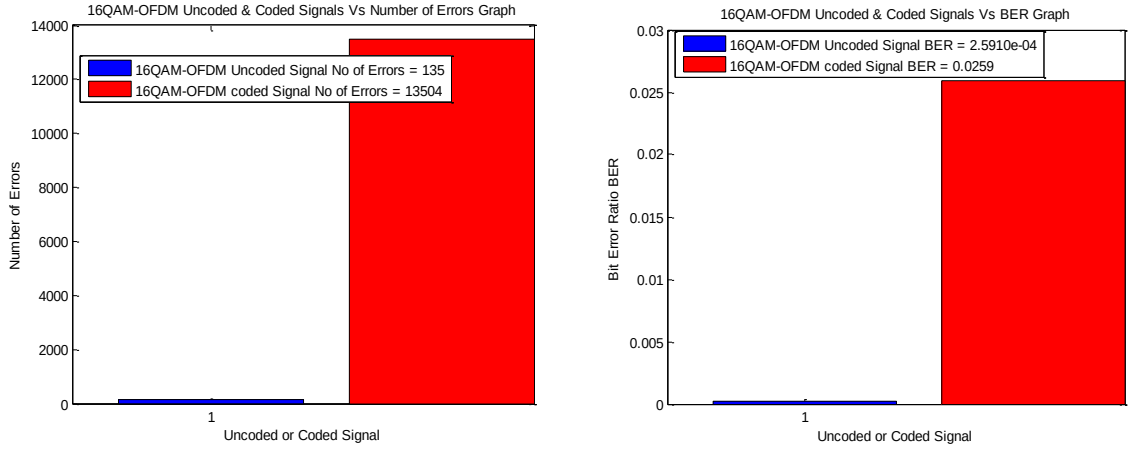

Figure 7.4: Comparison of 16QAM-OFDM with un-coded and coded signals at SNR 3 DB

Due to the fact that OFDM systems suffer from PAPR issue, since it is considered as the main drawback of the OFDM multicarrier systems. Subsequently, many PAPR decreasing techniques are proposed and evaluated by several Matlab simulations. As a result, the simulation results as illustrated in figure 7.5 show that both the RFC and RCF PAPR decreasing techniques enhance

the BER and the PAPR in the meanwhile. The simulations also show that the RFC performs better than the RCF with the same system complexity. It is also can be observed from the results that if the RCF and RFC are iterated better results can be achieved. After that another PAPR decreasing techniques that employ the principle of companding are investigated. Both AEXP and tanhR techniques are simulated. The simulation results show that AEXP performs better than RCF, RFC and tanhR in terms of PAPR. But in terms of BER it performs lower than RFC and RCF. Similarly, the tanhR performs better than the RCF and RFC in terms of PARP. But unfortunately lower than RFC and RCF regarding the BER. After that a DFT precoding technique is simulated with Matlab. The investigations show that it is performing better than RCF, RFC, AEXP and tanhR regarding to PAPR. This technique is adopted by 3GPP as SC-FDMA in the uplink transmission of the LTE-OFDM system. finally, a hybrid RFC and AEXP PAPR decreasing technique is simulated and investigated for performance. The simulation results illustrate that it gives a better performance than RFC alone and AEXP alone. The RFC improves the BER while the AEXP enhances the PAPR. To sum up, the hybrid PAPR decreasing techniques improve both the BER and PAPR but unfortunately increase the system complexity.

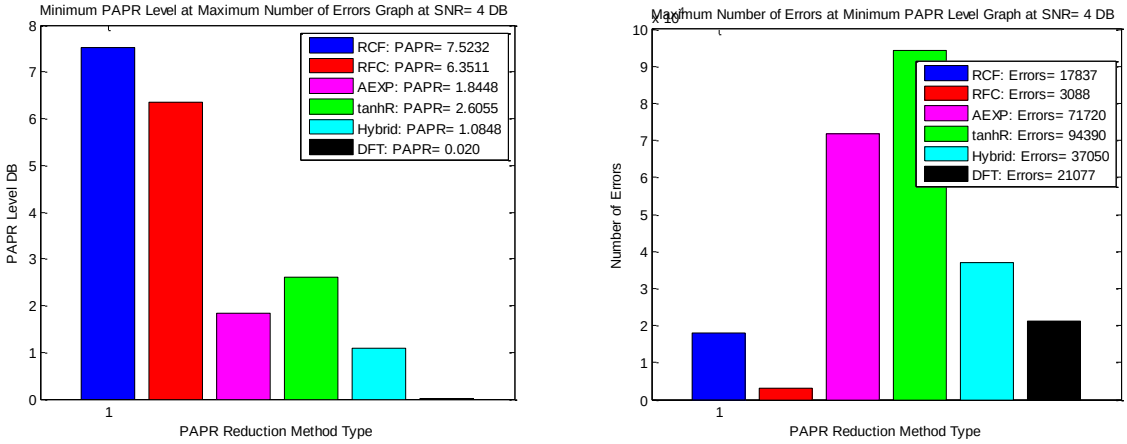

Figure 7.5: Comparison of different PAPR decreasing methods at SNR 4 DB

This thesis also simulates the impacts of CFO and STO which are considered as one of the important issues that degrade the efficiency of the OFDM systems. The simulation results show that the increments of STO and CFO distort the transmitted signals and cause both ICI and ISI. Three CFO estimators are simulated and evaluated for performance. CP-based training symbol, preamble and pilot tones. The simulation results show that these methods are capable of estimating

the CFO properly. And therefore, the receiver can compensate the estimated values on the received signal. The pilot tone method performs better in terms of MSE performance. Followed by the preamble method. And finally, the CP-based method. On the other hand, two STO estimation methods are simulated and evaluated. The maximum correlation CP based and the minimum squared difference CP based. Both methods calculate the estimated STO that can be compensated by the receiver to the received OFDM modulated signal. The maximum correlation method performs better than the minimum squared difference method. Also the channel is estimated by LS and MMSE pilot algorithms and both methods estimate the channel and their performances are reasonable but not excellent. As shown in figure 7.6 the MMSE estimator performs slightly better than LS estimator.

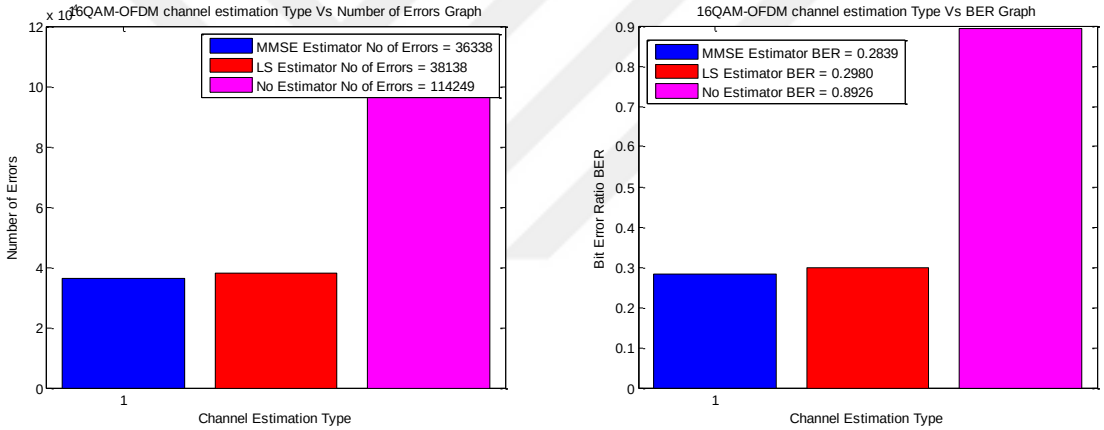

Figure 7.6: Comparison of LS & MMSE channel estimators in Rayleigh at SNR 10 DB

Both flat fading and frequency selective fading channels are simulated and investigated by a Matlab simulation model. The simulation results show that the performance is worst in the case of the frequency selective channel. The simulation demonstrates the principle of delay spread. Pulse shaping by raised cos filter is simulated and evaluated for improving the quality of the received signal. The simulation results demonstrate that it is extremely important to apply such filters in the OFDM system as a type of windowing. As it improves the received signal and avoids distortions.

7.1 FUTURE WORK

The analysis and the evaluation of LTE network will be further expanded to the LTE-A where MIMO-OFDM and multi-used theory are used. As well as demonstrates this study in more details.

REFERENCES

[1] W. Webb Ph. D., *The Future of Wireless Communications*, First Edition. Boston: Artech House Publishers, 2001.

[2] D. Tse and P. Viswanath, *Fundamentals of Wireless Communication*, 1 edition. Cambridge, UK; New York: Cambridge University Press, 2005.

[3] A. F. Molisch, *Wireless Communications*, 2 edition. Wiley-IEEE Press, 2012.

[4] H. Liu and G. Li, *OFDM-Based Broadband Wireless Networks: Design and Optimization*, 1 edition. Hoboken, N.J: Wiley-Interscience, 2005.

[5] C. Cox, *An Introduction to LTE: LTE, LTE-Advanced, SAE and 4G Mobile Communications*, 1 edition. Hoboken, NJ: Wiley, 2012.

[6] E. Krouk and S. Semenov, Eds., *Modulation and Coding Techniques in Wireless Communications*, 1 edition. Chichester, West Sussex: Wiley, 2011.

[7] S. Sesia, I. Toufik, and M. Baker, *LTE - The UMTS Long Term Evolution: From Theory to Practice*, 2 edition. Chichester, West Sussex, U.K.; Hoboken, N.J: Wiley, 2011.

[8] H. Zarrinkoub, *Understanding LTE with MATLAB: From Mathematical Modeling to Simulation and Prototyping*, 1 edition. Chichester, West Sussex, United Kingdom: Wiley, 2014.

[9] A. C. Brooks, S. J. Hoelzer, T. L. Stewart, and I. S. Ahn, "Design and Simulation of Orthogonal Frequency Division Multiplexing (OFDM) Signaling," *Electron. Publ. Digit. Object Identifiers DOIs*, pp. 1–4, 2001.

[10] Y. D. Dou and F. Z. Zhang, "Design and Implementation of OFDM Communication System Based on ARM," in *2018 10th International Conference on Intelligent Human-Machine Systems and Cybernetics (IHMSC)*, 2018, vol. 02, pp. 362–365, doi: 10.1109/IHMSC.2018.10188.

[11] S. K. Rony, F. A. Mou, and M. M. Rahman, “Performance Analysis of OFDM Signal Using BPSK and QPSK Modulation Techniques,” *Am. J. Eng. Res. AJER*, vol. 6, no. 1, p. pp-108-117, 2017.

[12] N. J. Borkar and Dattatray. S. Bormane, “BER performance of OFDM system with adaptive modulation,” in *2012 IEEE International Conference on Complex Systems (ICCS)*, 2012, pp. 1–8, doi: 10.1109/ICoCS.2012.6458547.

[13] Anuradha and N. Kumar, “BER analysis of conventional and wavelet based OFDM in LTE using different modulation techniques,” in *2014 Recent Advances in Engineering and Computational Sciences (RAECS)*, 2014, pp. 1–4, doi: 10.1109/RAECS.2014.6799622.

[14] E. Costa and S. Pupolin, “M-QAM-OFDM system performance in the presence of a nonlinear amplifier and phase noise,” *IEEE Trans. Commun.*, vol. 50, no. 3, pp. 462–472, Mar. 2002, doi: 10.1109/26.990908.

[15] S. Dixit and H. Katiyar, “Performance of OFDM in Time Selective Multipath Fading Channel in 4G Systems,” in *2015 Fifth International Conference on Communication Systems and Network Technologies*, 2015, pp. 421–424, doi: 10.1109/CSNT.2015.107.

[16] B. Tang, K. Qin, and H. Mei, “A Hybrid Approach to Reduce the PAPR of OFDM Signals Using Clipping and Companding,” *IEEE Access*, vol. 8, pp. 18984–18994, 2020, doi: 10.1109/ACCESS.2020.2968560.

[17] A. Singh and H. Singh, “Peak to average power ratio reduction in OFDM system using hybrid technique,” *Optik*, vol. 127, no. 6, pp. 3368–3371, Mar. 2016, doi: 10.1016/j.ijleo.2015.12.105.

[18] A. K. Yadav and Y. K. Prajapati, “PAPR Minimization of Clipped OFDM Signals Using Tangent Rooting Companding Technique,” *Wirel. Pers. Commun.*, vol. 105, no. 4, pp. 1435–1447, Apr. 2019, doi: 10.1007/s11277-019-06151-1.

[19] A. Mohammed, M. Shehata, A. Nassar, and H. Mostafa, “Performance Comparison of Companding-Based PAPR Suppression Techniques in OFDM Systems,” in *2019 8th*

International Conference on Modern Circuits and Systems Technologies (MOCAST), 2019, pp. 1–4, doi: 10.1109/MOCAST.2019.8742045.

[20] D. Gill and G. Saini, "PAPR Reduction in OFDM Systems using Non-Linear Companding Transform," *IOSR J. Electron. Commun. Eng.*, vol. 9, pp. 133–140, Jan. 2014, doi: 10.9790/2834-0928133140.

[21] S. Kaur, "A Survey on Various PAPR Reduction Techniques in OFDM Communication Systems," *Int. Res. J. Eng. Technol. IRJET*, vol. 2, pp. 24–28, Sep. 2015.

[22] M. B. Sutar and V. S. Patil, "LS and MMSE estimation with different fading channels for OFDM system," in *2017 International conference of Electronics, Communication and Aerospace Technology (ICECA)*, 2017, vol. 1, pp. 740–745, doi: 10.1109/ICECA.2017.8203641.

[23] A. Khlifi and R. Bouallegue, "Performance Analysis of LS and LMMSE Channel Estimation Techniques for LTE Downlink Systems," *Int. J. Wirel. Mob. Netw.*, vol. 3, no. 5, pp. 141–149, Oct. 2011, doi: 10.5121/ijwmn.2011.3511.

[24] M. K. Abboud and B. M. Sabbar, "Performance evaluation of high mobility OFDM channel estimation techniques," *Int. J. Electr. Comput. Eng. IJECE*, vol. 10, no. 3, pp. 2562–2568, Jun. 2020, doi: 10.11591/ijece. v10i3.pp2562-2568.

[25] C. Rajanandhini and S. P. K. Babu, "Comparison on Carrier Frequency Offset Estimation in Multi Band Orthogonal Frequency Division Multiplexing (OFDM) System," in *Innovative Data Communication Technologies and Application*, Cham, 2020, pp. 551–560, doi: 10.1007/978-3-030-38040-3_62.

[26] P. K. Nishad and P. Singh, "Carrier frequency offset estimation in OFDM systems," in *2013 IEEE Conference on Information Communication Technologies*, 2013, pp. 885–889, doi: 10.1109/CICT.2013.6558220.

[27] P. Krishna, K. K. Rao, and T. A. Kumar, "Carrier frequency offset estimations in OFDM-downlink LTE systems," in *2015 IEEE 9th International Conference on Intelligent Systems and Control (ISCO)*, 2015, pp. 1–5, doi: 10.1109/ISCO.2015.7282304.

[28] S. Younis, A. Al-Dweik, A. Hazmi, C. C. Tsimenidis, and B. S. Sharif, “Symbol timing offset estimation scheme for OFDM systems based on power difference measurements,” in *21st Annual IEEE International Symposium on Personal, Indoor and Mobile Radio Communications*, 2010, pp. 927–932, doi: 10.1109/PIMRC.2010.5672096.

[29] D.-C. Chang, “Effect and Compensation of Symbol Timing Offset in OFDM Systems with Channel Interpolation,” *IEEE Trans. Broadcast.*, vol. 54, no. 4, pp. 761–770, Dec. 2008, doi: 10.1109/TBC.2008.2002339.

[30] H.-T. Hsieh and W.-R. Wu, “Maximum Likelihood Timing and Carrier Frequency Offset Estimation for OFDM Systems with Periodic Preambles,” *IEEE Trans. Veh. Technol.*, vol. 58, no. 8, pp. 4224–4237, Oct. 2009, doi: 10.1109/TVT.2009.2019820.

[31] E. Dahlman, S. Parkvall, and J. Skold, *4G: LTE/LTE-Advanced for Mobile Broadband*, 1 edition. Amsterdam: Academic Press, 2011.

[32] J. Wang, Z. Zhang, Y. Ren, B. Li, and J.-U. Kim, “Issues toward networks architecture security for LTE and LTE-A networks,” *Int. J. Secur. Its Appl.*, vol. 8, no. 4, pp. 17–24, 2014.

[33] H. Holma and A. Toskala, Eds., *LTE for UMTS - OFDMA and SC-FDMA Based Radio Access*, 1 edition. Chichester, U.K: Wiley, 2009.

[34] M. Sauter, *From GSM to LTE: An Introduction to Mobile Networks and Mobile Broadband*, 1 edition. Chichester, West Sussex, U.K.; Hoboken, N.J: Wiley, 2011.

[35] G. M. Køien, “Mutual entity authentication for LTE,” in *2011 7th International Wireless Communications and Mobile Computing Conference*, 2011, pp. 689–694, doi: 10.1109/IWCMC.2011.5982630.

[36] N. Seddigh, B. Nandy, R. Makkar, and J. F. Beaumont, “Security advances and challenges in 4G wireless networks,” in *2010 Eighth International Conference on Privacy, Security and Trust*, 2010, pp. 62–71, doi: 10.1109/PST.2010.5593244.

[37] W. Ahmed, S. Anwar, and M. J. Arshad, “Security Architecture of 3GPP LTE Network and LTE-A Network,” vol. 7, no. 1, pp. 31–37, 2016.

[38] L. W. Couch, *Digital & Analog Communication Systems*, 8 edition. Upper Saddle River, N.J: Pearson, 2012.

[39] A. Goldsmith, *Wireless Communications*, 1 edition. Cambridge; New York: Cambridge University Press, 2005.

[40] H. Schulze and C. Lüders, *Theory and Applications of OFDM and CDMA: Wideband Wireless Communications*, 1st edition. Chichester, England; Hoboken, NJ: Wiley, 2005.

[41] T. S. Rappaport, *Wireless Communications: Principles and Practice*, 2 edition. Upper Saddle River, N.J: Prentice Hall, 2002.

[42] S. G. Glisic, *Advanced Wireless Communications: 4G Cognitive and Cooperative Broadband Technology*, 2 edition. Chichester, West Sussex, England; Hoboken, NJ: Wiley-Interscience, 2007.

[43] A.-E. M. Taha, N. A. Ali, and H. S. Hassanein, *LTE, LTE-Advanced and WiMAX: Towards IMT-Advanced Networks*, 1 edition. Chichester, West Sussex, U.K: Wiley, 2011.

[44] W. H. Tranter, K. S. Shanmugan, T. S. Rappaport, and K. L. Kosbar, *Principles of Communication Systems Simulation with Wireless Applications*, 1 edition. Upper Saddle River, NJ: Prentice Hall, 2004.

[45] M. Rupp, S. Schwarz, and M. Taranetz, *The Vienna LTE-Advanced Simulators: Up and Downlink, Link and System Level Simulation*, 1st ed. 2016 edition. New York, NY: Springer, 2016.

[46] C. Kappler, *UMTS Networks and Beyond*, 1 edition. Chichester, U.K: Wiley, 2009.

[47] K. Wesolowski, *Mobile Communication Systems*, 1 edition. New York: Wiley, 2002.

[48] Y. S. Cho, J. Kim, W. Y. Yang, and C. G. Kang, *MIMO-OFDM Wireless Communications with MATLAB*, 1 edition. Singapore; Hoboken, NJ: Wiley-IEEE Press, 2010.

[49] F. Wang and Y. Zhu, “An efficient CFO estimation algorithm for the downlink of 3GPP-LTE,” in *2011 International Conference on Wireless Communications and Signal Processing (WCSP)*, 2011, pp. 1–6, doi: 10.1109/WCSP.2011.6096788.

[50] K. Fazel and S. Kaiser, *Multi-Carrier and Spread Spectrum Systems: From OFDM and MC-CDMA to LTE and WiMAX*, 2 edition. Chichester, U.K: Wiley, 2008.

[51] A. Lipovac, “Qualifying CP length for LTE FDD downlink channel with small delay dispersion,” in *2015 23rd International Conference on Software, Telecommunications and Computer Networks (SoftCOM)*, 2015, pp. 367–370, doi: 10.1109/SOFTCOM.2015.7314116.

[52] H. Nourollahi and S. G. Maghrebi, “Evaluation of cyclic prefix length in OFDM system based for Rayleigh fading channels under different modulation schemes,” in *2017 IEEE Symposium on Computers and Communications (ISCC)*, 2017, pp. 164–169, doi: 10.1109/ISCC.2017.8024523.

[53] S. Sengar and P. Bhattacharya, “Performance improvement in OFDM system by PAPR reduction,” *Signal Image Process. Int. J.*, vol. 3, May 2012, doi: 10.5121/sipij.2012.3211.

[54] S. Mohammady, R. M. Sidek, P. Varahram, M. N. Hamidon, and N. Sulaiman, “Study of PAPR reduction methods in OFDM systems,” in *13th International Conference on Advanced Communication Technology (ICACT2011)*, 2011, pp. 127–130.

[55] H. Kaiho and T. Hattori, “Reduced complexity of spread spectrum OFDM for PAPR reduction and its basic performance,” in *TENCON 2009 - 2009 IEEE Region 10 Conference*, 2009, pp. 1–5, doi: 10.1109/TENCON.2009.5396030.

[56] R. Aishwarya Lal, M. N. Geetha, and M. S. Sahana, “The Relative Study of Peak-to-Average Power Ratio Reduction Techniques for LTE OFDM System,” in *2017 International Conference on Current Trends in Computer, Electrical, Electronics and Communication (CTCEEC)*, 2017, pp. 520–523, doi: 10.1109/CTCEEC.2017.8455037.

[57] T. Jiang and Y. Wu, “An Overview: Peak-to-Average Power Ratio Reduction Techniques for OFDM Signals,” *Broadcast. IEEE Trans. On*, vol. 54, pp. 257–268, Jul. 2008, doi: 10.1109/TBC.2008.915770.

[58] Ai Bo, Yang Zhi-xing, Pan Chang-yong, Zhang Tao-tao, and Ge Jian-hua, "Effects of PAPR reduction on HPA predistortion," *IEEE Trans. Consum. Electron.*, vol. 51, no. 4, pp. 1143–1147, Nov. 2005, doi: 10.1109/TCE.2005.1561836.

[59] S. Cha, M. Park, S. Lee, K.-J. Bang, and D. Hong, "A new PAPR reduction technique for OFDM systems using advanced peak windowing method," *IEEE Trans. Consum. Electron.*, vol. 54, no. 2, pp. 405–410, May 2008, doi: 10.1109/TCE.2008.4560106.

[60] Md. M. Mowla and S. M. Hasan, "Performance Improvement of Papr Reduction for OFDM Signal in LTE System," *Int. J. Wirel. Mob. Netw.*, vol. 5, pp. 35–47, Aug. 2013, doi: 10.5121/ijwmn.2013.5403.

[61] H. Sakran, M. Shokair, and A. Abouelazm, "Combined interleaving and companding for PAPR reduction in OFDM systems," *Prog. Electromagn. Res. C*, vol. 6, pp. 67–78, Jan. 2009, doi: 10.2528/PIERC08122211.

[62] M. Moharem, M. Gouda, and khalid shehata, "PAPR Reduction Performance for LTE OFDM Systems with Different Techniques," *Int. J. Sci. Eng. Res.*, vol. 4, pp. 2337–2344, May 2013.

APPENDIX A

A.1 REPEATED CLIPPING & FILTERING RCF SIMULATION RESULTS TABLE

Table A.1: RCF PAPR decreasing technique simulation results

Factor of Oversampling L	Clipping Rate CR	CCDF Reference PAPR After 4 Iteration	PAPR dB	SNR when Bit Errors=0
1.5	1.5	2.9419	7.5232	18
	2	3.6520	8.8703	15
	3	5.0175	11.7836	13
	4	6.1408	14.1735	11
2	1.5	3.5849	8.5905	18
	2	4.1374	9.5756	17
	3	5.3881	12.3207	14
	4	6.4839	14.5202	11
3	1.5	3.9146	9.3589	21
	2	4.5510	10.7291	15
	3	5.7154	13.1324	9
	4	6.7368	15.5365	9
4	1.5	3.6722	9.2112	21
	2	4.4314	10.7150	15
	3	5.7585	13.2022	9
	4	6.8049	15.5387	7

A.2 REPEATED FILTERING & CLIPPING RFC SIMULATION RESULTS TABLE

Table A.2: RFC PAPR decreasing technique simulation results

Factor of Oversampling L	Clipping Rate CR	CCDF Reference PAPR After 4 Iteration	PAPR dB	SNR when Bit Errors=0
1.5	1.5	2.3611	6.6785	28
	2	3.2821	8.4491	20
	3	4.8581	11.7276	12
	4	6.0549	14.4419	10
2	1.5	2.3961	6.3877	26
	2	3.2862	8.4540	22
	3	4.9041	11.7704	11
	4	6.4640	15.5695	9
3	1.5	2.3758	6.5167	24
	2	3.2888	8.4720	13
	3	4.8469	11.7129	9
	4	6.0580	14.1958	8
4	1.5	2.4333	6.3511	24
	2	3.2844	8.5226	12
	3	4.8451	11.7533	9
	4	6.0567	14.1969	7

A.3 AEXP COMPANDING PAPR DECREASING SIMULATION RESULTS TABLE

Table A.3: AEXP PAPR decreasing technique simulation results

AEXP Coefficient Constant	CCDF Reference PAPR	PAPR dB	SNR when Low Bit Errors Achieved
0.2	0.9295	1.8448	4349 At SNR=20 dB
0.6	2.3287	4.7969	141 At SNR=20 dB
1.0	3.3878	7.3001	2 At SNR=20 dB
1.4	4.2107	9.5375	0 At SNR=17 dB
1.8	4.860	11.587	0 At SNR=15 dB

A.4 ROOTING OF TANGENT TANHR SIMULATION RESULTS TABLE

Table A.4: tanhR PAPR decreasing technique simulation results

X Constant	Y Constant	CCDF Reference PAPR	PAPR dB	Low Bit Errors Achieved when high SNR (dB) Measured
1	1	9.8397	22.8623	0 errors when SNR=13
	0.8	8.1342	18.6852	0 errors when SNR=15
	0.6	6.2021	14.1359	3 errors when SNR=20
	0.4	4.0638	9.2314	1325 errors when SNR=20
	0.2	1.8521	4.2177	17853 errors when SNR=20
5	1	7.3514	16.9086	0 errors when SNR=13
	0.8	6.0146	13.9794	0 errors when SNR=15
	0.6	4.6108	10.7670	0 errors when SNR=17
	0.4	3.1076	7.2922	3 errors when SNR=20
	0.2	1.5327	3.6364	1861 errors when SNR=20
10	1	4.1583	8.8102	0 errors when SNR=17
	0.8	3.7439	8.0500	2 errors when SNR=20
	0.6	3.1613	6.8964	2 errors when SNR=20
	0.4	2.3491	5.2118	22 errors when SNR=20
	0.2	1.2889	2.9116	2463 errors when SNR=20
15	1	2.6088	5.2252	72 errors when SNR=20
	0.8	2.5171	5.2414	27 errors when SNR=20
	0.6	2.3329	5.0869	47 errors when SNR=20
	0.4	1.9546	4.4186	122 errors when SNR=20
	0.2	1.2301	2.8116	3112 errors when SNR=20
20	1	1.8064	3.3800	638 errors when SNR=20
	0.8	1.8273	3.5848	424 errors when SNR=20
	0.6	1.8120	3.7986	259 errors when SNR=20
	0.4	1.6553	3.6890	363 errors when SNR=20
	0.2	1.1387	2.6055	3764 errors when SNR=20

A.5 HYBRID RFC & AEXP PAPR DECREASING SIMULATION RESULTS TABLE

Table A.5: Hybrid RFC & AEXP PAPR decreasing technique simulation results

AEXP Constant	Factor of Oversampling L	Clipping Rate CR	CCDF Reference PAPR	PAPR dB	Low Bit Errors Achieved when high SNR (dB)
0.2	4	1.5	0.5123	1.0848	1471 errors when SNR=20
		2	0.6482	1.3673	731 errors when SNR=20
		3	0.7931	1.6604	432 errors when SNR=20
		4	0.8625	1.7684	194 errors when SNR=20
0.6	4	1.5	1.2812	2.6694	223 errors when SNR=20
		2	1.5917	3.4453	30 errors when SNR=20
		3	1.9823	4.2513	8 errors when SNR=20
		4	2.1365	4.5665	6 errors when SNR=20
1	4	1.5	1.7235	3.9033	152 errors when SNR=20
		2	2.2345	5.0815	0 errors when SNR=19
		3	2.8436	6.2792	0 errors when SNR=13
		4	3.0989	6.7964	0 errors when SNR=11
1.4	4	1.5	2.1118	5.1158	178 errors when SNR=20
		2	2.7350	6.5970	7 errors when SNR=20
		3	3.5123	7.9563	0 errors when SNR=11
		4	3.8590	8.6908	0 errors when SNR=9
1.8	4	1.5	2.3929	6.1580	146 errors when SNR=20
		2	3.1657	7.9298	4 errors when SNR=20
		3	4.0494	9.5320	0 errors when SNR=15
		4	4.4921	10.3172	0 errors when SNR=11